SUBMARINE CANYON EVOLUTION OF THE SOUTHWEST CAPE CONTINENTAL MARGIN

By

Kreesan Palan (BSc. Hons)

Submitted in fulfillment of the academic requirements for the degree of Master of Science

In the Discipline of Geological Sciences

School of Agriculture, Earth and Environmental Sciences

University of KwaZulu-Natal

Supervised by Prof. A.N. Green

Co-supervised by Dr. E.A. Wiles & Dr. K. Sink

December, 2017

PREFACE

The research described in this thesis was undertaken in the School of Geological Sciences (Marine Geology Unit), University of KwaZulu-Natal, under the lead supervision of Prof. A.N. Green and co-supervision of Dr. E.A. Wiles and Dr. K. Sink. The duration of the work performed spans January 2016 to December 2017. These studies represent original work by the author and have not been submitted in any form to another university. Where use was made of the work of others, it has been duly acknowledged in the text.

…… ……

Author **Date**

…… ……

Lead Supervisor **Date**

ABSTRACT

Submarine canyons are diverse geomorphological systems that are characterised by a wide variety of geomorphic and sedimentary processes. The complexities that arise during their evolution reveal changes in the tectonic and eustatic setting that actively sculpt continental margins. Newly acquired high-resolution bathymetry reveals 15 submarine canyon systems, most of which were previously undocumented, and a large fluid seep/pockmark field off the Cape continental margin of the west coast of South Africa. These are hosted in the Orange Basin, South Africa's largest gas producing basin. High resolution 2D seismic reflection and borehole data were used to establish a general seismic stratigraphy in which eight units are defined (Seismic Facies 1 – 8). Five key unconformity bounding surfaces are delineated (surfaces A – E) and related to major fluctuations in sea-level. Surface A marks the Albian sedimentation in the basin, B defines the Turonian – Conacian boundary and is imprinted by the first palaeo-canyons of the area, C characterises the Maastrichtian – Danian boundary and correlating with another episode of canyon formation, D marks the Palaeocene – Eocene surface, above which an assumed Oligocene canyon system was formed, and E defines the Mid-Miocene unconformity correlating to a pulse of uplift of the hinterland and further canyon incision.

The modern-day canyons observed from multibeam bathymetry are suspected to have initiated in the Pliocene. The contemporary canyon morphologies vary, with many canyon features yet to be described in the literature. These morphologies are broadly classed into linear, sinuous, hooked and shelf-indenting types. Pockmarks are situated in close proximity to the sinuous, hooked and shelf-indenting canyon types and were quantified using hydrological extraction techniques to a total of 2219. These pockmarks represent the terminus of stratigraphic fluid migration from an Aptian gas reservoir, evidenced in the form of blowout pipes and brightened reflectors. Various pockmark morphologies are exhibited including circular, elongate, crescentic, composite and stringed-types. This pockmark morphological diversity is explained through localised bottom current controls which modify a point-sourced circular pockmark to establish the more complicated morphologies.

The morphometric analyses of the canyons suggest contemporaneous down- and upslope eroding paradigms, that later were dominated by the influences of vertical fluid flows and gas seepage. It is proposed that fluid flow plays a key role in establishing the morphological variability of canyons

along the Cape continental margin. Vertical fluid migration within the study area has the potential to mobilise sediments, evidenced by the occurrences of blowout pipes, pockmarks and neighbouring mass wasting deposits. The youngest (or most immature) canyons are considered to be the linear-types, produced by the amalgamation of intra-slope rills and with a notable absence of fluid flow features. Succeeding these are the sinuous canyons, their sinuous form dictated by the spatially irregular control of fluid flow on the sea-floor stability. The hooked canyons are defined by their arcuate heads and dense pockmark associations, suggesting further fluid flow interaction around the canyon head, producing erosion patterns associated with neither up, nor downslope mass wasting. A single shelf indenting/breaching canyon is observed. This is considered the most mature canyon system. The meandering mid-components of this canyon formed by fluid-interactions, however slumping may have been of sufficient magnitude to have extended beyond the pockmark fields, the canyon head thus gaining access to sediment flows from the upper slope. The head then subsequently retrogressed beyond the shelf-break to its present position.

This thesis provides the first opportunity for a glimpse into seafloor fluid venting and escape features from the South African margin and how they affect canyon morphologies.

ACKNOWLEDGEMENTS

To my lead supervisor Andy Green, this was an enjoyable journey under your guidance. I appreciate all the advice and mentorship you've provided throughout the duration of this project. Thank you for everything.

My mother, thank you for all you've done for me. None of it goes unnoticed. My father, spreading wisdom to me contrary to conventional beliefs. Chrysantha, you're a good sister to me.

Errol Wiles, it's been a pleasure working with you as my co-supervisor. Brian Andrews of the United States Geological Survey (USGS), thank you for your hours spent unselfishly helping me halfway across the globe. I truly appreciate it! Nigel Hicks is thanked for providing a crash course in Kingdom Suite.

To Arissa Shanganlall, what a fun voyage during these MSc years – hikes, camps, roadtrips, drinks, food, silly songs, pranks etc. I'll never forget it! You have helped me overcome tough times in my life and brought much cheerfulness. Thank you.

To Leigh and the rest of the Gordon family, only good memories. To the rest of my friends and family: Brendan Naiker (I am the dominant FIFA king), Mike Jacobs, Lauren Pretorius, Shivani Keshav, Chetan Ramlall, Dean De Villiers – you may be few, but you are treasured!

This thesis was funded by the South African National Biodiversity Institute (SANBI) via grants from the National Research Foundation (NRF). Thank you, Dr. Kerry Sink, for securing the dataset. Anadarko Petroleum Corporation is thanked for the collection of multibeam data used in this thesis. The Petroleum Agency of South Africa (PASA) is thanked for supplying the seismic and well data.

TABLE OF CONTENTS

PREFACE ..... **i**

ABSTRACT ..... **ii**

ACKNOWLEDGEMENTS ..... **iv**

TABLE OF CONTENTS ..... **v**

CHAPTER 1: INTRODUCTION **1**

CHAPTER 2: BACKGROUND **4**

2.1. SUBMARINE CANYON SYSTEMS 4

2.2. FLUID FLOW FEATURES 8

CHAPTER 3: REGIONAL SETTING **14**

3.1. LOCALITY 14

3.2. TECTONIC AND GEOLOGICAL FRAMEWORK 14

3.3. OCEANIC CURRENTS ALONG THE CAPE MARGIN 18

CHAPTER 4: METHODOLOGY **20**

4.1. DATA COLLECTION AND PROCESSING 20

4.2. POCKMARK EXTRACTION PROCESS 22

CHAPTER 5: RESULTS **24**

5.1. GENERAL SEISMIC STRATIGRAPHY 24

5.2. SUBMARINE CANYON SPECIFIC OBSERVATIONS 35

5.3. FLUID FLOW AND POCKMARK FEATURES 68

CHAPTER 6: DISCUSSION **80**

6.1. GENERAL SEISMIC STRATIGRAPHY 80

6.2. SUBMARINE CANYONS 83

6.3. FLUID FLOW AND POCKMARK FEATURES 89

6.4. MODELS FOR FLUID MIGRATION AND CANYON DEVELOPMENT 92

CHAPTER 7: CONCLUSIONS **96**

REFERENCES **98**

APPENDIX A **116**

CHAPTER 1

INTRODUCTION

Submarine canyon systems serve as major conduits for sediment from the continental shelf to deep abyssal areas (Shepard & Dill, 1966; Carlson & Karl, 1988; Harris & Whiteway, 2011). An intimate knowledge of these systems, especially regarding their evolution, is key to understanding deep water sediment transport and delivery processes and their ensuing depositional products. In particular, cycles of sea-level change, evolving sediment supply rates and tectonic instability may imprint on these systems (Pratson et al., 2007), revealing subtle fluctuations in these three controlling influences on the evolution of the continental margin. This has direct relevance to the general understanding of slope and abyssal-hosted petroleum plays and their reservoir potentials.

The recent collection of multibeam bathymetry from the continental slope of the Cape continental margin of South Africa has revealed the presence of numerous submarine canyons (Fig. 1.1), the majority of which are hitherto undescribed from the literature and therefore informally named in this thesis. A large fluid seep/pockmark field was similarly revealed and has provided the first opportunity for a glimpse into seafloor fluid venting and escape features from the South African margin. In many areas, these vents occur in association with canyons of particularly striking geomorphologies.

This thesis aims to understand the evolution of the canyons from the Cape continental margin. The canyons are examined in the context of downslope-eroding gravity flows (Piper & Normark, 2009) or retrogressive slumping (Pratson et al., 1994; Green et al., 2007), but also include the possible role of gas seepage-induced sediment failures (Hovland et al., 2002). These three influences are examined within the general bedrock framework of the margin. This study therefore provides a surface, sub-surface and structural analysis of the canyons and their host stratigraphy, in order to understand the broad scale evolution of erosion patterns on the Cape continental margin. This increases the understanding of the erosional and unconformity forming processes of the area which can then be tied to trends in sea-level change.

The objectives of this thesis are:

1. To provide a sub-surface and structural analysis of the canyons and their associated host stratigraphy using 2D seismic reflection data.
2. To delineate unconformity bounding surfaces, match these with pre-existing and published biostratigraphic frameworks, and to then relate them to the state of sea-level at that time.
3. To track changes in canyon position and evolution.
4. To examine, using morphometric and statistical means, the current canyon morphology. This is in order to reveal the dominant processes that influenced their evolution.
5. To explain the effect localised fluid (gas) flow has on canyon evolution and to relate this to particular and unusual canyon morphologies documented in the study area.

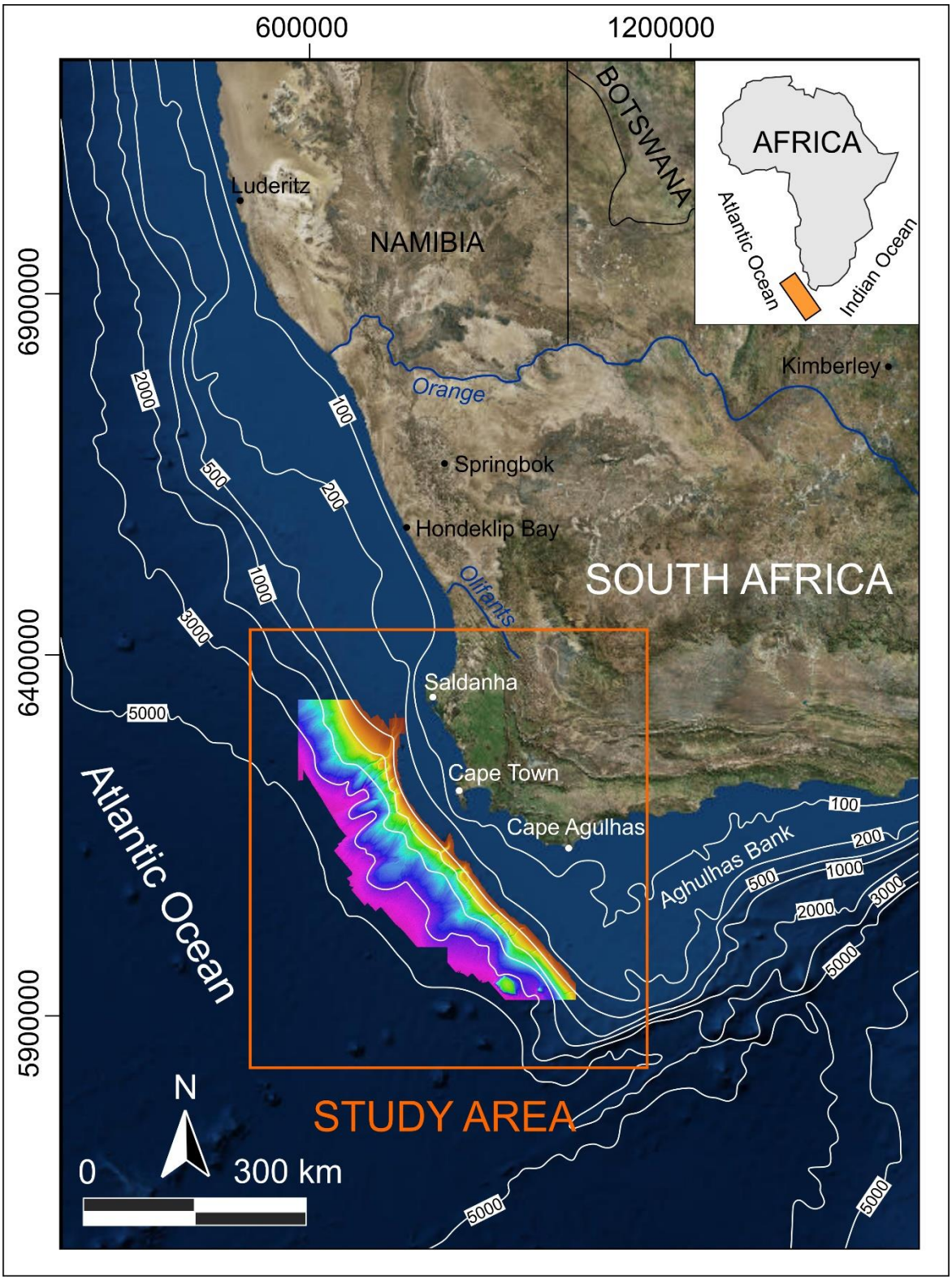

Figure 1.1: Locality map of the study area showing the extent of the bathymetric data between 315 – 3125 m depth. Satellite altimetry imagery acquired from NOAA.

CHAPTER 2

BACKGROUND

2.1. SUBMARINE CANYON SYSTEMS

Submarine canyons are incisions on the seafloor that serve as major conduits for sediment transportation from the continental shelf to the adjacent basins (Shepard & Dill, 1966; Canals et al., 2006; Jobe et al., 2011; Puig et al., 2014). Broadly, canyons may be classified into shelf-indenting and slope-confined features (Jobe et al., 2011; Huang et al., 2014), the latter of which is considered as immature in its evolutionary pathway and the former considered the end-point in canyon evolution (Farre et al., 1983). In some cases, shelf-indenting canyons may have a distinct connection to a fluvial system (e.g. Harris & Whiteway, 2011). Regardless of their evolutionary state, all canyons are considered as global biodiversity hotspots due to their topographical complexity which shelters many important and unique benthic ecosystems (Huvenne & Davies, 2013). Periods of sediment flushing (e.g. Canals et al., 2006) and submarine landsliding (e.g. Green & Uken, 2008) further result in dynamic systems that promote diversity and favour the development of ecological niches.

During the early applications of sequence stratigraphy, canyons were considered key erosional surfaces that formed during sea-level regression and through lowstand intervals (cf. Catuneanu, 2006). With the advent of better mapping systems, coring techniques, and dating methods, it is now known that canyons may form at any point in the sea-level cycle, including sea-level highstands (Boyd et al., 2008; Covault et al., 2007; Covault & Graham, 2010), provided the canyon head, or most proximal point of the canyon system, has already incised the shelf (Posamentier et al., 1991). In this case, the canyon will remain active for the transport of sediment from terrigenous sources such as coastal mountain belts, fluvial systems or longshore drift cells (Jobe et al., 2011) to the deep sea depositional systems (Covault & Graham, 2010). In contrast, those canyon heads that are detached from terrestrial sediment sources and are located entirely on the slope are considered as active during lowstands and marine transgression (Covault & Graham, 2010).

Canyon systems are typically associated with point source distal submarine fan deposition (Covault & Graham, 2010; Covault, 2011; Shanmugam, 2016). Therefore, an understanding of

their role in sediment transfer is critical in the context of potential exploration targets for petroleum and organic carbon reservoirs (Harris et al., 2007). Depending on the local conditions, specifically the sediment supply and oceanographic circulation, fans may be reduced or completely absent (Wiles et al., 2013). Fan morphology, internal structure and composition is dictated in many ways by the erosion styles that predominate in the canyon itself (Emery & Myers, 1996). This, in turn, is influenced by the local stratigraphy and prevailing sea-level states.

Shelf-indenting vs. slope-confined canyons

Shelf-indenting canyons have erosional characteristics such as tributaries, multiple thalwegs, slumped walls and V-shaped cross-sectional profiles (Cunningham et al., 2005; Lastras et al., 2009; Jobe et al., 2011) (Fig. 2.1.1). Typically, these canyons most frequently occur on active continental margins (Ortega-Sánchez et al., 2014) and are thus linked to areas of high sediment supply such as adjacent aeolian dune fields (Henrich et al., 2010), fluvial systems (Green & Uken, 2008; Huang et al., 2014) or longshore drift cells (Covault et al., 2007) (Fig. 2.1.1).

Slope-confined canyons are typically more a U-shaped in profile, and lacking terraces along their lengths (Zhu et al., 2009; Jobe et al., 2011). Sediment transported through their channels are thought to be sourced from mass wasting events on the slope (Kennett, 1982; Pratson et al., 1994; Brothers et al., 2013) (Fig. 2.1.1), as opposed to the terrestrial associations of shelf-indenting systems. Slope-confined canyons may frequently exhibit axial incisions, defined as small v-shaped incisions at the base of the canyon floor in which recent flows have eroded the main axis only (Baztan et al., 2005). These are believed to destabilise sediments from canyon walls as they oversteepen the walls relative to the canyon floor, preconditioning the materials for slides, slumps and debris flows (Baztan et al., 2005; Puga-Bernabeu et al., 2013). Slope confined canyons typically occur in close association with mass transport deposits (MTDs) either along the canyon walls or on the adjacent slope from the mentioned processes (Li et al., 2016).

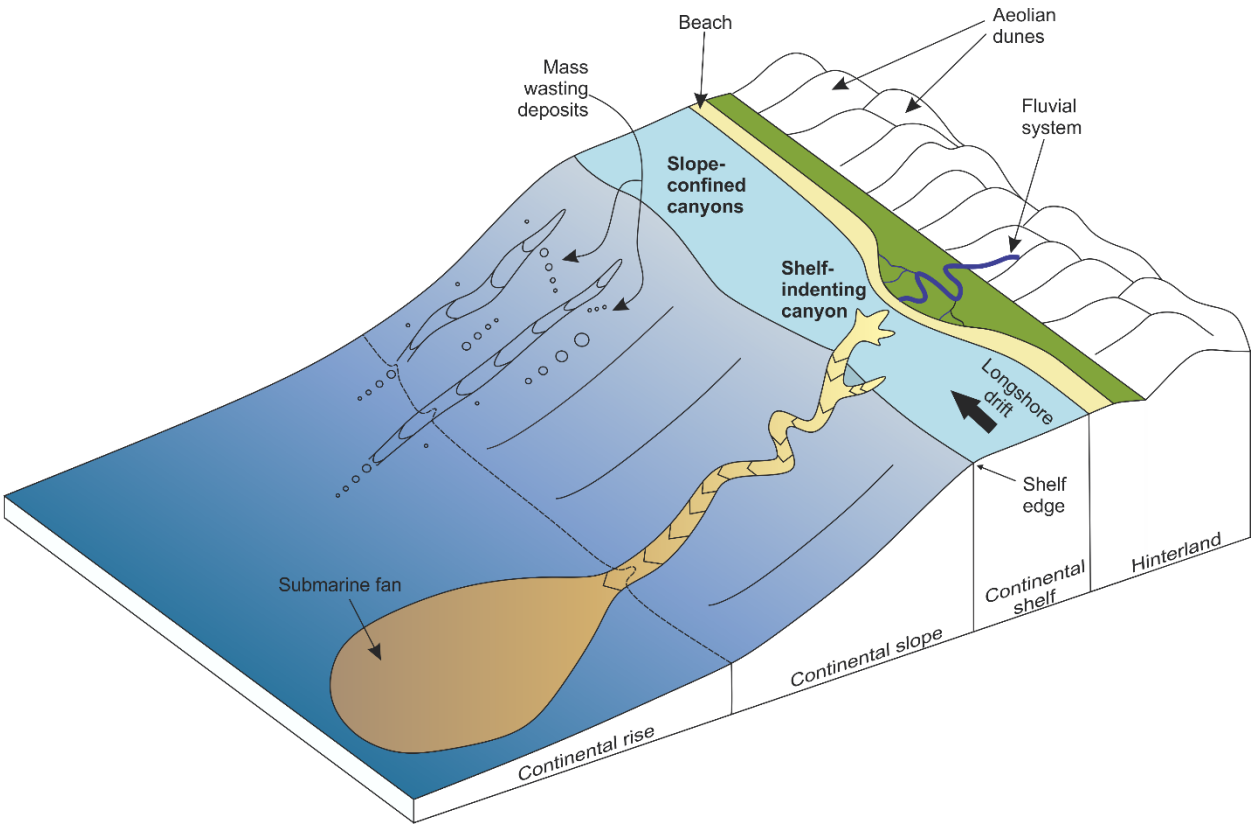

Figure 2.1.1: Characteristics of shelf-indenting and slope-confined canyons. Shelf-indenting systems are highlighted by sediment transfer from longshore drift cells, direct fluvial linkages and/or aeolian dune fields whereas slope-confined systems are characterised by increased occurrences of mass wasting deposits. Figure modified from Jobe et al. (2011).

Key processes in canyon formation

Many authors explain the evolution of modern canyon systems through two main components, downslope or upslope eroding regimes (cf. Green et al., 2007). The former requires sculpting by turbidity currents akin to fluvial flows (Mitchell, 2004), the latter revolving around retrogressive failures of the head and flanks of a canyon (Pratson et al., 1994).

With regards downslope eroding paradigms, the turbidity currents required to erode the continental slope are considered "accelerated turbidity currents" (Piper & Normark, 2009). Piper & Normark (2009) propose three fashions in which turbidity currents can be ignited (to initiate erosion). These include:

1. Downslope transformation of failed sediments (e.g. slides, slumps and/or debris flow materials) by fluid entrainment or grain plucking.
2. Continuous or sporadic discharge of fluvial or glacial meltwater to create a dense hyperpycnal plume.
3. Suspension of coastal, shelf or upper-slope sediment and entrainment downslope by gravity.

Initiation by sediment failure is often associated with tectonic activity where earthquakes are required to trigger the turbidity current and subsequent sedimentation. This is termed a "lock exchange turbidity current", where sediment is released into a slump, and progressively evolves to a debris flow and finally a turbidity current (Piper & Normark, 2009). From passive margins, oversteepening of the continental slope and pore water sapping may introduce sufficient instability to the slope, thus resulting in the initiation of slope failures which may similarly transform (Hampton, 1972; Pratson & Coakley, 1996; Mohrig & Marr, 2003).

Hyperpycnal flows occur when dense, sediment-laden river water enters the ocean. When sediment concentrations are greater than 1 $kg.m^{-3}$ (Parsons et al., 2001), a negatively buoyant plume is set up causing undercurrents that spill sediment across the shelf (Talling, 2014). The flow tries to overcome the density contrast which generates the turbulence and initiates the turbidity current.

Storm-initiated turbidity currents are produced during the process of offshore advection of sediment, especially fluid muds from the nepheloid layer (Piper & Normark, 2009). This occurs through the phenomenon of down-welling by conduit erosion. Associated with a down-welling flow is enough suspended sediment to generate a turbidity current and become auto-suspending (Palanques et al., 2006).

In conjunction with a predominant downslope turbidity current, it is believed that simultaneous retrogressive mass wasting processes on the slope may also influence canyon formation (Pratson et al., 1994; Pratson & Coakley, 1996). This is triggered either by slope oversteepening (Pratson & Coakley, 1996), earthquake activity (Mosher et al., 2010) or gas liberation within shallow sediments (Judd & Hovland, 2007).

2.2. FLUID FLOW FEATURES

Fluid (gas) flow features have a dynamic influence over numerous geological, ecological and chemical systems (Judd & Hovland, 2007). Typically, many of these features can be used to track gas reservoirs as they indicate the flow pathway from source to seafloor (Løseth et al., 2009). Owing to this fluid activity, these features also include areas of sediment mobilisation and subsequent failure (Van Rensbergen et al., 2003).

Pockmarks

Pockmarks are crater-like, concave-up features that are produced from the escape of free gas into the water column (King & MacLean, 1970; Hovland & Judd, 1988; Løseth et al., 2009; Ostanin et al., 2013; Panieri et al., 2017). Hovland & Judd (1988) propose that pockmarks form from the vertical migration of thermogenic gas, hosted within a hydrocarbon reservoir at depth, through sub-surface sediments. This leaves depressions on the seafloor known as "pockmarks" (Fig. 2.2.1). This process may either be continuous by fluid escape through slow seepage (Cartwright et al., 2007) or episodic in response to rapid hydrothermal venting (Davies et al., 2002). Sustained thermogenic methane leakage is oxidized by bacteria when vented at pockmark sites (Cathles et al., 2010) promoting the formation of vent communities resulting in cementation by in situ carbonate to produce hardgrounds (Gay et al., 2006). In cases where pockmarks cease venting, they are subsequently covered by sediments (Long, 1992), and are then referred to as "buried pockmarks" (Hovland & Judd, 1988). Buried pockmarks are significant as they represent the time at which gas expulsion was active and record the end of gas expulsion prior to burial (Judd & Hovland, 2007).

The global distribution of pockmarks is vast, examples include the North Sea (e.g. Judd & Hovland, 2007; Hustoft et al., 2010; Mazzini et al., 2016), with several accounts from offshore Namibia (Moss & Cartwright, 2010), Angola (Gay et al., 2007; Maia et al., 2016), Nigeria (Løseth et al., 2011), India (Dandapath et al., 2010), China (Chen et al., 2015), New Zealand (Netzeband et al. 2010), USA (Brothers et al., 2014) and Canada (Zühlsdorff & Spiess, 2004).

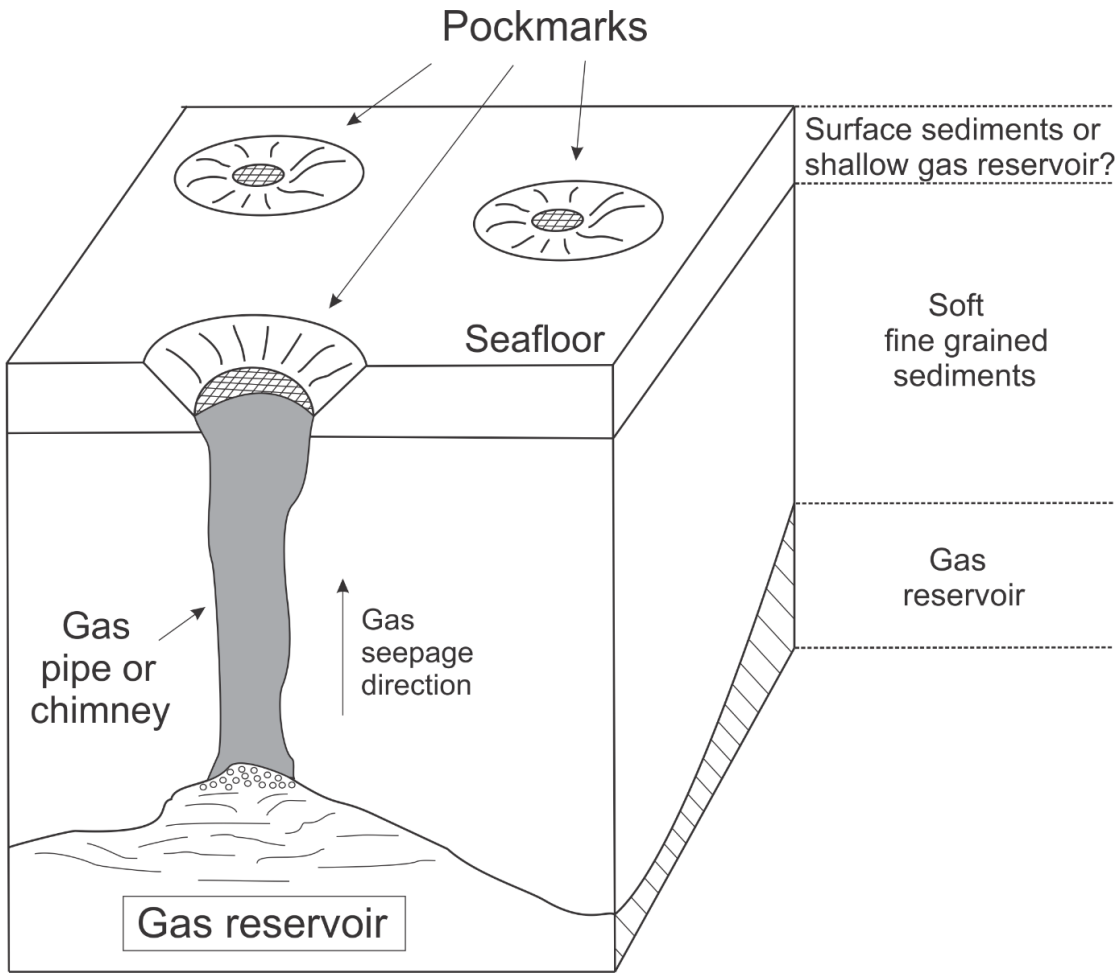

Figure 2.2.1: Idealised model of pockmark formation, showing the vertical gas seepage direction from a gas reservoir, through fine grained soft sediments which terminates at the seafloor – modified from Cathles et al. (2010).

Classification of pockmarks according to morphology

Pockmarks encompass a variety of morphologies, including: circular, elongate, crescentic, elliptical, composite or string-like (Judd & Hovland, 2007; Dandapath et al., 2010; Chen et al., 2015). These morphologies are suggested to have evolved from a single circular morphology due to the influence of the prevailing bottom current activity (Sun et al., 2011).

There are six recognised morphological classes:

1. Circular
2. Elliptical
3. Crescentic
4. Elongate
5. Composite
6. String-like

The circular morphology (Fig. 2.2.2a) conventionally measures between 10 – 750 m in diameter and 1 – 45 m in relief (Hovland et al., 2002). Ideally, their cross section is symmetrical with the same slope around the crater, and the greatest relief in the centre of the depression (Chen et al., 2015). They can also occur as asymmetrical depressions (Sun et al., 2011). The mechanism responsible for creating a circular pockmark requires point source gas ascent (Hovland et al., 2002).

Elliptical pockmarks (Fig. 2.2.2b) are generally located in deep water settings, governed by faults, bottom currents and slumping (Dandapath et al., 2010), which may all occur simultaneously. These pockmarks are common throughout all the ocean basins globally.

Crescentic pockmarks (Fig. 2.2.2c) are rare occurrences and are thus poorly understood. They are believed to be associated with bottom current activity (Verdicchio & Trincardi, 2006), ideally situated above inclined curved faults which likely control the gas migration and fluid transport responsible for its shape (Chen et al., 2015). Duarte et al. (2010) suggests an alternative genetic mechanism in the form of turbidity current-induced alteration.

Elongate pockmarks (Fig. 2.2.2d) are defined by a long and short axis in plan view. It is suggested that multiple, individual, circular pockmarks, within a close proximity to one another (Pilcher & Argent, 2007), coalesce to form a single elongate pockmark through bottom current activity, with the long axis parallel to current the direction (Chen et al., 2015; Dandapath et al., 2010). Josenhans et al. (1978) examined these features in tidal settings and considered that their long axes form parallel to the dominant tidal flow direction.

Composite pockmarks (Fig. 2.2.2e) are a product of numerous single pockmarks which are in the process of merging with one another thus creating unusual, complex, crater morphologies (Judd & Hovland, 2007). A pockmark string comprises multiple pockmarks (Fig. 2.2.2f) of various morphologies, over a kilometer scale, that are arranged in a linear or chain-like fashion (Hasiotis et al., 2002). This can form in response to (re)activation of major faults and the resultant gas migration along the fault plane (Andresen, 2012). In some cases, the multiple pockmarks may amalgamate to develop a single extensive pockmark (Judd & Hovland, 2007).

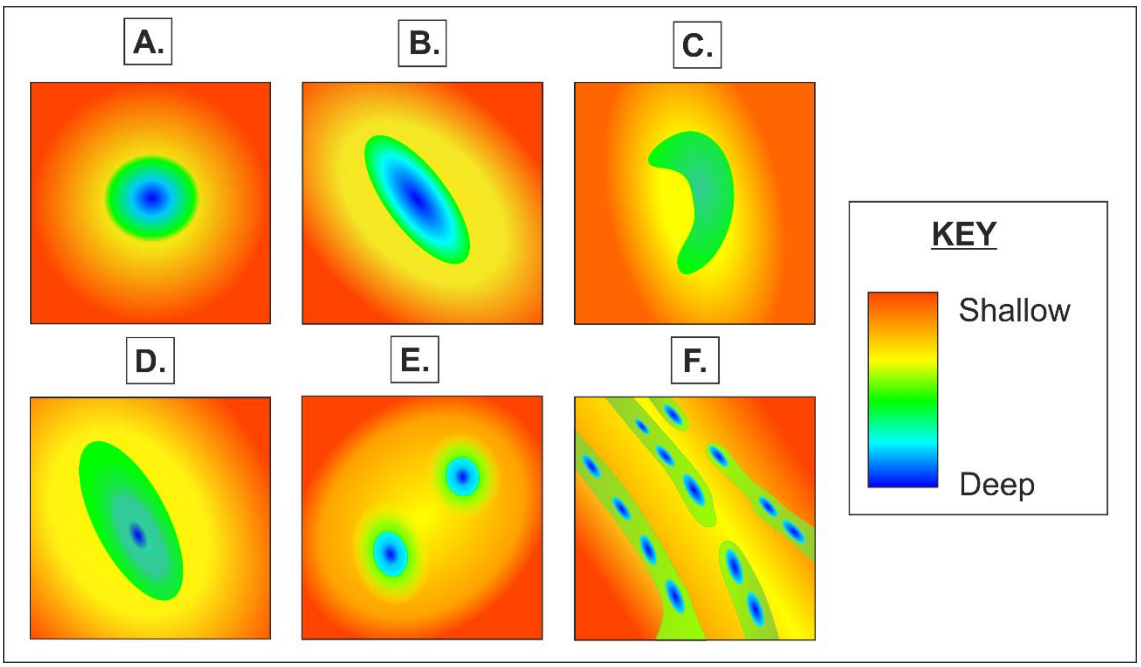

Figure 2.2.2: Morphological classes of pockmarks illustrating a plan/bathymetric view (A – F). **A.** Circular pockmark. **B.** Elliptical pockmark. **C.** Crescentic pockmark. **D.** Elongate pockmark. **E.** Composite pockmarks that are in the process of merging. **F.** Strings of pockmarks forming a chain. Figure modified from Chen et al. (2015).

Classification of pockmarks according to size

Size classification schemes are based on the surficial extent of the pockmark, independent of morphology. These are summarised in Table 2.2.1 (after Chen et al., 2015). Larger pockmarks indicate larger expulsions of gas via vertical gas migration processes (Pilcher & Argent, 2007). Strong bottom current activity also plays a critical role in controlling the size of pockmarks as currents enlarge pockmarks over time in accordance with minimizing sediment infill by

winnowing (Hammer et al., 2009; Sun et al., 2011). Where a lack of active seepage is evident from seismic data, bottom currents are suggested to have maintained and enlarged pockmarks over time (Paull et al., 2002).

Table 2.2.1: Classification of pockmarks according to size proposed by Chen et al. (2015).

Size	**Meters**	**Tens of meters**	**Hundreds of meters**	**Kilometres**
Type of pockmark	Small pockmarks	Normal pockmarks	Giant pockmarks	Mega-pockmarks
Reference	King & Maclean, 1970	Orange et al., 2002	Hasiotis et al., 2002 Ostanin et al., 2013 Marcon et al., 2014	Sun et al., 2011 Duarte et al., 2010

Seismic characteristics of fluid flow features

The seismic evidence for vertical gas migration is evidenced by features known as gas chimneys or pipes (Løseth et al., 2009). The terminological discrimination between the two is unclear with many authors using the terms inter-changeably (e.g. Cathles et al., 2010; Cartwright & Santamarina, 2015; Chen et al., 2015). Andresen (2012) differentiates the terms based on their seismic character. A chimney consists of distorted amplitude anomalies (Fig. 2.2.3a), whereas pipes take on vertically stacked high or low amplitude anomalies (Fig. 2.2.3b). The reflectors that comprise a pipe may be stacked either convex up- or down (Plaza-Faverola et al., 2010). Both chimneys and pipes are related to vertically focused fluid flow that originates atop shallow gas pockets (Cathles et al., 2010). Chimneys and pipes facilitate gas transport through low permeability sequences that terminate at the seafloor as pockmarks (Fig. 2.2.3c) (Moss & Catwright, 2010; Andresen et al., 2011; Løseth et al., 2011).

Polygonal fault systems act as conduits for fluid migration (Maia et al., 2016) and therefore have a direct influence on pipe and pockmark formation (Berndt et al., 2003; Gay et al., 2006, 2007). Pipe and chimney features emanate from these faulting systems (Chen et al., 2015; Maia et al.,

2016) (Fig. 2.2.3c) which are considered to have formed during early sediment compaction (Judd & Hovland, 2007). These grow progressively post-burial (Cartwright, 1996).

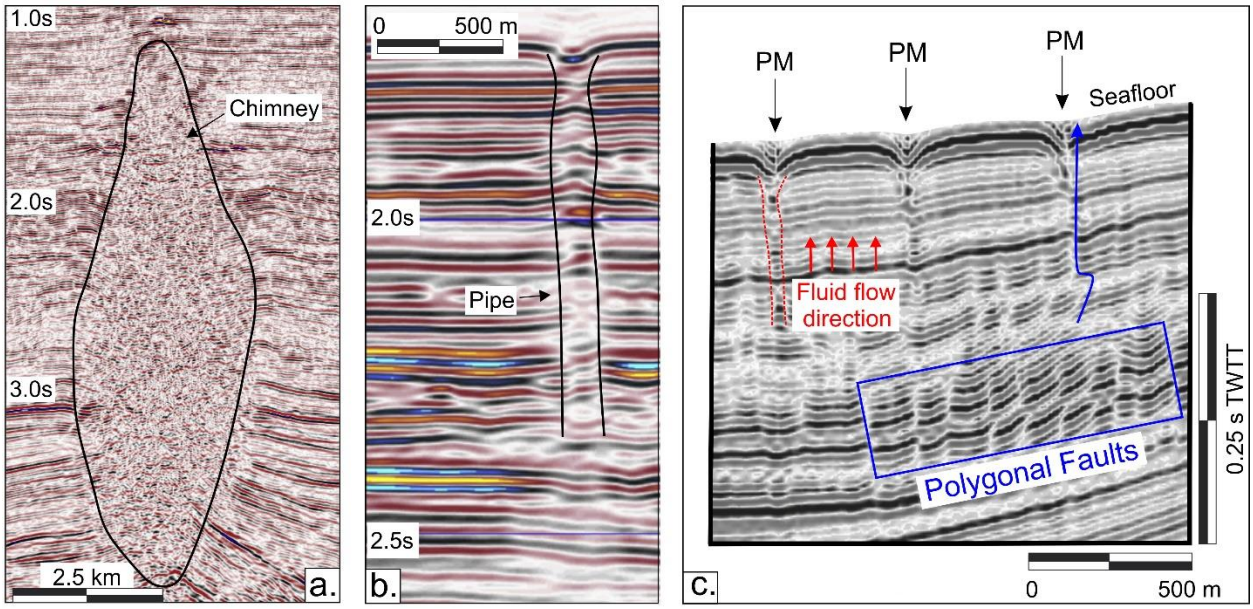

Figure 2.2.3: Features of vertically focused fluid flow (A – C). **A.** Gas chimney with chaotic reflectors that truncates the lateral stratigraphy (modified from Løseth et al., 2009). **B.** Gas pipe which consists of stacked reflectors (modified from Løseth et al., 2011). **C.** Gas pipes depicting vertical fluid flow direction (indicated by the red arrows) which terminate at the seafloor as a pockmark. There is also a system of polygonal faults suggesting a seepage route for fluid migration (indicated by the blue arrow) (modified from Maia et al., 2016).

CHAPTER 3

REGIONAL SETTING

3.1. LOCALITY

The study area is located ~60 km offshore the southwestern coast of South Africa within the Atlantic Ocean, spanning an area of 46 000 km^2 (Fig. 1.1). The bathymetric dataset lies just below the shelf break (~450 m), from depths 315 to 3925 m. There are two prominent wide points of the shelf, one off the Olifants River and the second west of Cape Agulhas (Dingle et al., 1983). The shelf is narrowest west of both the Cape Town and Saldanha Bay (Birch, 1977). The slope has a low gradient and reaches 1.267° off Hondeklip Bay and 2.917° west of the Cape Town (Birch, 1977). The slope and rise stretch out ~200 km into the Orange Basin and a further 400 km offshore into the Cape Basin (Dingle et al., 1983; Dingle & Robson, 1992).

3.2. TECTONIC AND GEOLOGICAL FRAMEWORK

The western coast of South Africa is forms a passive continental margin, produced by the Early Cretaceous break up of Gondwana (Fouché et al., 1992; Macdonald et al., 2003; Watkeys, 2006). This margin lies between two major orthogonal crustal lineaments, the Walvis Ridge abutment in the north and the Agulhas Fracture Zone in the south (Dingle, 1992). This facilitated the separation of South America and Africa to form the 160 000 km^2 Orange Basin along the west coast of South Africa and southern Namibia (Dingle, 1992; Gladczenko et al., 1998; Kuhlmann et al., 2010) (Fig. 3.2.1). The Orange Basin has an overall thickness of 8 km and hosts significant oil and gas interest (Brown et al., 1995).

The synrift phase (Oxfordian – Valanginian) of the Orange Basin is characterised by the presence of N-S trending grabens and half-grabens that consist of predominantly volcanic successions with sporadic siliciclastic and lacustrine deposits (Kuhlmann et al., 2010) (Fig. 3.2.2). The volcanic strata are marked by seaward dipping reflectors (SDR) (Fig. 3.2.1) which define the initial continental break-up and lithospheric stretching (Light et al., 1993; Scarselli et al., 2016).

The transitional phase of the basin is marked by the Barremian break-up unconformity (117 Ma) (Fig. 3.2.2) that truncates the previously mentioned key seaward dipping reflectors (Falvey, 1974). The transitional sequence (Barremian – Aptian) comprises continental flood basalt deposits overlain by fluvial and sandy marine deposits (Dingle et al., 1983; Broad et al., 2006).

The Aptian unconformity (112 Ma) marks the onset of the drift phase of sedimentation within the basin (Brown et al., 1995). This surface is key for identifying Aptian source rocks for oil and gas (Kuhlmann et al., 2010). This is supported by the favourable tectonic and climatic shale-forming conditions of the time (Kuhlmann et al., 2010).

Notably, distally deposited Turonian strata comprise a succession of basinal shales which are interpreted to be an important source rock for oil and gas (Aldrich et al., 2003). The Turonian – Coniacian boundary is defined by a heavily-incised surface, interpreted as a series of palaeo-canyons which can be traced throughout the basin (Fig. 3.2.2) (Broad et al., 2006). This corresponds to both local relative, and global sea-level lowstands (Siesser & Dingle, 1981; Haq et al., 1987).

Campanian and Maastrichtian-age strata are truncated in many parts of the basin. This is interpreted to have occurred in response to a margin-uplift event at ~80 Ma (Hirsch et al., 2010), evidenced by a Maastrichtian – Danian unconformity (Scarselli et al., 2016).

The overlying Cenozoic strata are defined by marine sediments that comprise siltstones and sandstones, overlain by shelly limestones (Gerrard & Smith, 1982). There is a notable Mid-Miocene erosional unconformity in the basin, which can be traced throughout southern Africa. This was caused by a Miocene-aged pulse of uplift of the hinterland (Partridge & Maud, 1987; Hicks & Green, 2017).

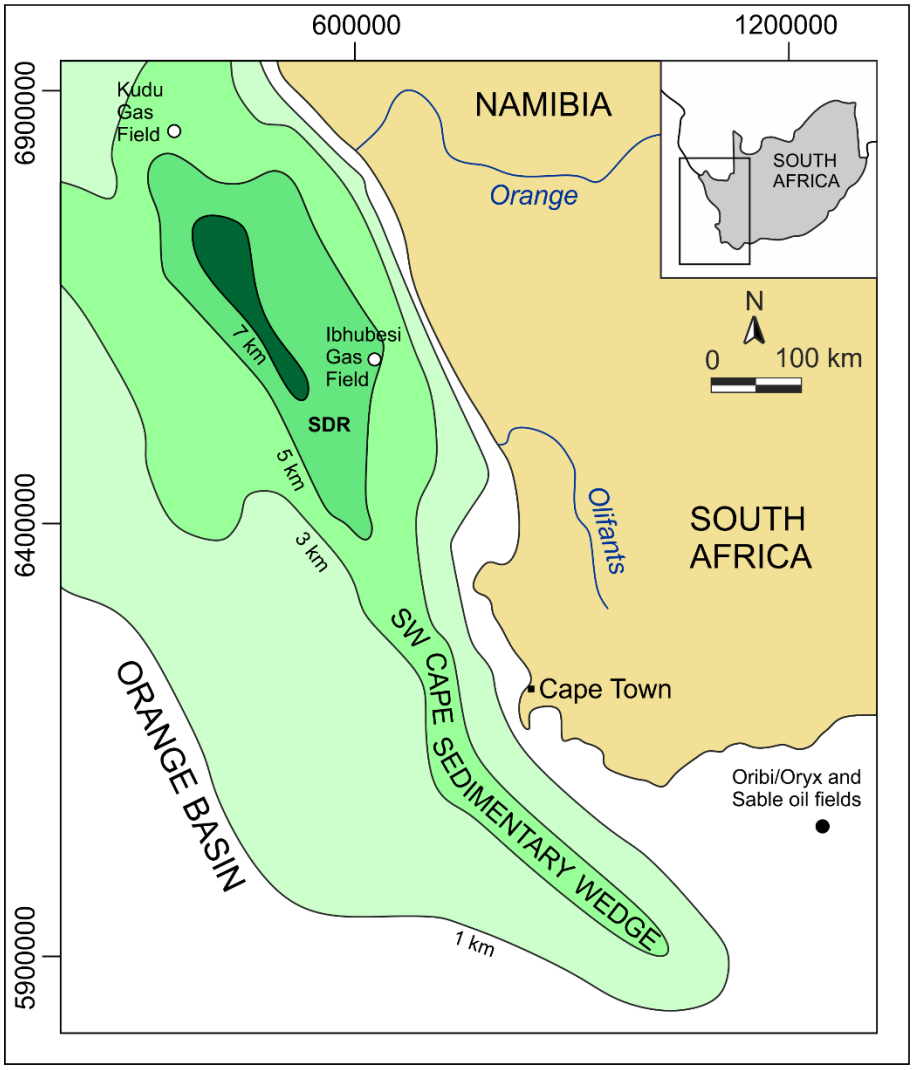

Figure 3.2.1: The extent of the Orange Basin, with the isopach distribution of post-rift strata as well as major gas and oil fields. SDR = seaward dipping reflectors. Modified from Broad et al. (2006).

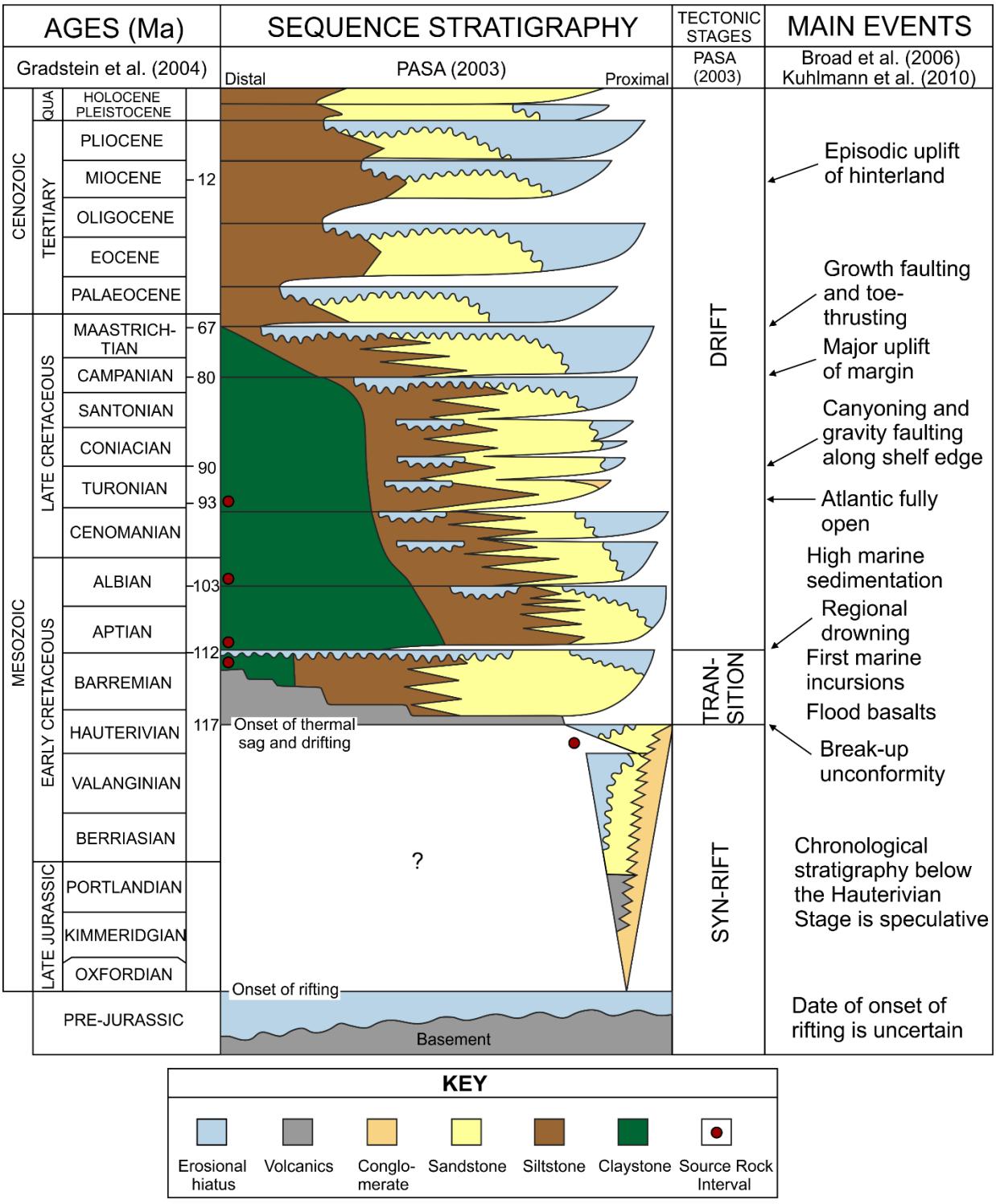

Figure 3.2.2: Wheeler diagram and major margin sculpting episodes for the Orange Basin, including oil and gas source rock intervals. Modified from Broad et al. (2006) and Kuhlmann et al. (2010).

3.3. OCEANIC CURRENTS ALONG THE CAPE MARGIN

There are four main oceanic current systems that circulate along the Cape margin at different depths. These are the Antarctic Bottom Water (AABW), North Atlantic Deep Water (NADW), Antarctic Intermediate Water (AAIW) and Benguela Coastal Currents (BCC) (Fig. 3.3.1) (Weigelt & Uenzelmann-Neben, 2004).

The AABW system is the deepest bottom current (>4000 m) of the margin (Weigelt & Uenzelmann-Neben, 2004). It is believed to have developed in the Late Miocene in response to the growth of the Mid-Miocene Antarctic ice sheet (Zachos et al., 2001). The AABW is suspected to undercut the lower slope and thus set off instabilities further upslope (Dingle & Robson, 1992). The NADW system is considered to have originated at 10 Ma (Berger & Wefer, 2002) and is defined by a net southeasterly flow between 1500 and 4000 m depth (Fig. 3.3.1) (Weigelt & Uenzelmann-Neben, 2004). The AAIW overlies the NADW and occupies water depths between 500 and 1500 m, forming a northwesterly flow (Weigelt & Uenzelmann-Neben, 2004). These two countercurrents (NADW and AAIW) are capable of triggering extensive mass wasting events at their contact at 1500 m (Weigelt & Uenzelmann-Neben, 2004). The BCC is a shallow surface current which flows northwesterly between the water surface and 500 m depth (Shannon, 1985). It has matured throughout the Neogene (Diester-Haass et al., 2001) and does not have the potential to erode the shelf or upper slope (Weigelt & Uenzelmann-Neben, 2004). The BCC is associated with prominent coastal upwelling waters that are cold and rich in nutrients such as phosphates, nitrates and silicates (Currie, 1953). As a consequence, there is an accumulation of organic-rich sediments in the shelf regions (Wefer et al., 1998).

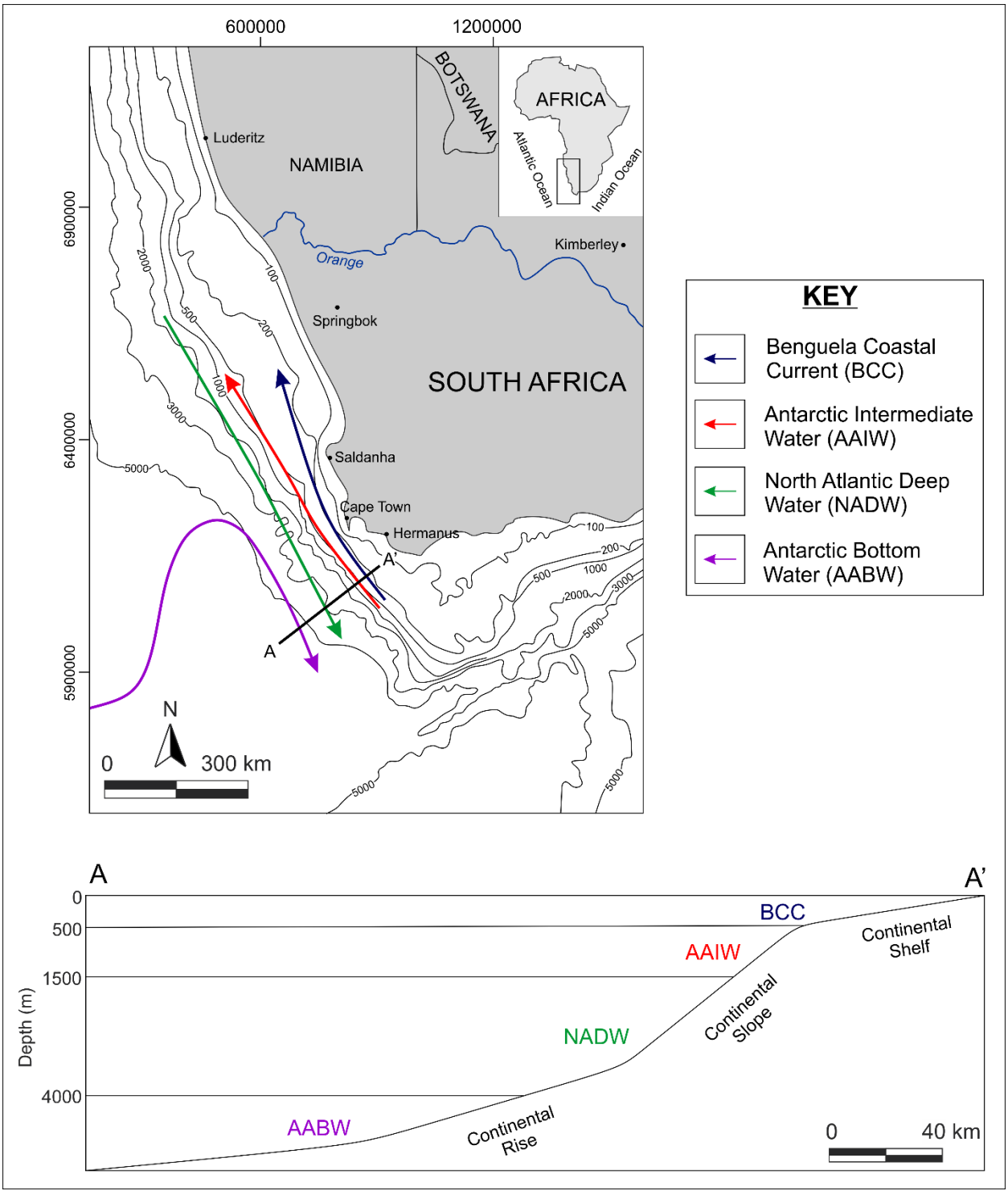

Figure 3.3.1: The oceanic currents off the west coast of southern Africa, note the paths of the AABW, NADW, AAIW and BCC. An idealised cross-section (A – A') (below) showing the depths at which these currents interact. Modified from Lutjeharms & Stockton (1987).

CHAPTER 4

METHODOLOGY

4.1. DATA COLLECTION AND PROCESSING

4.1.1. Multibeam bathymetry

The multibeam bathymetric data were collected by Anadarko Petroleum Corporation in 2013 to examine the fluid seep features that were alluded to by seismic data from the area. A Kongsberg EM 710 multibeam sensor with an operating frequency of 100 kHz was used to collect the soundings. Routine sound velocity profiles were collected in order to reduce the sounding data to depths relative to mean sea-level (MSL). The data were processed using CARIS and resolved to approximately 1 m in the Z-domain. These were then exported as several files in XYZ format which were imported into ArcGIS 10.3 and merged to create a uniform 25 × 25 m grid in ASCII format. The merged data were then used to create a single raster file using the "ASCII to Raster" conversion tool in ArcGIS 10.3 with a final 25 m grid output with a World Geodetic System (WGS) 1984 datum, and Universal Tranverse Mercator (UTM) Zone 33 S projection.

4.1.2. Seismic and well log data

Thirteen seismic lines are presented in this study which comprise legacy data stored by the Petroleum Agency of South Africa (PASA) (Fig. 4.1.1). The data were all pre-stacked and migrated, and provided in segy format with their respective navigation files. Each file was interpreted in IHS Kingdom Suite 2017, whereby bounding surfaces and faults were picked. The well-data (well C-B1) for the area were also examined for sound velocity corrections, allowing the conversion from two-way travel time to depth in metres. Lithological logs were further compiled, and biostratigraphic correlations based on palaeontological assemblages were made following other authors (e.g. McMillan, 2003).

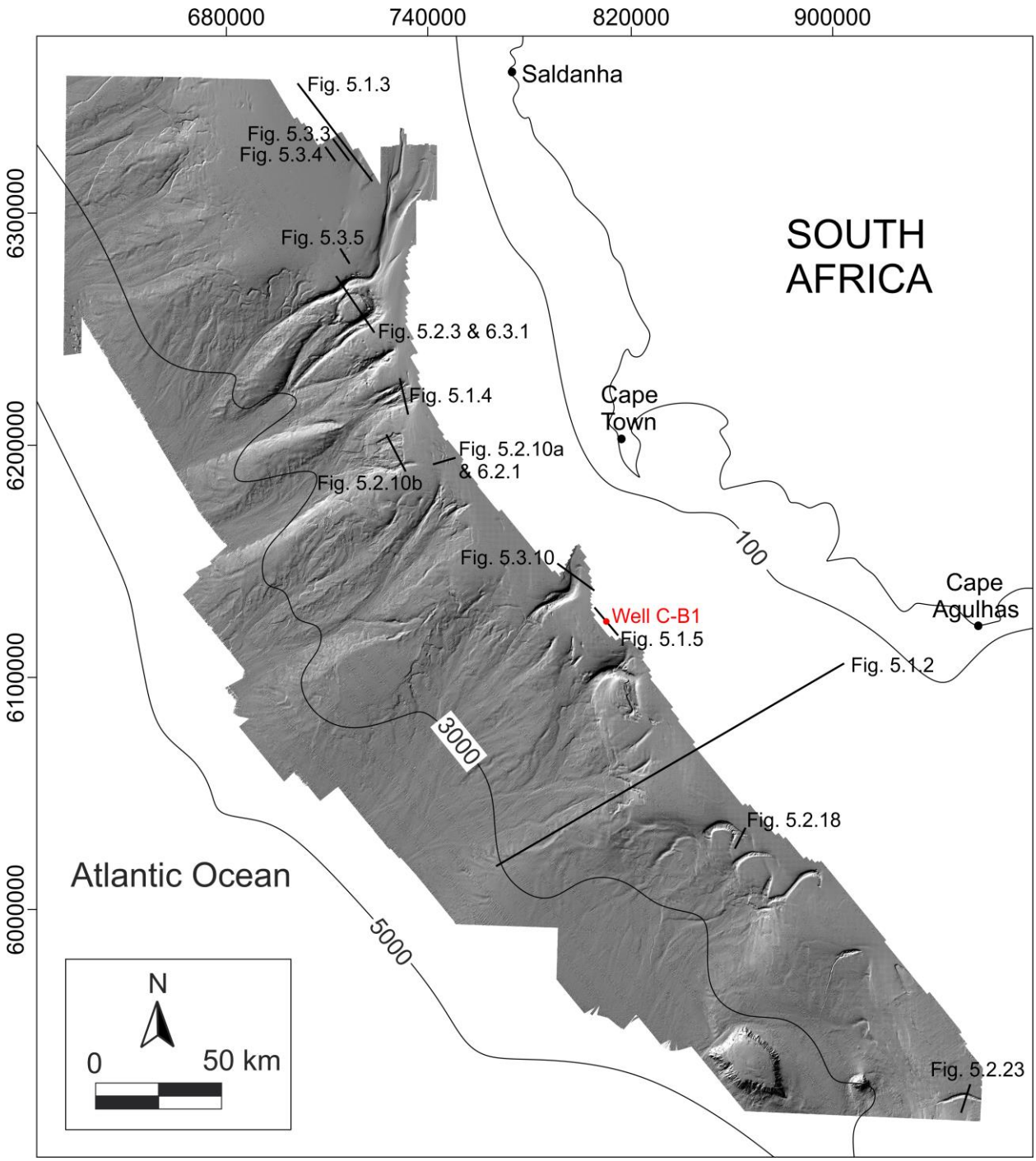

Figure 4.1.1: Hillshaded bathymetric image showing the location of seismic lines (labelled by their respective figure numbers) and well C-B1 used in this study.

4.2. POCKMARK EXTRACTION PROCESS

The numerical analysis of the spatial distribution of pockmark features were performed according to the extraction method proposed by Andrews et al. (2010) (Fig. 4.2.1). This uses a series of hydrologic algorithm techniques available in ArcGIS 10.3. The sink tool was used to input the gridded bathymetry, which revealed the spatial distribution of pockmarks. This identified pockmarks as single point features (i.e. sinks), with each sink defined as a cell or succession of adjoining cells that has an abnormally lower value than that of the neighbouring cells. Each sink thus defines the pockmark bottom (Z_2). The flow direction tool was then used to establish the critical point at which a change in curvature and gradient occurs. This defines the depth of the pockmark rim (Z_1). From this, the actual pockmark depth (d) was determined using the raster calculator function to solve:

$$d = Z_2 - Z_1 \qquad \text{(eq. 1)}$$

This method only works for circular pockmarks, hence the sink tool recognised multiple sinks in the other complex pockmark morphologies (e.g. elongated or crescentic). These were manually corrected to a single pockmark feature. A further manual correction was performed to delete artifacts or mass wasting features that have notably lower-elevation cells than the surrounding seafloor.

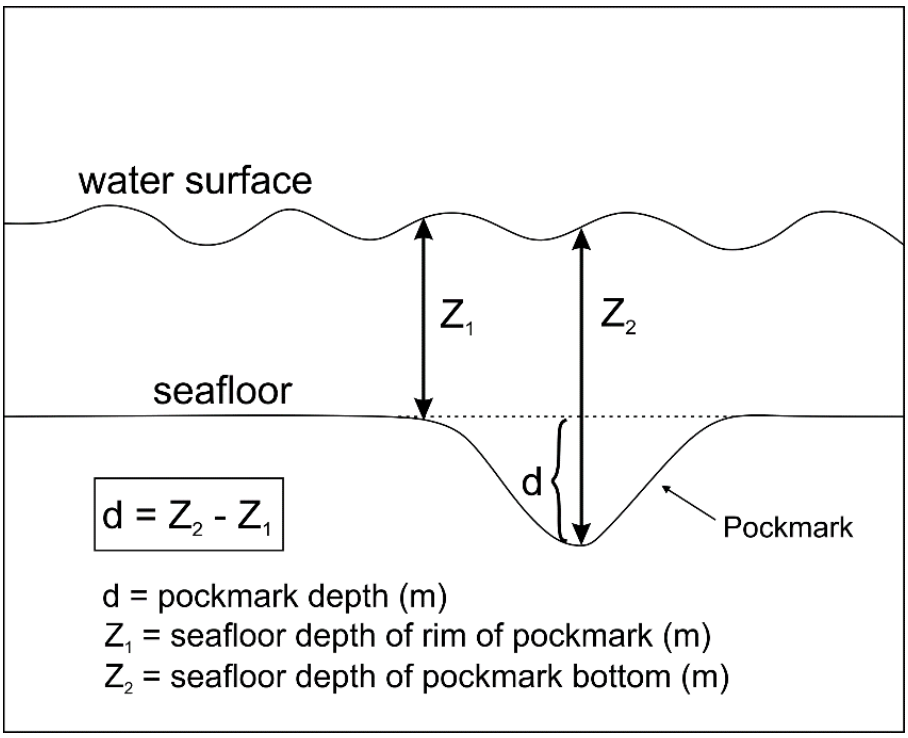

Figure 4.2.1: An illustration of the pockmark extraction process, whereby the pockmark bottom is defined by Z_2, the pockmark rim defined by Z_1 and the pockmark depth defined by *d*. Diagram modified from Andrews et al. (2010).

CHAPTER 5

RESULTS

5.1. GENERAL SEISMIC STRATIGRAPHY

The study area consists of 15 submarine canyon systems, and is subdivided into three domains (Zone A, B and C) based on distinct canyon morphologies, occurrences of pockmark fields and mass wasting features. This chapter describes the shallow (<2000 m) seismic stratigraphy that underpins the canyon and fluid flow features of the study area (Fig. 5.1.1). Eight main units are documented, Seismic Facies 1 to 8 (SF 1 – 8), each established on the basis of their seismic character and bounding surfaces (surfaces A – E) (Figure 5.1.2). These overlie the Seismic Basement Unit (SBU), defined as that layer not associated with any canyon and/or pockmark features, and which also represents the limits of the data analysis (marked by the red surface in Figure 5.1.2). Along-strike profiles are provided in Figures 5.1.3, 5.1.4 and 5.1.5, in order to examine the relationship of the present canyons to those of the surrounding stratigraphy more closely. Well data (C-B1) are examined in the context of the stratigraphy (Fig. 5.1.5). The well is located ~5000 m inshore of the bathymetry, but assumed to be an along-strike continuation of the stratigraphy of Zone C (defined in the following sections).

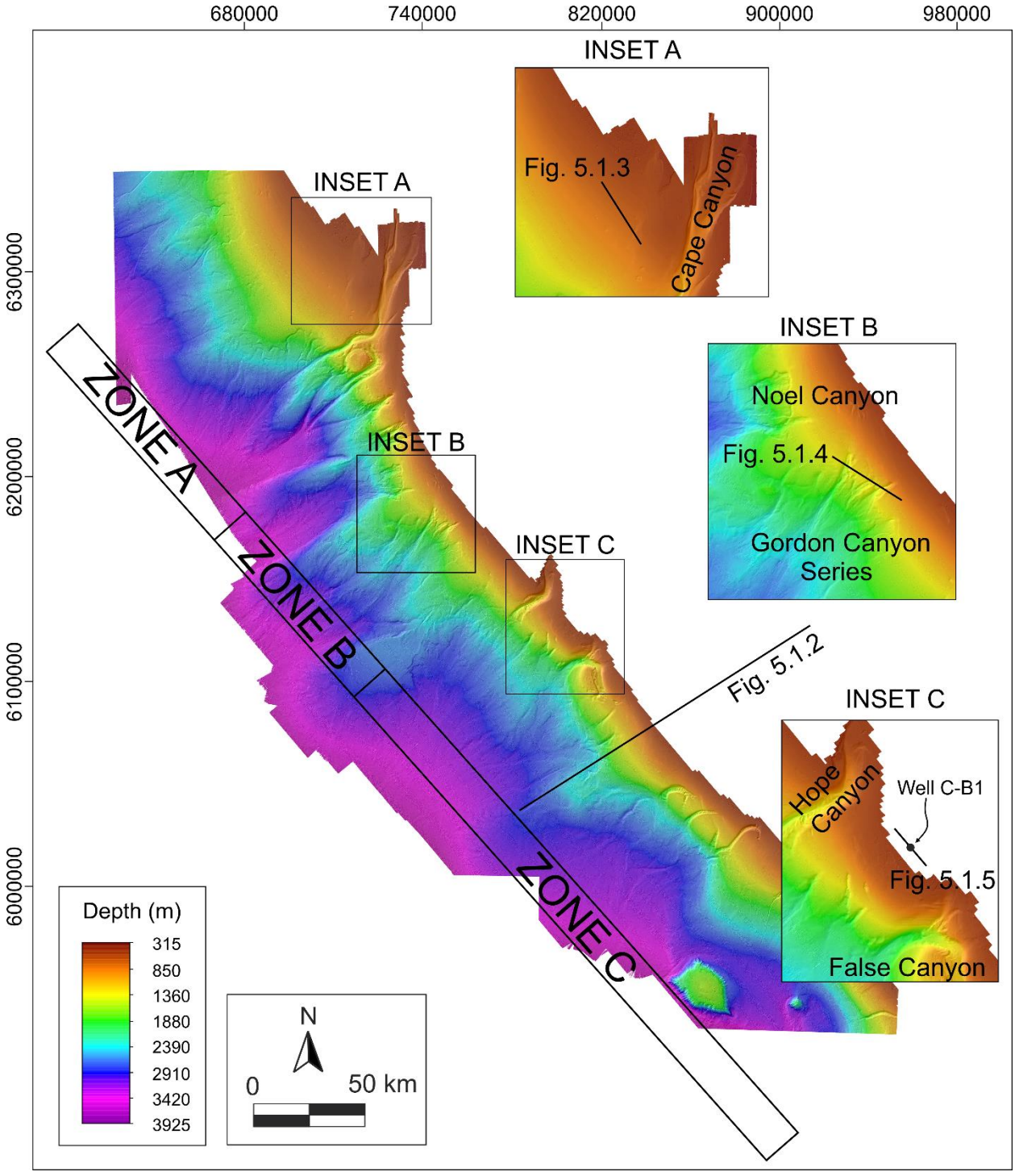

Figure 5.1.1: Bathymetric data of the study area showing seismic line locations: down-dip profile extending inshore of the bathymetry (Fig. 5.1.2) and along-strike profiles of Zone A, B and C (Figs 5.1.3-5.1.5).

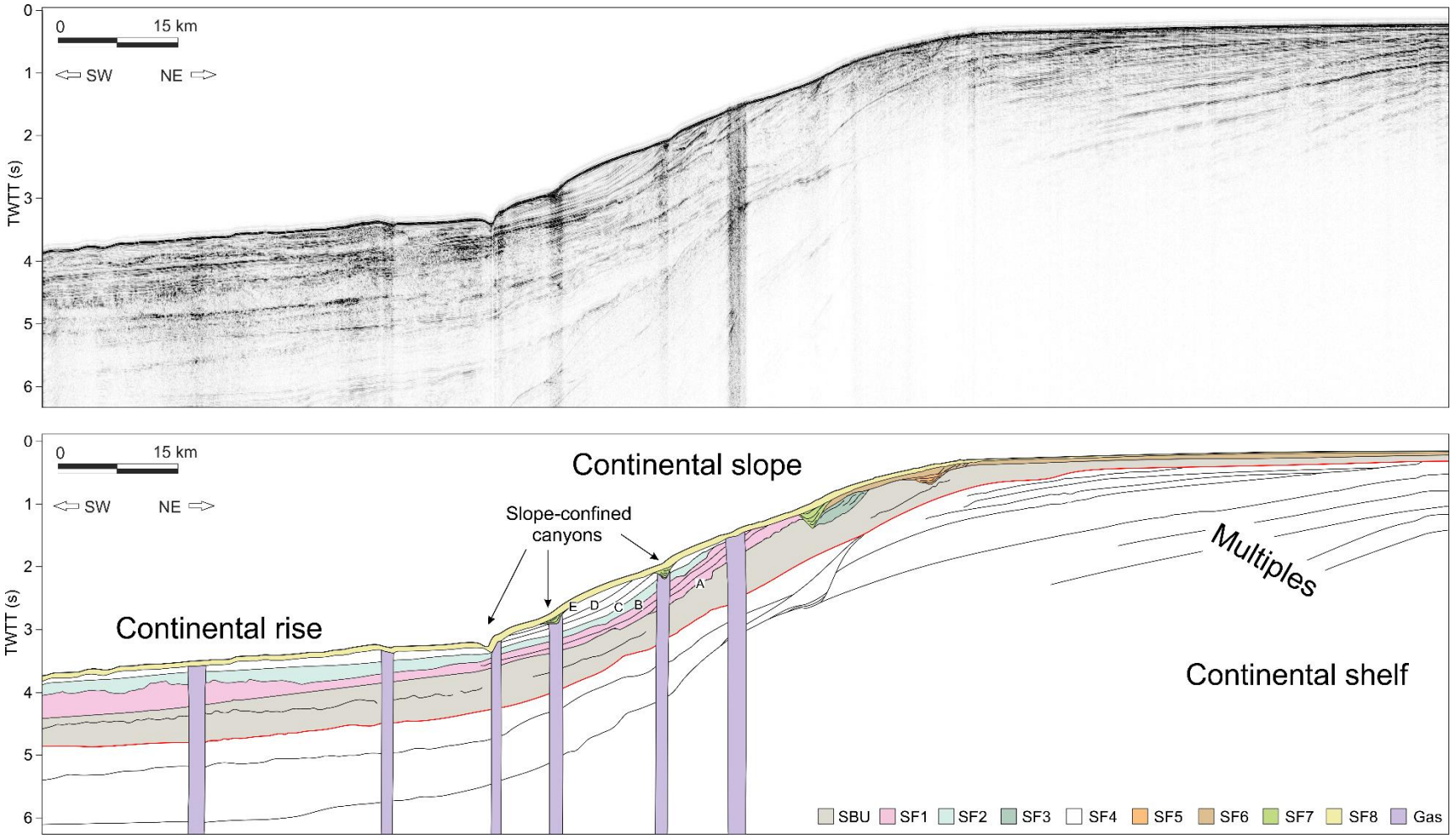

Figure 5.1.2: Down-dip seismic profile showing the seismic stratigraphy (including gas features) of the continental shelf, slope and rise. Eight facies are identified based on their reflector arrangement and bounding surface geometries.

Seismic Basement Unit (SBU)

The Seismic Basement Unit (SBU) is the lowermost unit of interest in the stratigraphy and is continuous throughout the extent of the available seismic data. Most of the body of the SBU comprises low-amplitude wavy reflectors that are weakly stratified (Fig. 5.1.2). There are, however, frequently occurring signal attenuations within the unit (Fig. 5.1.2). The SBU increases thickness in a seaward direction from 1000 m along the shelf to 7000 m along the rise (Fig. 5.1.2).

Seismic Facies 1 (SF1)

This is the basal-most unit associated with the present-day canyon systems, reaching a thickness of 240 m. The base of this sequence is defined by surface A (Fig. 5.1.3, 5.1.4 & 5.1.5), a high amplitude, laterally extensive reflector. Above this base, characterising the body of this unit, are a series of bright, high amplitude reflectors with strict horizontal parallel configurations that is only found in Zone A and C (Fig. 5.1.3 & 5.1.5). In Zone B, SF1 is strictly parallel but lacking in brightness and amplitude.

Seismic Facies 2 (SF2)

The base of SF2 is defined by a corrugated surface, marked by surface B (Fig. 5.1.3 & 5.1.5). These corrugations are between 150 to 300 m apart and up to 200 m in relief. The body of this unit comprise wavy to sub-parallel high amplitude reflectors (Fig. 5.1.2 & 5.1.4), with a maximum thickness of 480 m. Mainly, SF2 occurs as a drape facies that appears to cover older palaeo-canyon systems that have formed incisions into surface B. Notably, these canyons are situated stratigraphically below the current canyon systems and form a stacked arrangement of incisions (Fig. 5.1.4). Along its boundaries, the reflectors of SF2 onlap onto SF3 (Fig. 5.1.4).

Seismic Facies 3 (SF3)

This unit is characterised by high-amplitude oblique tangential reflectors that downlap onto SF1 and SF2 (Fig. 5.1.4). It reaches a maximum thickness of 800 m and is found adjacent to SF1 and

SF2 with a wedge-type geometry (Fig. 5.1.4). In the upper slope region, SF3 can be seen to downlap on palaeo-canyon systems that are defined by SF6 (Fig. 5.1.2).

Seismic Facies 4 (SF4)

Overlying SF3 is SF4, which is separated by surface D, therefore requiring further sub-division into SF4a and SF4b.

Seismic Facies 4a (SF4a)

Seismic Facies 4a comprises high-amplitude, laterally extensive reflectors in Zone A and C (Fig. 5.1.3 & 5.1.5) and low-amplitude in Zone B draping the palaeo-canyon systems formed in surface C (Fig. 5.1.4). The geometries of the reflectors in this unit vary as they can either be wavy to chaotic in Zone A and C (Fig. 5.1.3 & 5.1.5) or parallel to the seafloor in Zone B (Fig. 5.1.4). The thickness of this succession is also variable, reaching 25 m in Zone A and C, and increasing to 100 m thick in Zone B.

Seismic Facies 4b (SF4b)

This unit consists of sub-parallel to wavy reflectors (Fig. 5.1.3, 5.1.4 & 5.1.5) reaching a maximum thickness of 80 m. Characteristically, there are packages of brightened reflectors that are found throughout the body of this unit (Fig. 5.1.4).

Seismic Facies 5 (SF5)

Seismic Facies 5 is a sequence that is defined as a palaeo-canyon fill unit that breaches the shelf-slope break (Fig. 5.1.2). It comprises a set of convex upward reflectors and reaches a maximum thickness (equivalent of canyon relief) of 180 m.

Seismic Facies 6 (SF6)

This particular facies is only found in the upper slope and shelf regions. It has a uniform thickness of 75 m. It mainly comprises poorly defined reflectors, however a series of inclined downlapping reflectors can be observed (Fig. 5.1.2).

Seismic Facies 7 (SF7)

This unit forms another palaeo-canyon fill facies that lies just beneath the youngest stratigraphic unit (SF8). The palaeo-canyons range in widths between 500 and 800 m and have reliefs up to 200 m. In some cases, buried stacked axial incisions and adjacent terraces are evident (Fig. 5.1.4).

Seismic Facies 8 (SF8)

This is the youngest facies and comprises high amplitude reflectors which are parallel to sub-parallel to the seafloor. Seismic Facies 8 is laterally continuous across all canyon systems in the study area (Fig. 5.1.3, 5.1.4 & 5.1.5) and surrounding regions (Fig. 5.1.2). It maintains an approximate, uniform, thickness of 80 m throughout. Notably, in the linear canyon systems (see next section), SF8 is incised by canyon channels such as the G2 Canyon (Fig. 5.1.3).

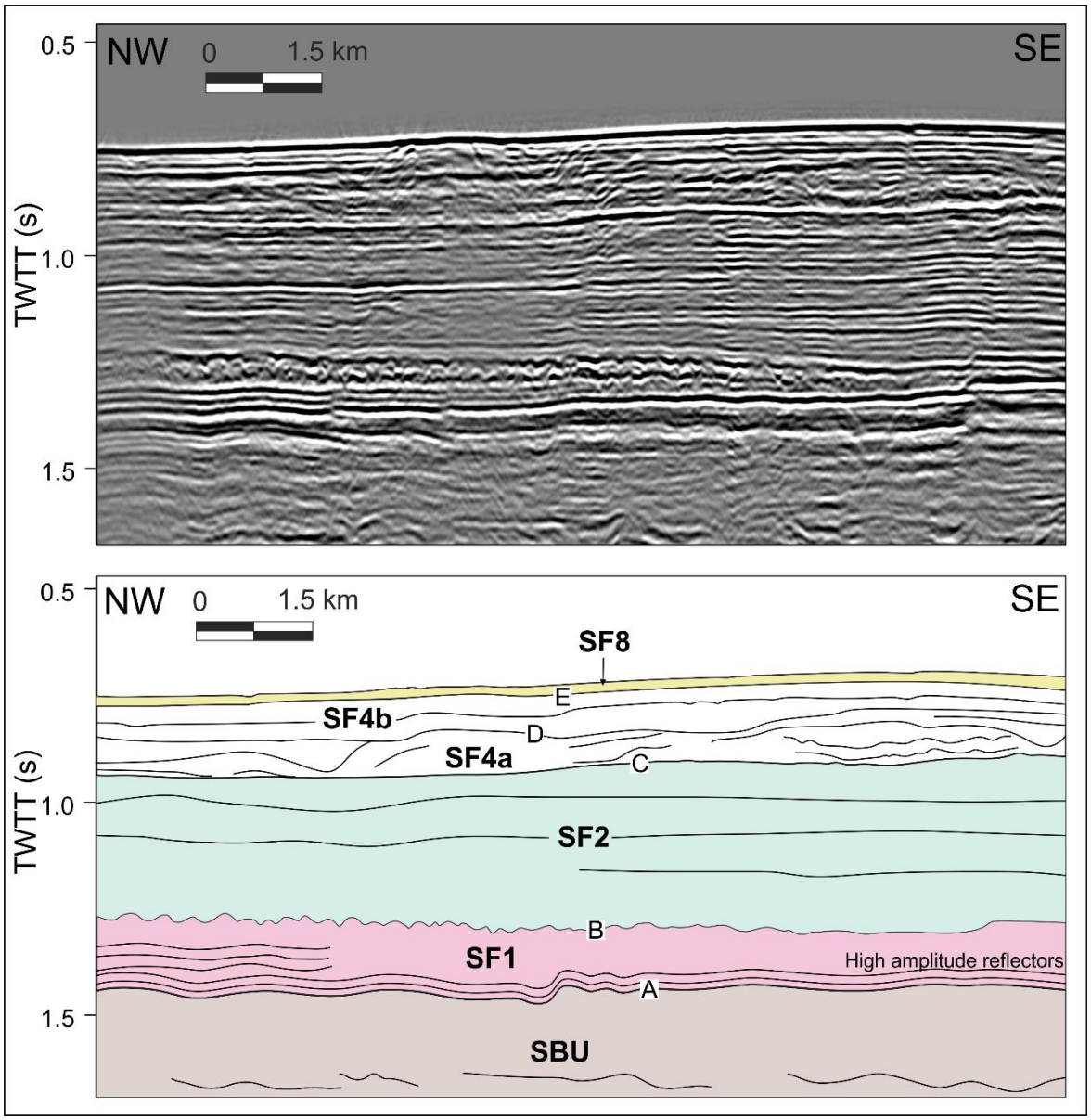

Figure 5.1.3: The lateral continuity of seismic facies in Zone A: SBU = Seismic Basement Unit; SF1 = Seismic Facies 1; SF2 = Seismic Facies 2; SF4a = Seismic Facies 4a; SF4b = Seismic Facies 4b; SF8 = Seismic Facies 8. The raw data are displayed in the above image and the image below shows the seismic facies interpretation. Major bounding surfaces are labelled A – E.

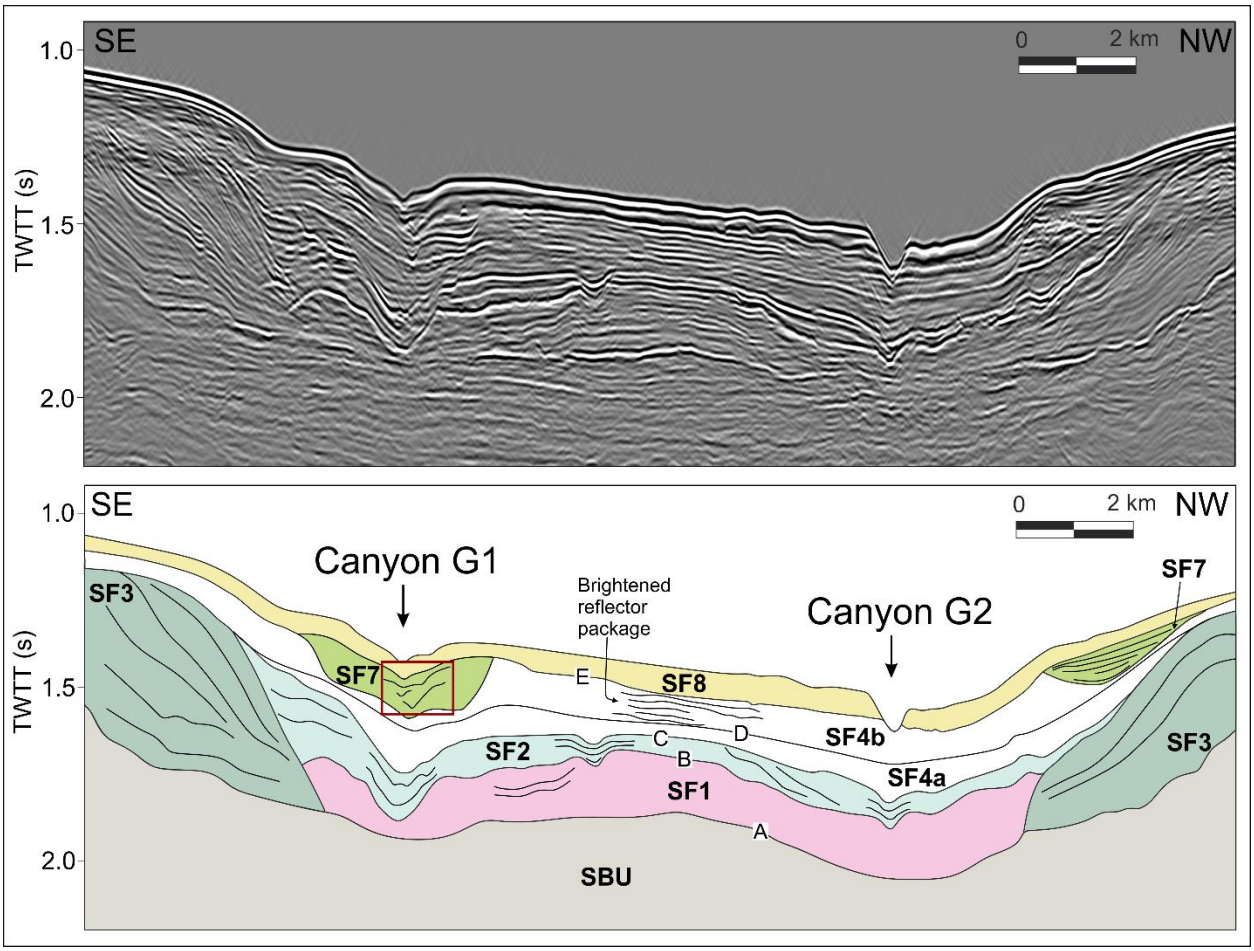

Figure 5.1.4: The lateral continuity of seismic facies in Zone B: SBU = Seismic Basement Unit; SF1 = Seismic Facies 1; SF2 = Seismic Facies 2; SF3 = Seismic Facies 3; SF4a = Seismic Facies 4a; SF4b = Seismic Facies 4b; SF7 = Seismic Facies 7; SF8 = Seismic Facies 8. The raw data is displayed in the above image. The image below shows the seismic facies interpretation. Major bounding surfaces are labelled A – E. The red box indicates the stacked axial incisions recognised below Canyon G1.

Sedimentology and chronology

The lithologies of the units are established from log data obtained for well C-B1 (Fig. 5.1.5), located ~5000 m inshore of Zone C (Fig. 5.1.1). Continuous samples from this well were acquired after depths of 600 m, at shallower depths only chip samples were collected. The palaeontological ages of the major bounding surfaces are based on these samples, together with the continuous log data and are summarised in Table 5.1.1. The ages of the upper units are postulated based on these bracketing surfaces (Table 5.1.2).

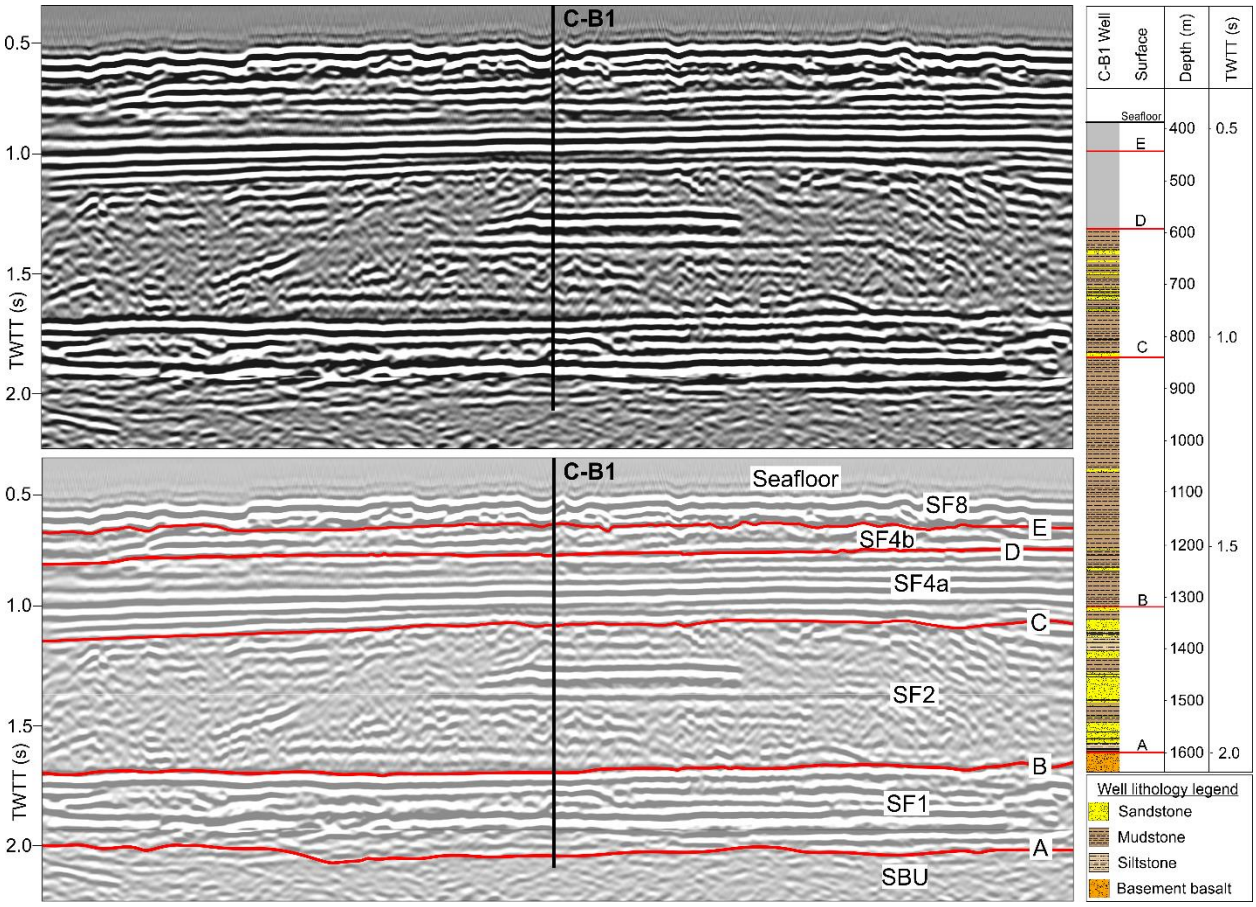

Figure 5.1.5: Seismic and well data of an along-strike tie line showing the various seismic units (Table 5.1.2) and their bounding surfaces (Table 5.1.1). Note the prominent stratigraphic obscuration in SF2.

Table 5.1.1: The dates of the major bounding surfaces.

Surface	Age
E	Mid-Miocene surface (12 Ma)
D	Palaeocene – Eocene boundary (56 Ma)
C	Maastrichtian – Danian boundary (65 Ma)
B	Turonian – Conacian boundary (89 Ma)
A	Aptian – Albian boundary (113 Ma)

Table 5.1.2: A summary of the seismic units, their respective lithologies and proposed ages.

Unit	Lithology	Surface (base)	Age
SF8	Hemipelagic drape	E	Holocene
SF7	Muddy/sandy canyon fill?	?	Late Oligocene
SF6	?	?	Oligocene?
SF5	?	?	Oligocene?
SF4b	Mudstone with sand lenses	D	Oligocene?
SF4a	Sandstone with mud fills	C	Coniacian - Maastrichtian?
SF3	?	?	Coniacian - Maastrichtian?
SF2	Mudstone with sand lenses	B	Coniacian - Maastrichtian?
SF1	Sandstone with intercalated mudstone and siltstone	A	Turonian
SBU	Basalt	*N/A*	Late Aptian

Based on the available well and seismic data, surface A marks the base of SF1 which comprises a sandstone that is intercalated with muddy and silty components, between Albian and Turonian in age. Surface B represents the Turonian – Conacian boundary, separating SF1 from SF2. This marks the start of thicker mudstone packages intercalated with sporadic sandy lenses. Surface C (Maastrichtian – Danian) separates SF2 from SF4a and surface D (Palaeocene – Eocene) separates

SF4a from SF4b. Lithologically, SF4a comprises sandstones with mud lenses and SF4b is composed of mudstones with intercalated sand lenses. Surface E denotes a Mid-Miocene erosional boundary, overlying this is SF8 which is identified as a muddy Holocene drape from a single chip sample. This may however span several older ages, but the lack of data precludes a more precise age.

Gas Features

The gas characteristics within the seismic data typically take the form of laterally brightened zones, gas pipes and chimneys (Fig. 5.1.2). The latter two are columnar units which cut across existing stratigraphy. They may measure up to 30 km in length (e.g. Fig. 5.1.2), and could possibly extend beyond this. They are defined as either a confinement of acoustic blanking, stacked reflectors and/or chaotic reflectors. Brightened zones consist of parallel reflectors that have an abnormally higher amplitude than its neighbouring stratigraphy.

5.2. SUBMARINE CANYON SPECIFIC OBSERVATIONS

Bathymetric and seismic analysis

As previously mentioned, the study area consists of 15 submarine canyon systems, and is subdivided into three domains (Zones A, B and C from northwest to southeast respectively) (Fig. 5.2.1). The canyon morphologies recognised in this dataset are either linear, sinuous or hooked. The hooked type-morphology is defined when the head of a particular canyon exhibits a pronounced arcuate thalweg morphology. All morphometrics associated with these canyon systems are displayed in Appendix A. Apart from the well-known Cape Canyon (Dingle et al., 1983; Wigley & Compton, 2006; Compton & Wiltshire, 2009), the remaining 14 canyon systems are informally named as they are previously unreported. In some instances, a particular canyon system may comprise multiple individual canyons that feed into the same trunk which is then termed a "canyon system".

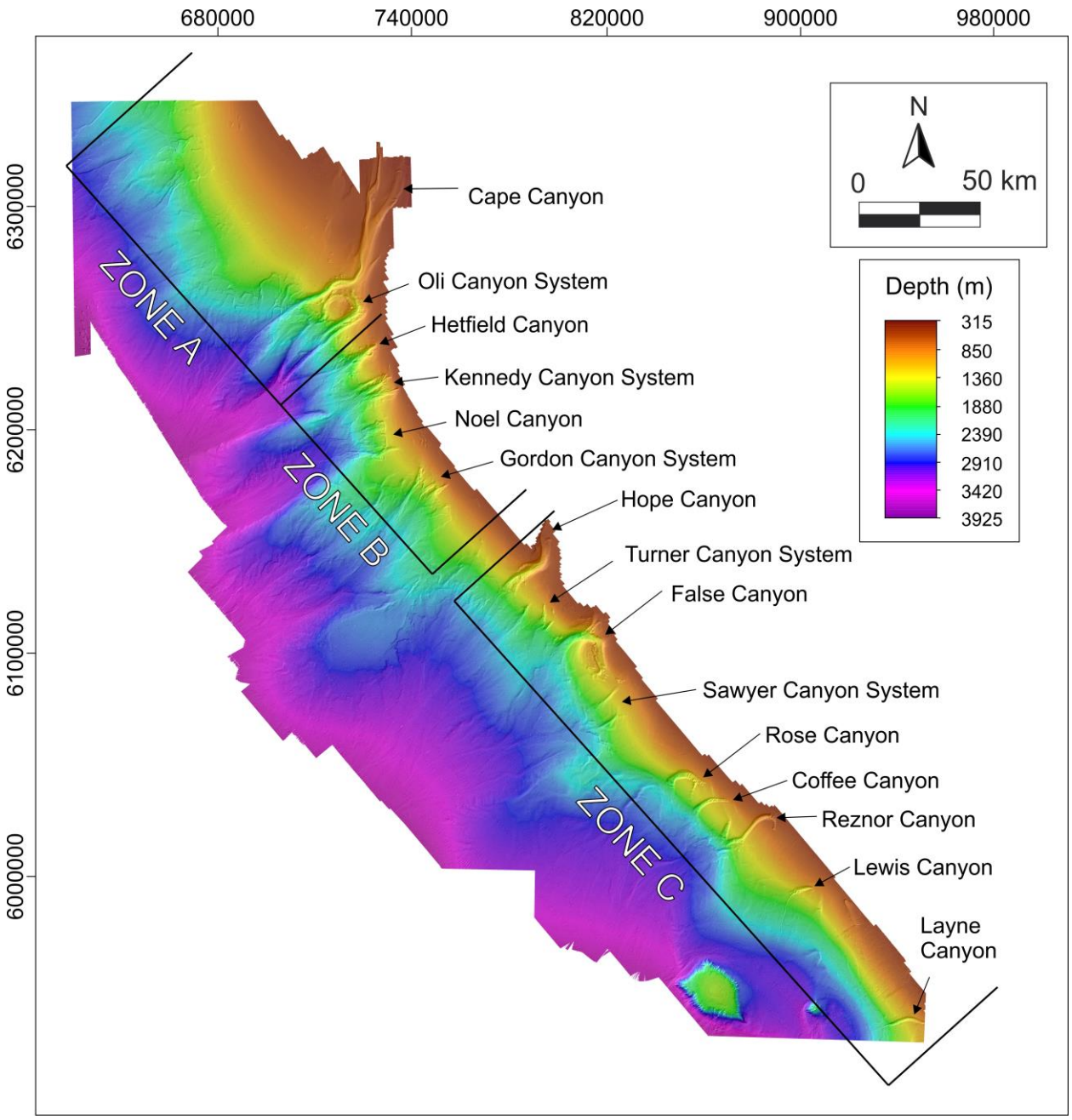

Figure 5.2.1: Submarine canyon domains of the southwestern Cape continental margin of South Africa; separated into Zones A, B and C from northwest to southeast respectively.

ZONE A CANYONS

Zone A consists of two sinuous canyons, the Cape Canyon and the Oli Canyon System. The Cape Canyon is the northernmost canyon recognsied here, unfortunately they head is not fully covered within the extent of the bathymetric dataset. The head region is inferred according to satellite altimetry imagery (NOAA data of Google Earth, Fig. 5.2.2) and from previous work of Wigley & Compton (2006) and Compton & Wiltshire (2009).

The Cape Canyon

The mid-canyon exhibits a smooth U-shape geometry, where it is 4000 m wide with a vertical relief of 300 m (Fig. 5.2.2). A key feature of this canyon is its unusual meandering of the channel from an approximate N-S to strict NE-SW orientation. The walls of the canyon along this meander are associated with five mega-pockmarks that are between 500 and 1200 m in diameter (Fig. 5.2.2). The canyon toe shows a narrower V-shape channel that is 300 m wide and with a relief of 50 m.

The Cape Canyon cuts into the underlying SF3 and SF4 units and is draped by SF8 (Fig. 5.2.3). Notably, the seismic architecture beneath this canyon is mostly flat-lying high amplitude and chaotic reflectors of SF2 and SF3 which show no palaeo-incision but rather localised brightening beneath the canyon floor (Fig. 5.2.3).

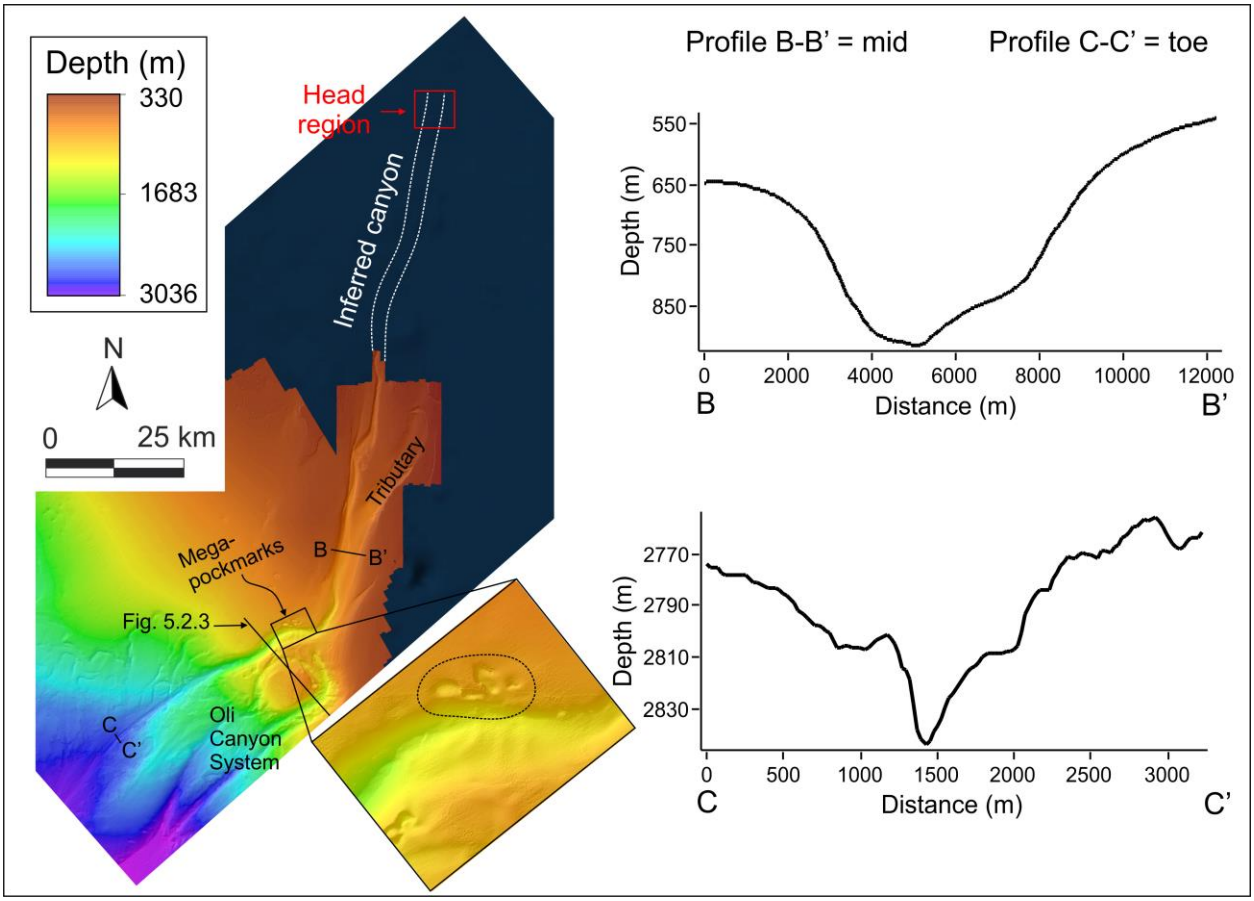

Figure 5.2.2: The bathymetric data of the Cape Canyon and cross sections of the mid-canyon (B-B') and toe (C-C') regions. The upper limits of this canyon is not covered by this dataset and is therefore inferred (indicated by the white dashed line). There is an enlarged portion of this canyon which shows mega-pockmarks adjacent to the meandering canyon walls.

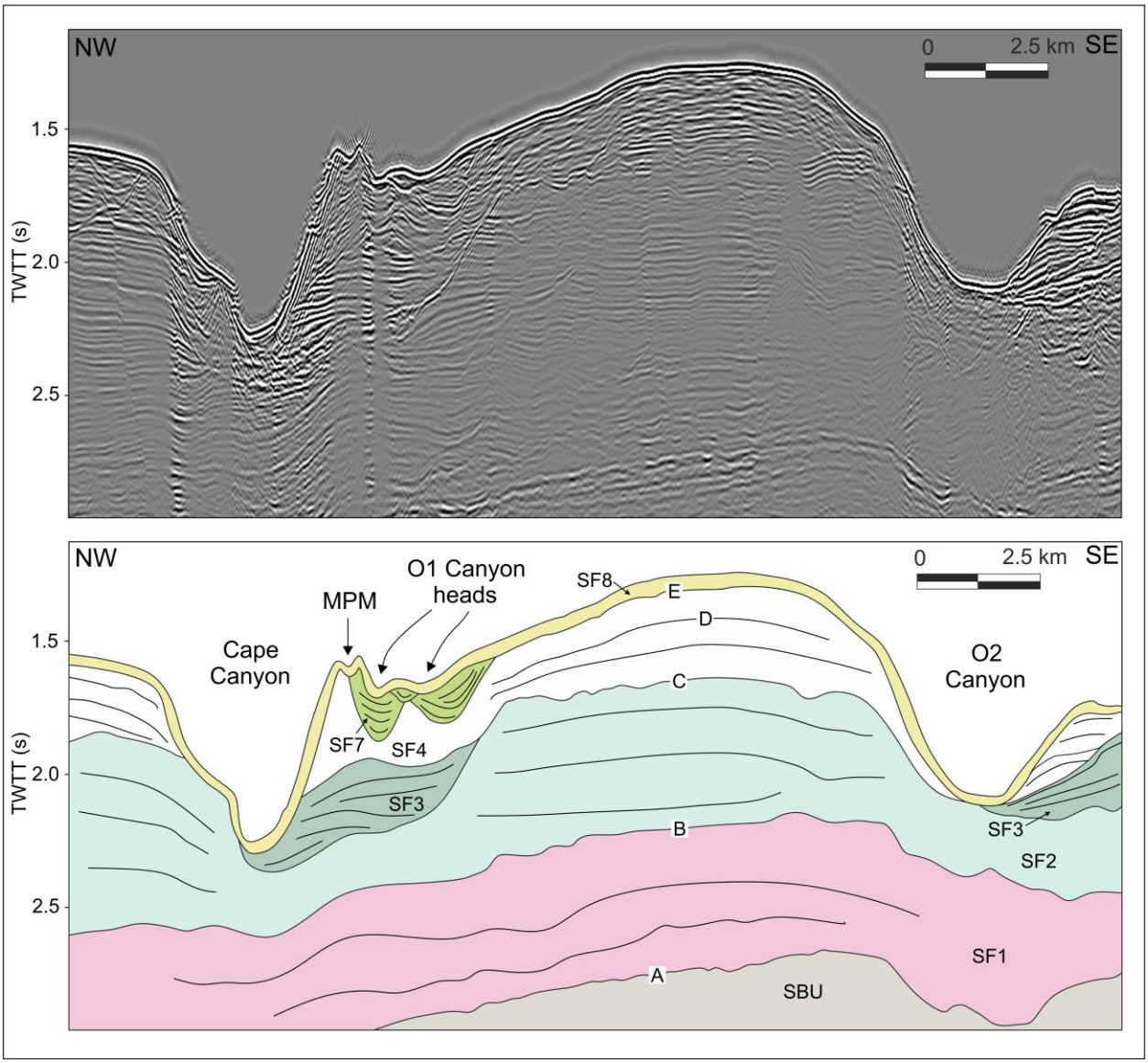

Figure 5.2.3: Raw seismic data (above) and interpretation (below) through the Cape Canyon and the Oli Canyon System. There is an occurrence of a mega-pockmark adjacent to the wall of the northeastern O1 head (indicated by "MPM"). This is associated with two underlying infilled canyons systems in SF7.

The Oli Canyon System

This system comprises three distinct canyons (O1, O2 and O3) which feed into a single trunk (Fig. 5.2.4). The heads of these canyons are located at the same depth (990 – 1200 m) where the Cape Canyon changes its orientation with the mega pockmarks.

Canyon O1 has a length of 51 km, with an overall low sinuosity of 1.10 (Fig. 5.2.4). The canyon head is particularly arcuate and bifurcates (Fig. 5.2.4), the northern segment of which is ~1000 m wide with a V-shaped geometry and a minor axial incision starting at a depth of ~1200 m. In contrast, the southern segment is more U-shaped in geometry. A substantial number of pockmarks cluster around the canyon heads and range from 200 m to 2000 m in diameter (Fig. 5.2.5a). One pockmark of particular importance is located adjacent to the northern head of the O1 Canyon, ~750 m in diameter (Fig. 5.2.3). This is associated with two underlying infilled canyons systems in SF7.

The canyon does not widen into the mid-canyon region, but does widen towards the canyon toe to ~2000 m width. Seismic data through the bifurcated heads of the O1 feature shows three palaeo-canyons comprising SF7 (Fig. 5.2.3). These are up to 1800 m wide and 400 m in vertical relief and are draped by the "Holocene" SF8 (Fig. 5.2.3). Notably, these palaeo-canyons consist of brightened reflectors at the base of their channels.

Canyon O2 is a relatively straight, 27 km long canyon that has a similarly bifurcating head (Fig. 5.2.4). Overall, this canyon is a flat-bottomed feature. The bifurcating head sections are each ~750 m wide (Fig. 5.2.4), with two pockmarks occurring adjacent to the heads. These are each ~1000 m in diameter (Fig. 5.2.5a). Further downslope, the mid-canyon has a concave up cross section with gentle flanks (Fig. 5.2.4). The toe is characteristic of rill features, up to 200 m wide and 10 m in vertical relief (Fig. 5.2.4). These rills proceed downslope for a further 12 km (Fig. 5.2.5b). The underlying stratigraphy of the O2 canyon lacks any palaeo-incisions and it incises instead into mostly flat laying SF2-4.

The O3 Canyon has an arcuate head which is attached to the mid-O2 Canyon (Fig. 5.2.4 & 5.2.5a). This forms a nearly complete circular feature on the seafloor. Overall, this canyon is linear over the 42 km it spans. There is a prominent region of mass wasting around the head that hosts a number of pockmarks within it (Fig. 5.2.5a). The zone of mass wasting covers an area of 26 km^2.

At the mid-canyon (20 km from the head), there is a notable axial incision (Fig. 5.2.4 & 5.2.5b) which proceeds downslope for 20 km and terminates before the canyon toe.

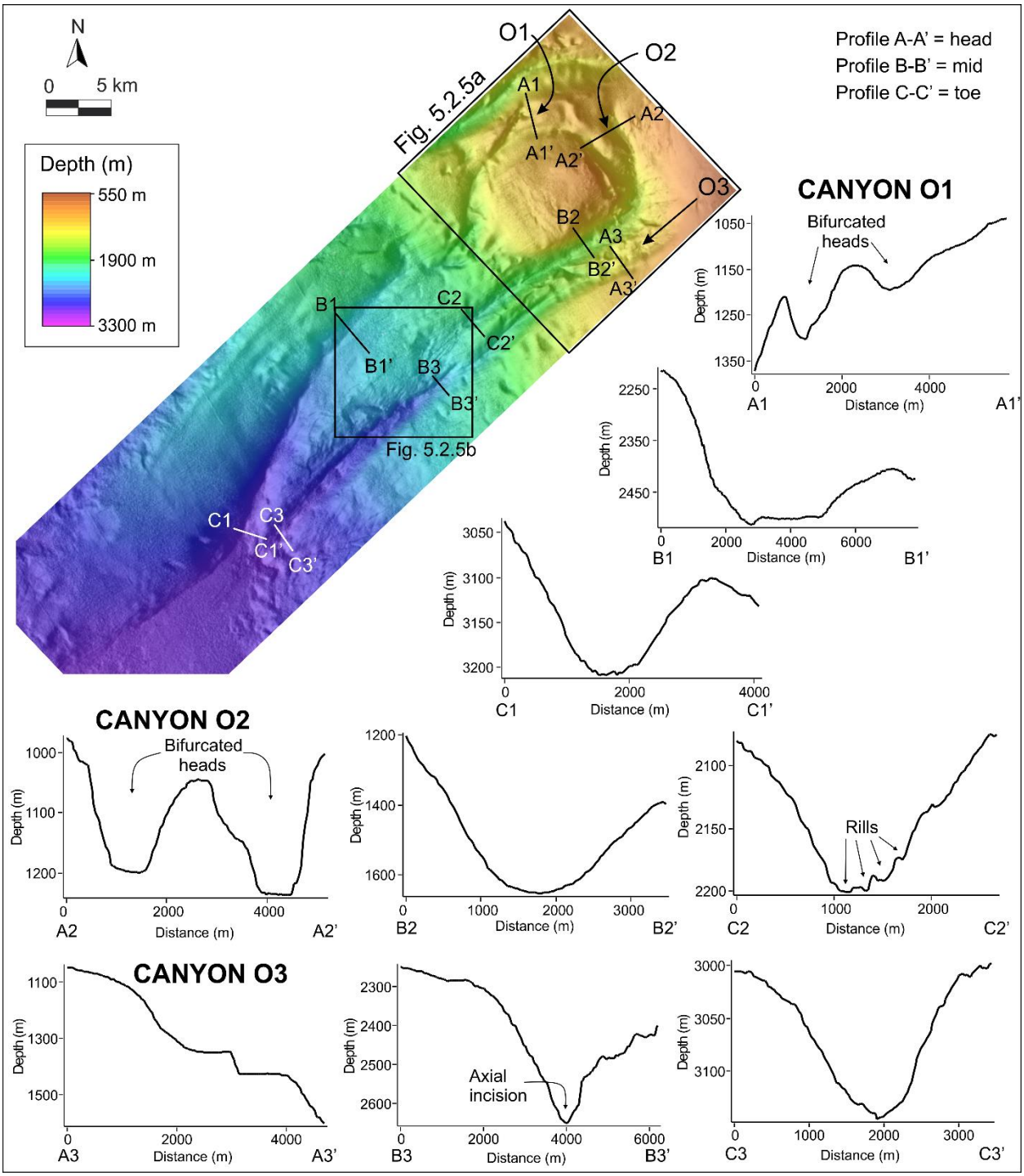

Figure 5.2.4: Multibeam bathymetry detailing the Oli Canyon System consisting of canyons O1, O2 and O3. There are nine accompanying cross-sectional profiles for this system: the O1 Canyon head (A1-A1'), mid-canyon (B1-B1')

and toe (C1-C1'); the O2 Canyon head (A2-A2'), mid-canyon (B2-B2') and toe (C2-C2'); the O3 Canyon head (A3-A3'), mid-canyon (B3-B3') and toe (C3-C3').

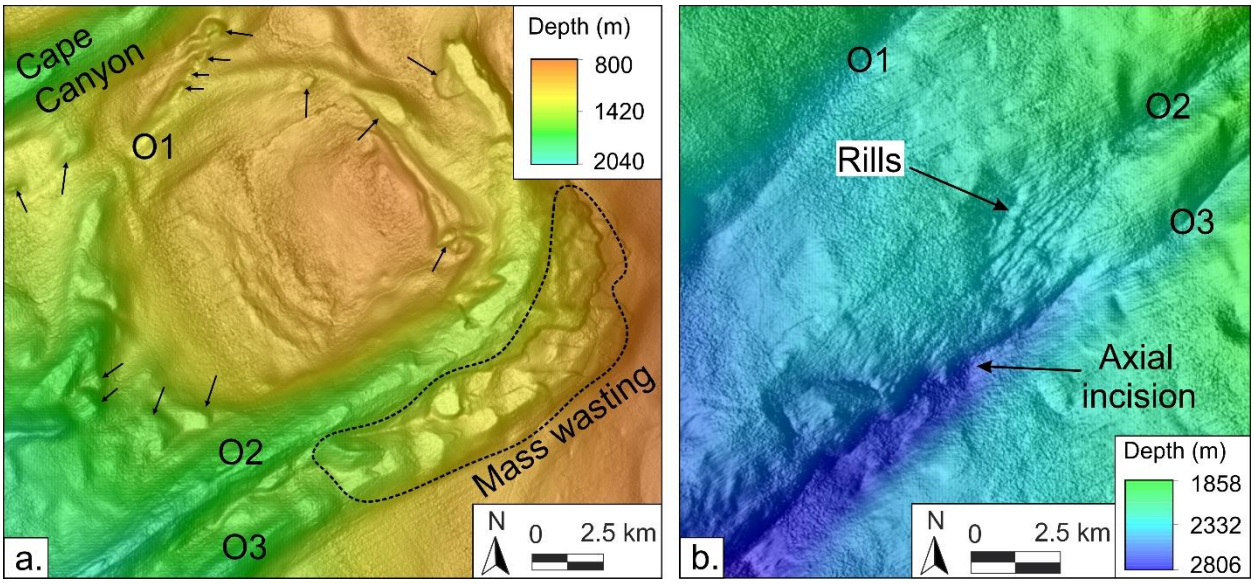

Figure 5.2.5: Characteristic features of the Oli Canyon System (A – B). **A.** The heads of the O1, O2 and O3 Canyons emphasizing numerous pockmark occurrences (indicated by the black arrows), together with a region of disturbed seafloor considered as indicative of mass wasting. **B.** Rill features at the terminus of the O2 Canyon and an axial incision within the thalweg of the O3 Canyon.

ZONE B CANYONS

There are four canyon systems within Zone B; the Hetfield, Kennedy, Noel and Gordon Canyon systems (Fig. 5.2.6). Three of these four systems have a linear morphology and are thus collectively documented below, whereas the Noel Canyon is decidedly more sinuous.

Linear canyons of Zone B

The Hetfield Canyon, Kennedy Canyon System (K1, K2 and K3) and Gordon Canyon System (G1 and G2) range in length from 17 km to 30.5 km, with a net NE-SW orientation (Fig. 5.2.6). The Kennedy and Gordon systems are separated by the sinuous Noel Canyon. Notably, there are no pockmarks associated with these canyons. There are a series of rills that follow the toe of Canyon G1, which trend downslope and reach 50 m in width and 5 m in relief (Fig. 5.2.8).

The majority of the canyon heads are located at depths of between 600 and 1200 m. They express a common V-shape profile no wider than 1800 m and range in vertical relief between 100 and 300 m. The canyon walls are typically smooth (Fig. 5.2.6) with the exception of the G1 Canyon which shows a U-shape profile with a gullied channel bottom. The first sub-canyon of the Kennedy System (K1) has a low-relief head (Fig. 5.2.6) as compared with the higher relief heads of the other systems.

In the mid-canyon areas, the bathymetric profiles are generally wide (up to 4500 m) and U-shaped, with reliefs of between 110 and 200 m (Fig. 5.2.7). These areas of the canyons encompass multiple irregular gully features that are no wider than 250 m, the exception being Canyon K1 and G2 which have steep and narrow V-shaped profiles with greater relief (220 m deep, 500 m wide) (Fig. 5.2.7).

The toe segments (at depths between 2400 and 1700 m) of the linear canyons are morphologically diverse. Canyons K1 and G2 have axial incisions up to 20 m in relief (Fig. 5.2.8). Canyon G1 has a wider channel (~3000 m), and the K3 and Hetfield canyons have steeper sided walls (up to 100 m deep and 1000 m wide), marked by numerous gullies (Fig. 5.2.8). The deepest portions of Canyon K2 are remarkably subdued in relief when compared to the other canyons.

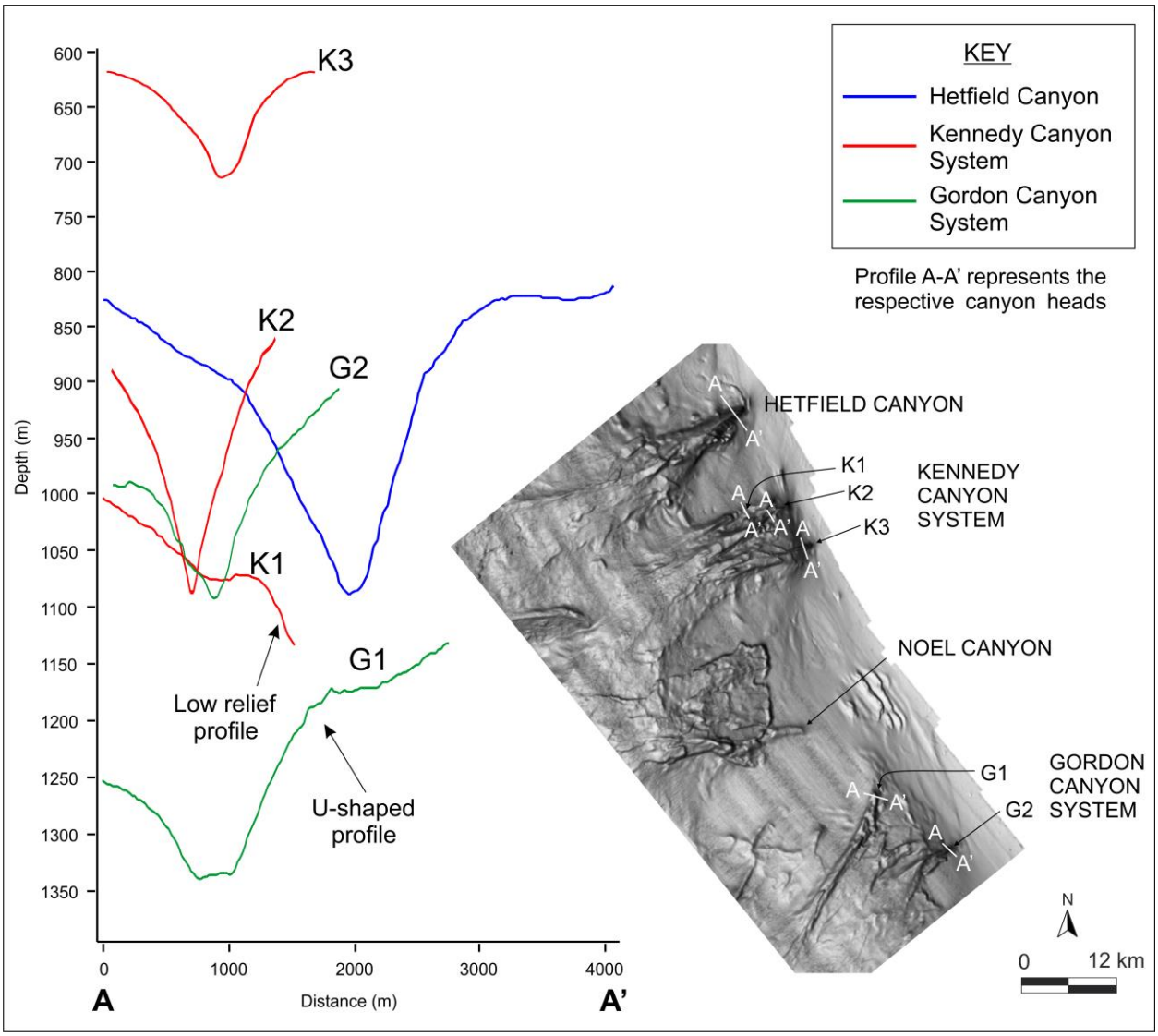

Figure 5.2.6: Cross-sectional profiles (A-A') of canyon heads from the corresponding hillshaded bathymetric image for the Hetfield, Kennedy and Gordon Canyon Systems.

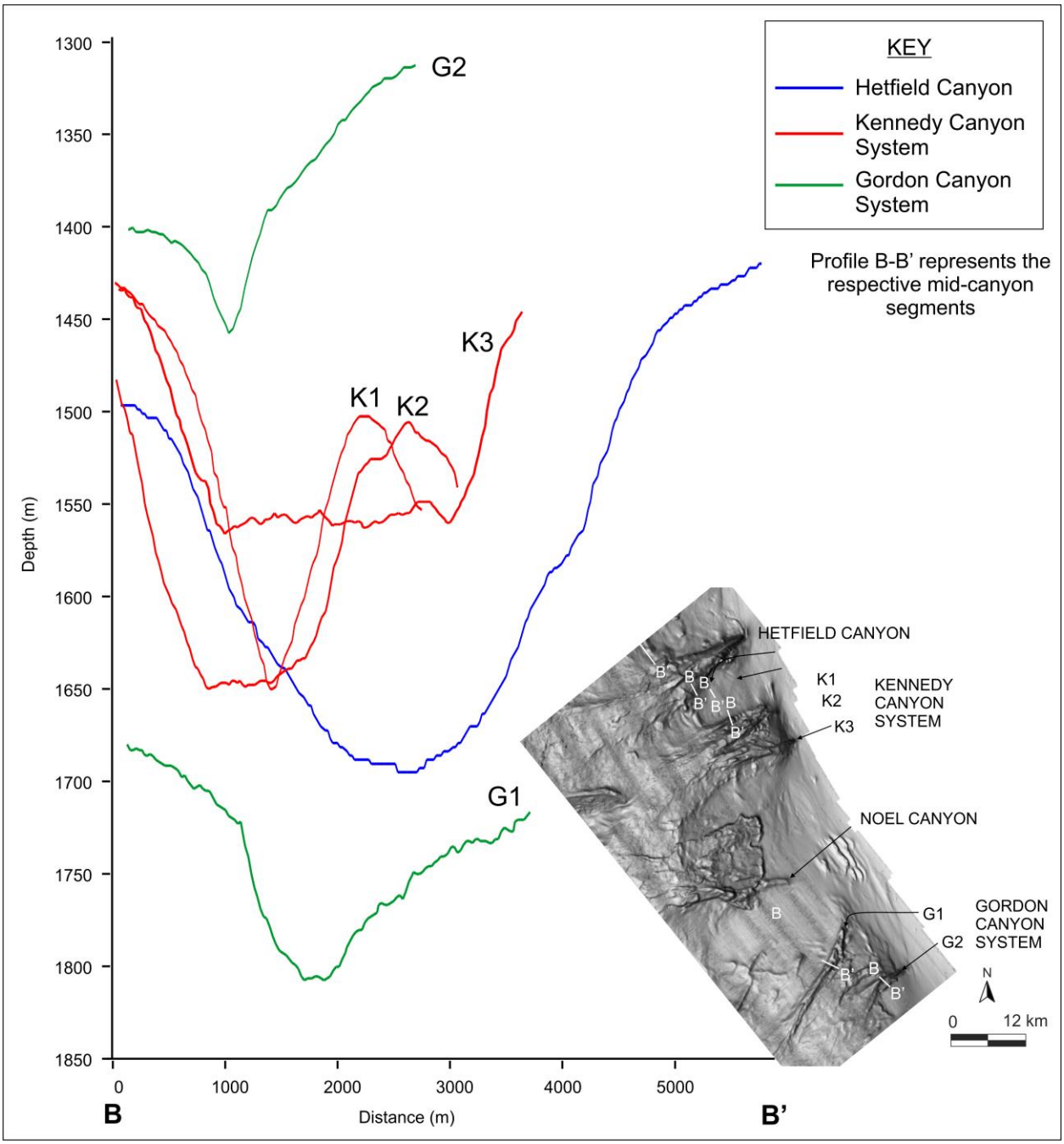

Figure 5.2.7: Cross-sectional profiles (B-B') of the mid-canyon segments from the corresponding hillshaded bathymetric image for the Hetfield, Kennedy and Gordon Canyon Systems.

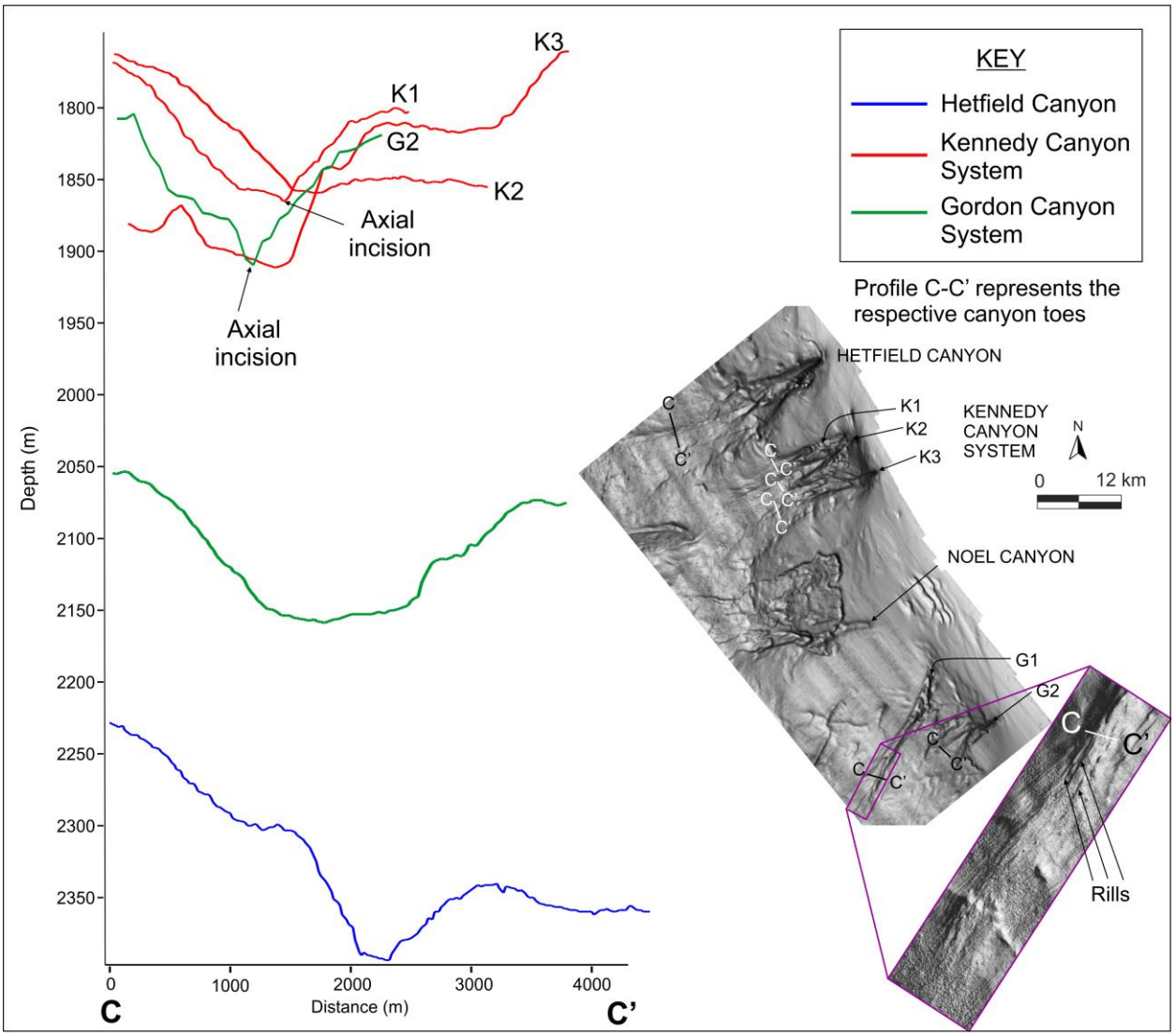

Figure 5.2.8: Cross-sectional profiles (C-C') of canyon toes from the corresponding hillshaded bathymetric image for the Hetfield, Kennedy and Gordon Canyon System. The purple box enhances the detail of a series of rills that occur downslope from the toe of the G1 Canyon.

The Noel Canyon System

Upslope from the Noel Canyon are a series of subdued headscarps (Fig. 5.2.9 & 5.2.10a) that cover an area of 62 km^2, interspersed by promontories of smooth continental slope (Fig. 5.2.9). The subsurface beneath these subdued headscarps comprises hummocky chaotic reflector packages that are housed within the neighbouring linear reflectors (Fig. 5.2.10a). There appears to be numerous faults downslope of this zone that offset the parallel to oblique-parallel seaward dipping reflectors of SF4a and SF4b (Fig. 5.2.10a).

Figure 5.2.10b shows the 4000 m wide N1 Canyon channel, characterised by a series of intra-canyon rill features measuring up to 1000 m in width and 20 m in relief (Fig. 5.2.10b). The inter-canyon space between the N1 and N2 Canyons is defined by a series of inter-canyon rills that are more subdued in width and relief (Fig. 5.2.10b). The N1 channel and inter-canyon rill features appear to be coalesced mass wasting features in SF8 that produce an irregular, hummocky topography confined to a zone ~312 km^2 on the bathymetric data (Fig. 5.2.9). Upslope of this zone are the headscarps and faulted zones of SF4a and SF4b.

The N2 Canyon is weakly sinuous (1.10). The head and mid-canyon portions have narrow, V-shaped features approximately 500 m wide, with minor gullies at their bases respectively (Fig. 5.2.9). The canyon narrows towards the toe (~150 m at its base) (Fig. 5.2.9) and is underlain by SF7 and draped by SF8 (Fig. 5.2.10b).

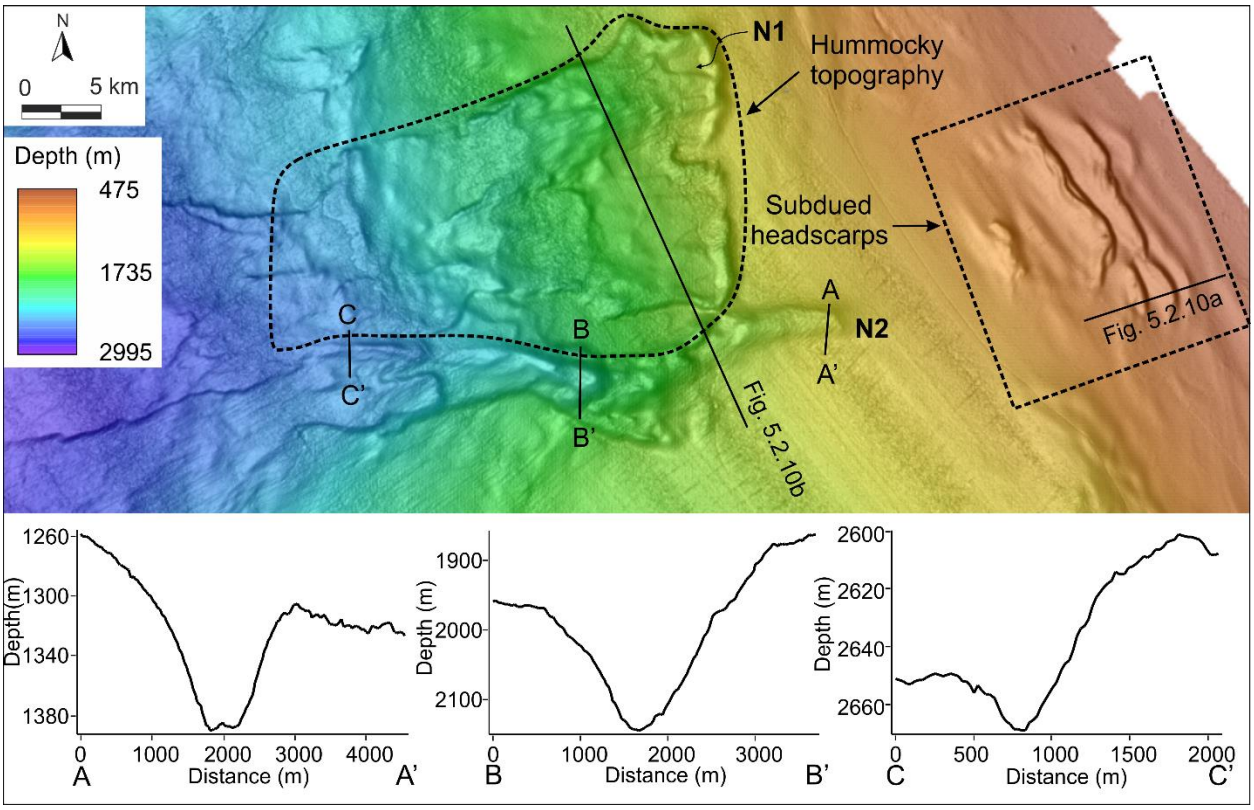

Figure 5.2.9: Cross-sectional profiles of the head (A-A'), mid-canyon (B-B') and toe (C-C') from the corresponding bathymetric image for the N2 Canyon. Also shown is an adjacent zone of mass wasting giving a hummocky topography which engulfs the N1 Canyon, upslope of which are a series of subdued seafloor headscarps.

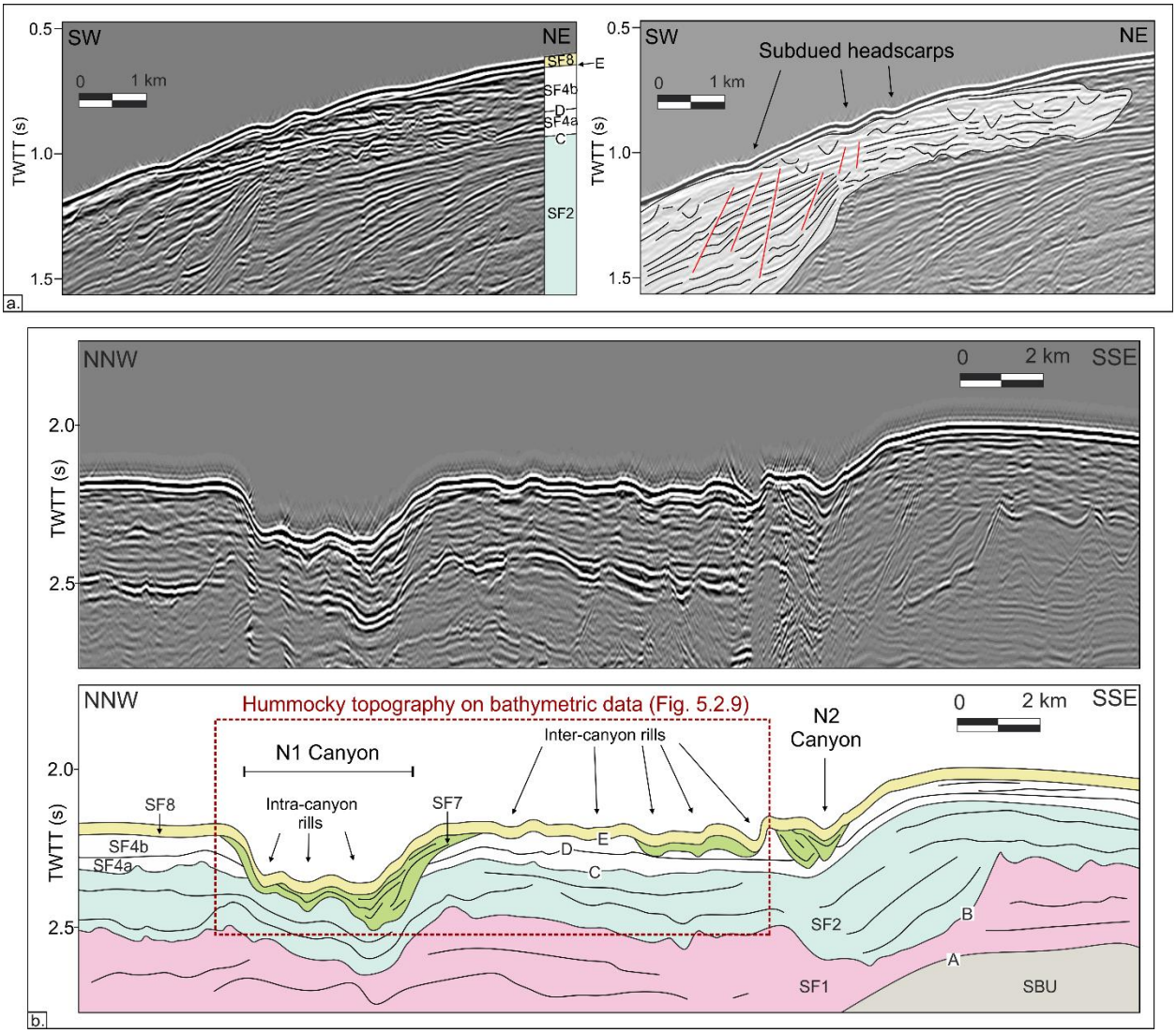

Figure 5.2.10: Seismic data and interpretations of the Noel Canyon System and associated features (A – B). **A.** Subdued headscarps (left) and the interpretation (right) showing disorientated, hummocky and chaotic reflectors of SF4a and SF4b and downslope faulting (indicated by the red lines) **B.** Along-strike seismic profile and interpretation through the mid-canyons of the Noel Canyon System (N1 and N2 Canyons) and the adjacent patch of mass wasting features. The mass wasting features produce a hummocky topography (observed in Figure 5.2.9).

ZONE C

Zone C comprises nine canyon systems: one sinuous (Hope Canyon); two linear (Turner and Sawyer Canyon Systems); and six hooked (False, Rose, Coffee, Reznor, Lewis and Layne Canyons). The linear systems are collectively documented whereas individual descriptions are provided for the other morphologies due to their complex nature which requires more intimate levels of descriptive detail.

The Hope Canyon

This canyon is moderately sinuous (1.12) and is associated with a multitude of densely clustered pockmarks, particularly around the head (Chapter 5, Section 5.3). The head is characterised by a strong asymmetric cross section with a skewed thalweg that is 5000 m wide and ~150 m deep (Fig. 5.2.11a). The mid-canyon is defined by a U-shaped cross section (Fig. 5.2.11a) that is dominated by crescentic bedforms and sediment lobes that converge on the axial incision along the main canyon channel (Fig. 5.2.11b). This incision has a total length of 27 km. These crescentic bedforms have wavelengths of ≤1500 m and heights of ~50 m. There is a single distributary (1300 m wide; 100 m relief) on the western flank of the mid-canyon that similarly hosts numerous crescentic bedforms and sediment lobes (Fig. 5.2.11b). The toe shows the downslope extension of the axial incision which deepens to ~40 m at this point (Fig. 5.2.11a).

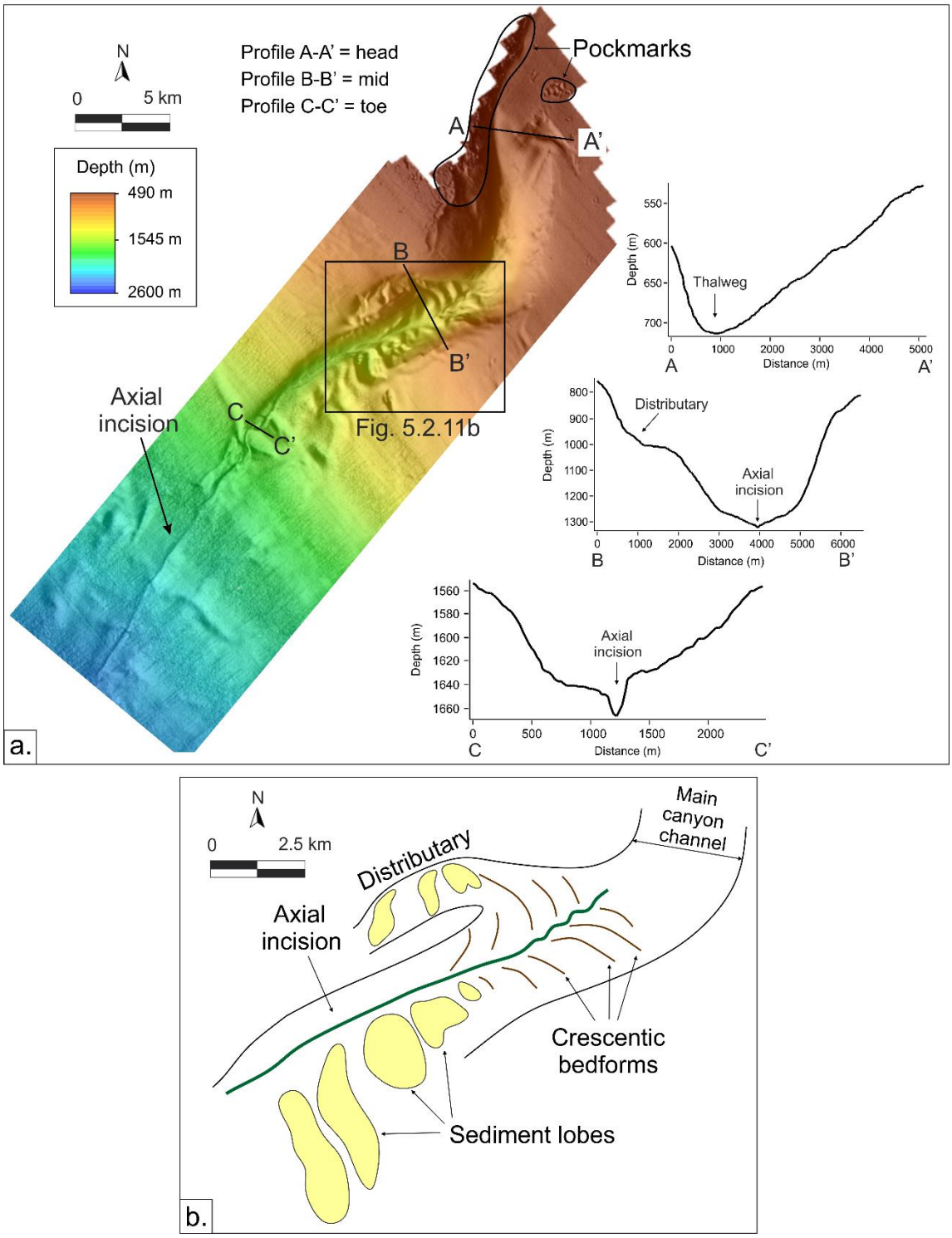

Figure 5.2.11: Characteristic features of the Hope Canyon (A – B). **A.** The bathymetric image and corresponding cross-sections of the head (A-A'), mid-canyon (B-B') and toe (C-C') of the Hope Canyon. A 27 km-long axial incision can be observed downslope from the canyon toe. **B.** Interpretation of the seafloor features that occur along the mid-canyon. Note the axial incision, crescentic bedforms, lobes of sediment and single distributary.

Linear canyons of Zone C

The Turner (T1 – T3) and Sawyer (S1 – S2) Canyon Systems make up the linear canyons of Zone C and have a total of five small individual canyons (described collectively below). These two canyon systems are separated by the hooked False Canyon. They are orientated in an overall NE-SW alignment and range in length from 5 to 12 km. These canyons are generally featureless, with no axial incisions and limited terracing or rilling. Some minor rills occur, with reliefs of between 50 - 100 m, except for the T2 Canyon which appears to have a smooth profile (Fig. 5.2.12). There is no evident mass wasting outside of the adjacent wall and head areas (Fig. 5.2.12).

The linear canyon heads occur between depths of 1000 and 1500 m. At their start, the canyons are U-shaped, with a gentle reliefs of up to 1700 m wide and 120 m deep (Fig. 5.2.12). In the mid-canyon, the channels are still U-shaped, with increasing relief (150 m) and slightly narrower thalwegs (1500 m) (Fig. 5.2.13). Canyon S1, is however steeper and more V-shaped (Fig. 5.2.13). In this region, the T3 Canyon has a 250 m wide terrace.

The canyons terminate in water 1400 to 2000 m deep. Here their profiles have become more V-shaped, with widths of 1200 and 1800 m and a relief of 50 to 150 m (Fig. 5.2.14). In this region, the S1 Canyon is entered by a small distributary ~800 m wide and ~20 m deep (Fig. 5.2.14).

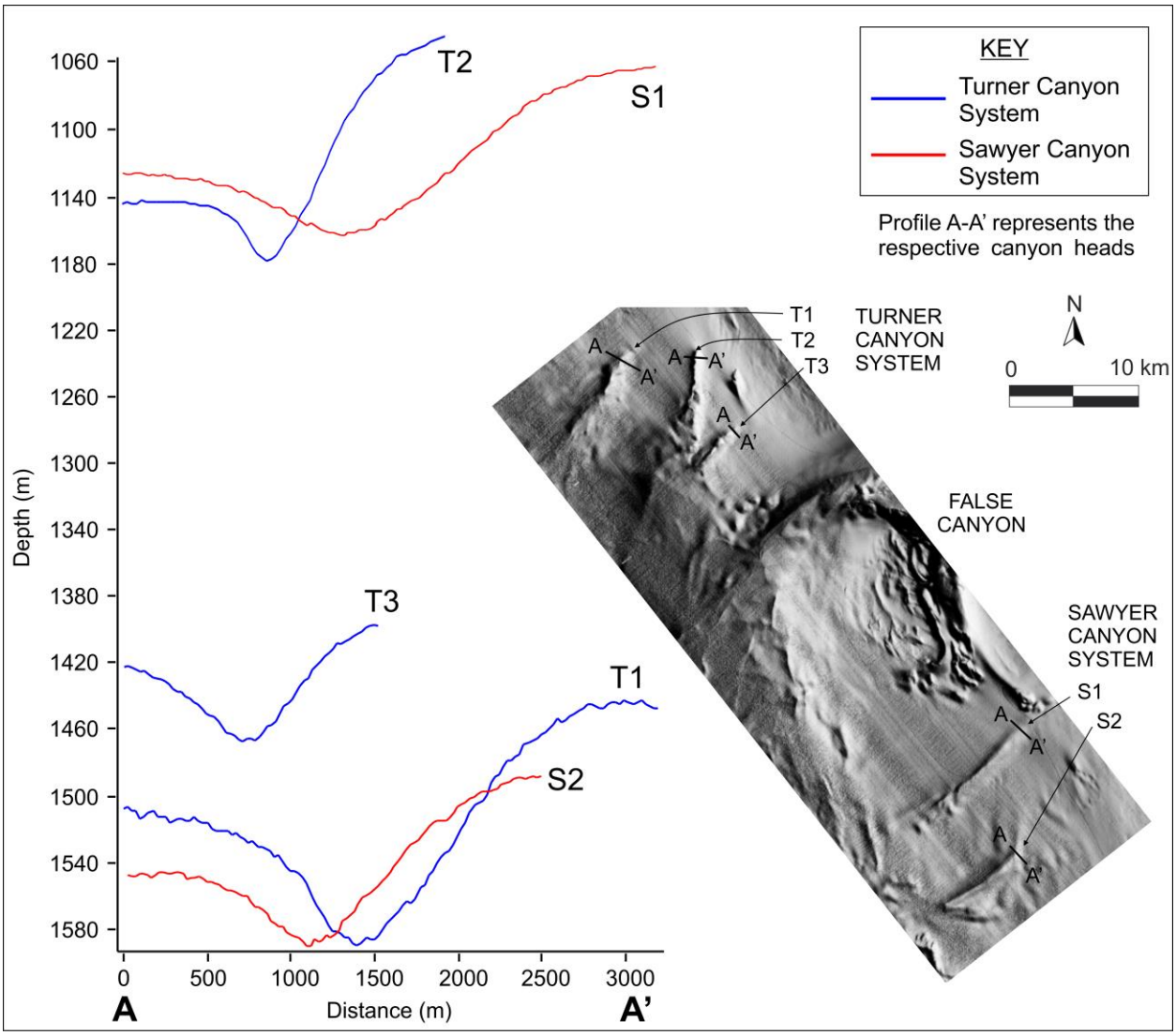

Figure 5.2.12: Cross-sectional profiles (A-A') of canyon heads from the corresponding hillshaded bathymetric image for the Turner and Sawyer Canyon Systems.

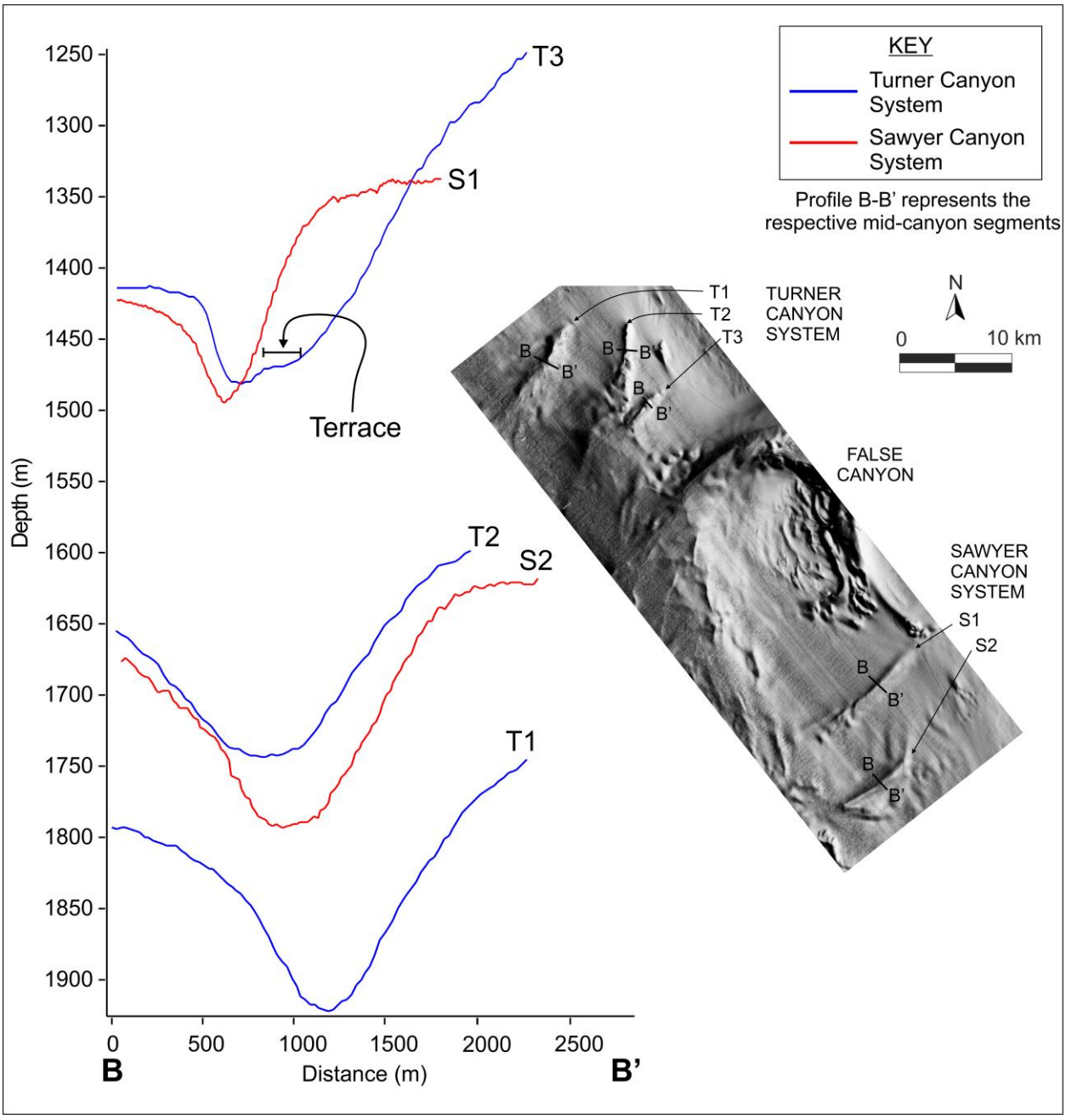

Figure 5.2.13: Cross-sectional profiles (B-B) of mid-canyon segments from the corresponding hillshaded bathymetric image for the Turner and Sawyer Canyon Systems.

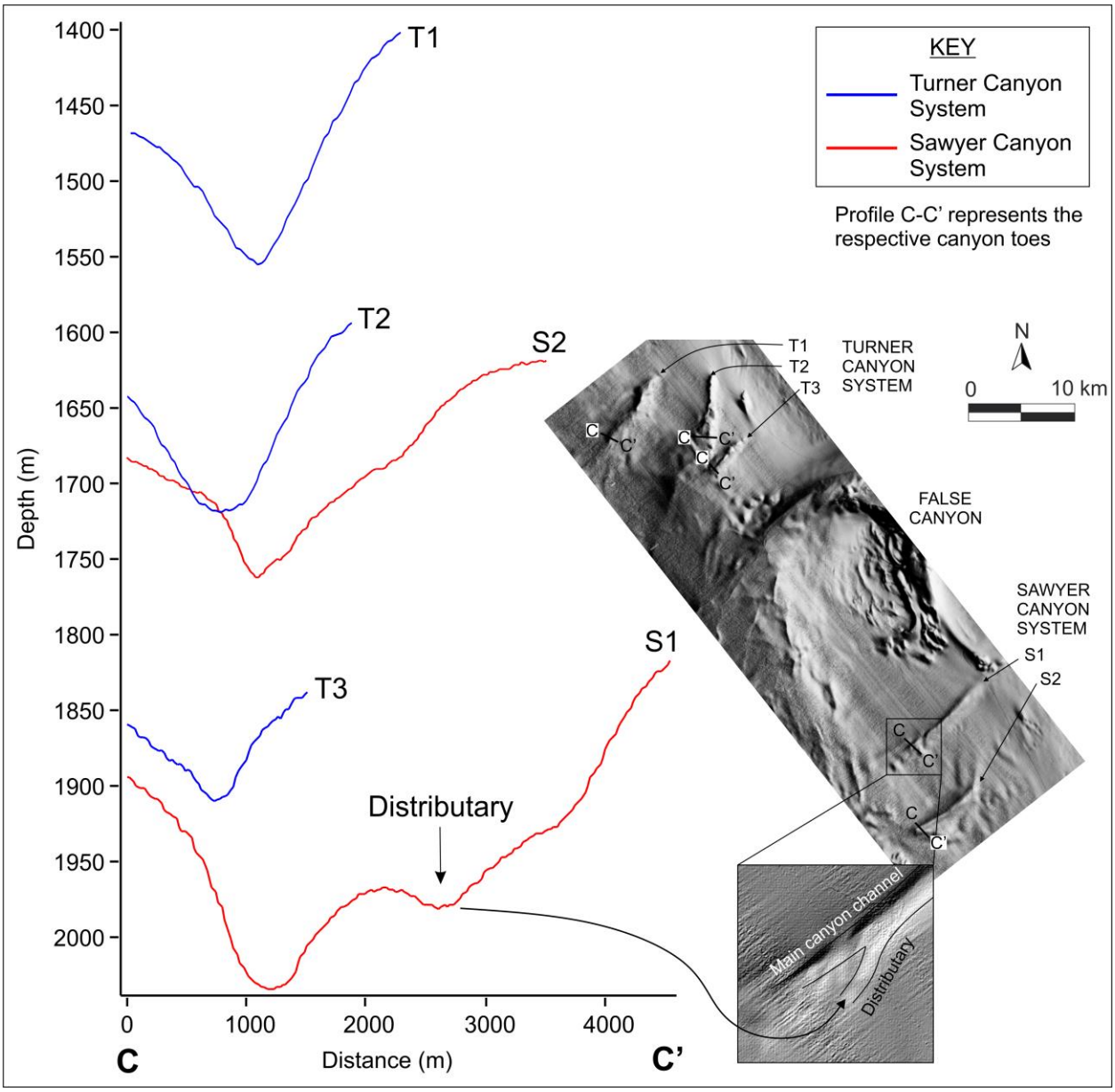

Figure 5.2.14: Cross-sectional profiles (C-C') of canyon toes from the corresponding hillshaded bathymetric image for the Turner and Sawyer Canyon Systems.

Hooked canyons of Zone C

There are seven canyon systems that comprise the hooked-type canyon morphology in Zone C. Of these, six are found in the southernmost parts of the study area, with exception of the False Canyon which occurs between the Turner and Sawyer Canyon Systems. These canyons are individually described from northwest to southeast.

The False Canyon

The False Canyon is a moderately sinuous (1.55) canyon that stretches for 34 km from a depth of 650 to 2325 m. The head bifurcates (Fig. 5.2.15); each component is ~1000 m wide with a V-shaped geometry. Associated with these bifurcating heads is a zone of mass wasting with a surface area of 53 km^2 (Fig. 5.2.15) that extends along the western flank (downslope) of the upper to mid-canyon regions. These heads coalesce around the mid-canyon which then forms a discrete, symmetrical U-shaped channel 3500 m wide (Fig. 5.2.15), the wall of which is associated with a mega-pockmark. There are two tributaries that join the main channel around this mid-canyon region, each of which have a series of crescentic bedforms in their channels (Fig. 5.2.15). The most distal canyon reaches form the widest segment (~4000 m). Where the canyon terminates, five mega-pockmarks are found (Chapter 5, Section 5.3).

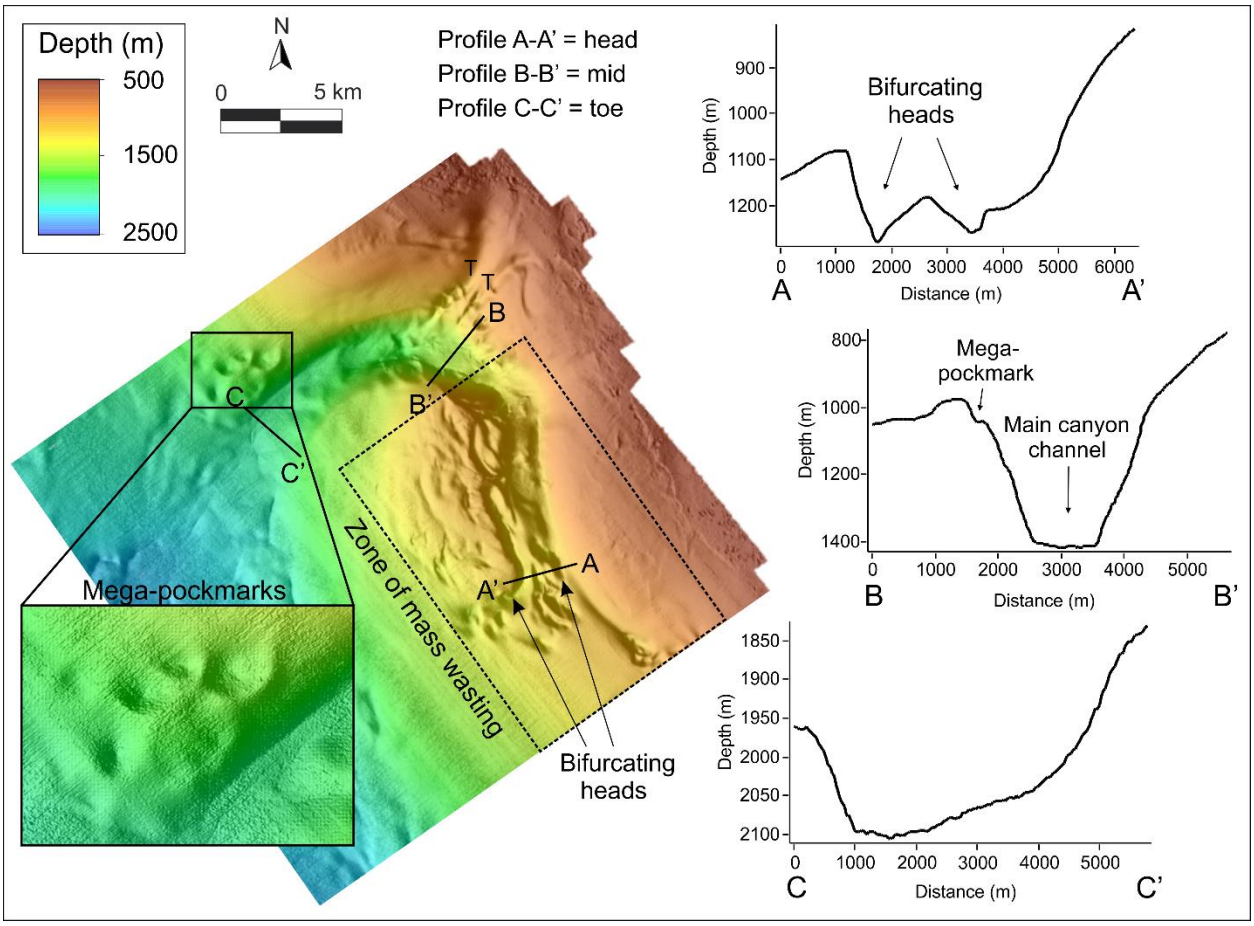

Figure 5.2.15: The bathymetric image and corresponding cross-sections of the head (A-A'), mid-canyon (B-B') and toe (C-C') of the False Canyon. The morphological aspects are displayed on the bathymetric image which shows a hook-type morphology with an arcuate bifurcated head that is engulfed by a zone of mass wasting. The tributaries are indicated by "T" and there is a cluster of mega-pockmarks adjacent to the canyon toe.

The Rose Canyon

This canyon is particularly sinuous (1.78), dominated by a strong hook morphology in the head regions (Fig. 5.2.16). The head bifurcates (each sub-head ~1500 m wide) and is underlain by a series of palaeo-canyon features cut into surface C, filled by Oligocene-age SF7 and draped by the Holocene-age SF8 (Fig. 5.2.18). The stratigraphy here is strongly normally-faulted, the faults disrupt the Late Cretaceous and Palaeocene units (SF2 and SF4), and terminate against the younger Oligocene and Holocene strata (SF7 and SF8).

There is a prominent train of curvilinear bedforms which attach to the main canyon channel with wavelengths up to 1500 m (Fig. 5.2.16 & 5.2.17). There are occurrences trains of canyon-hosted crescentic bedforms along the upper to mid-regions of this canyon which become more subdued towards the toe regions (Fig. 5.2.16). These bedforms have wavelengths up to 1000 m with an alternating steeper lee (~30°) and gentler stoss (~10°) repetition with a depression pool in between successive bedforms (Fig. 5.2.17). Overall, the canyon progressively broadens downslope from 2100 to 4000 m.

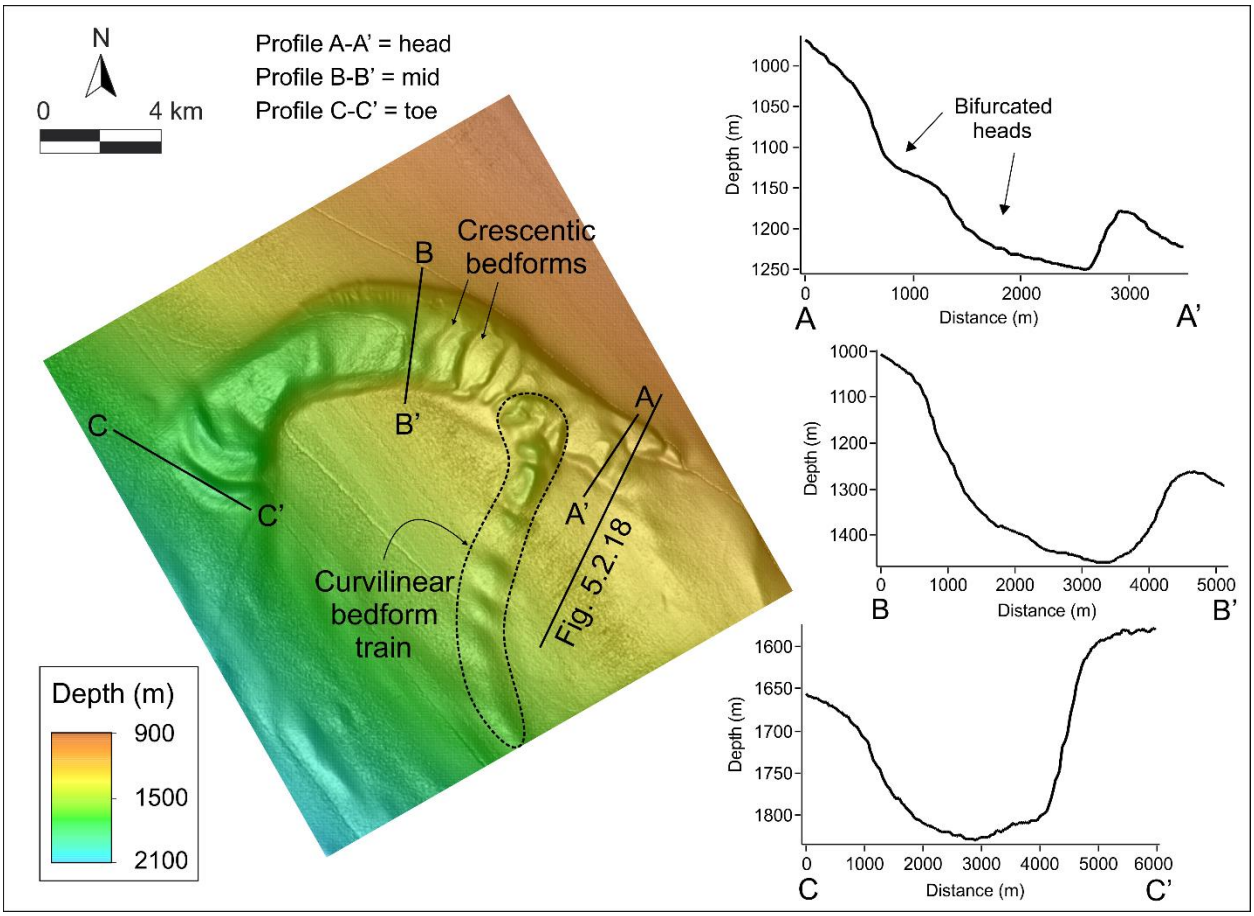

Figure 5.2.16: The characteristics of the Rose Canyon showing multiple crescentic bedforms and an external train of bedforms extending from the main canyon channel. The corresponding cross sections of the head (A-A'), mid-canyon (B-B') and toe (C-C') are also shown.

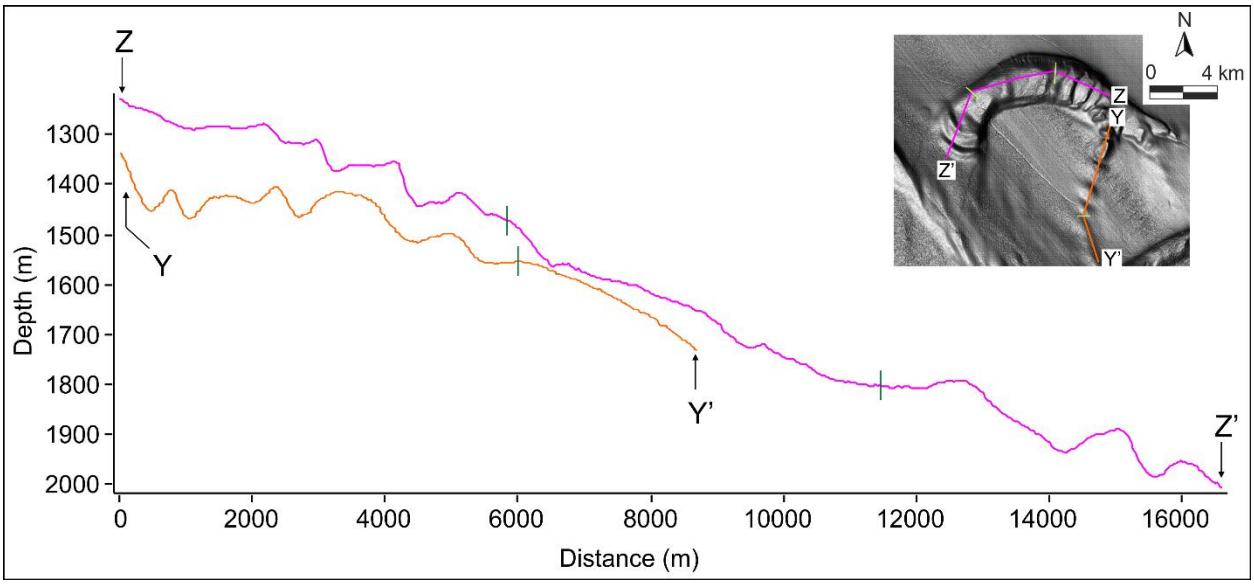

Figure 5.2.17: Cross sections through the bedforms of the Rose Canyon (Z-Z') and the bedforms that attach to it (Y-Y').

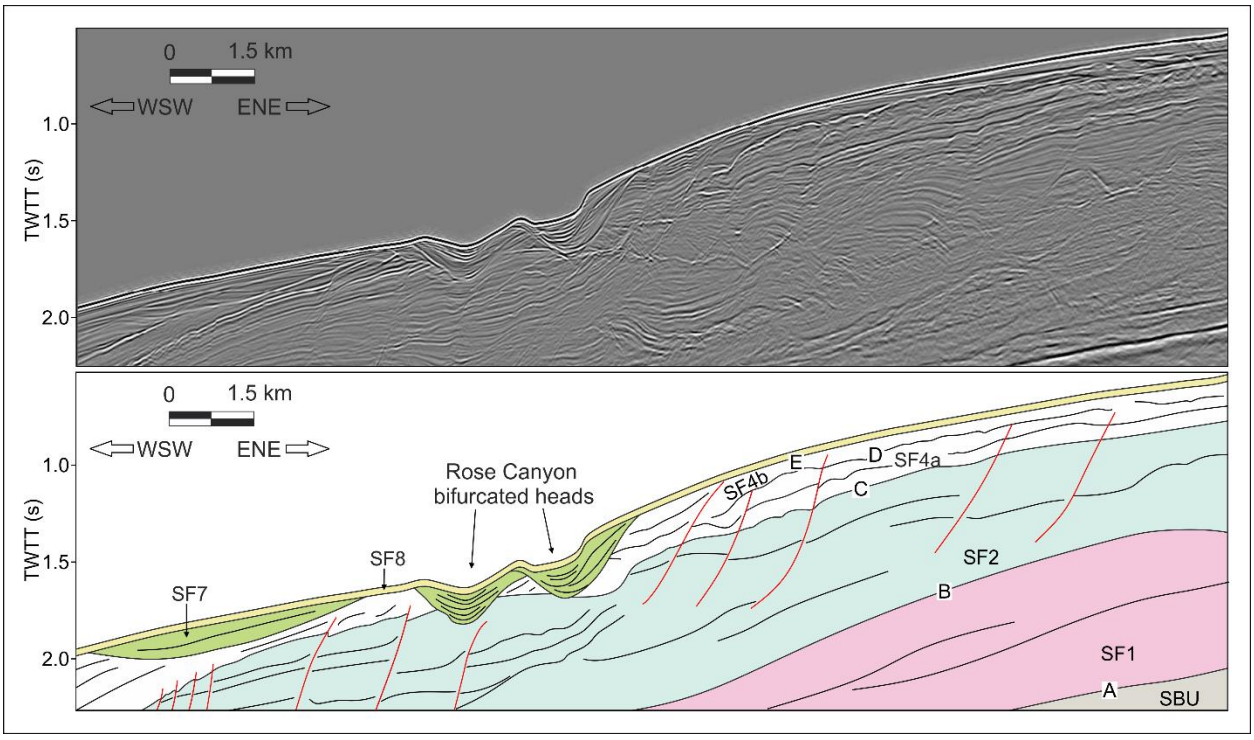

Figure 5.2.18: Seismic profile (upper) and interpretation (lower) through the heads of Rose Canyon. The red lines indicate multiple faults within the region that disrupt the Late Cretaceous and Palaeocene units (SF2 and SF4), terminating against the younger Oligocene and Holocene strata (SF7 and SF8).

The Coffee Canyon

The Coffee Canyon is a moderately sinuous (1.20), relatively short (~17 km) feature. The arcuate head is a low relief feature (50 m) and is associated with multiple crescentic bedforms (Fig. 5.2.19). A minor axial incision (~20 m relief) develops in the mid-canyon portions (Fig. 5.2.19), where crescentic bedforms overlap. The toe comprises a U-shaped channel with subdued bedforms (Fig. 5.2.19). Overall, the canyon width increases downslope from 1000 to 2500 m.

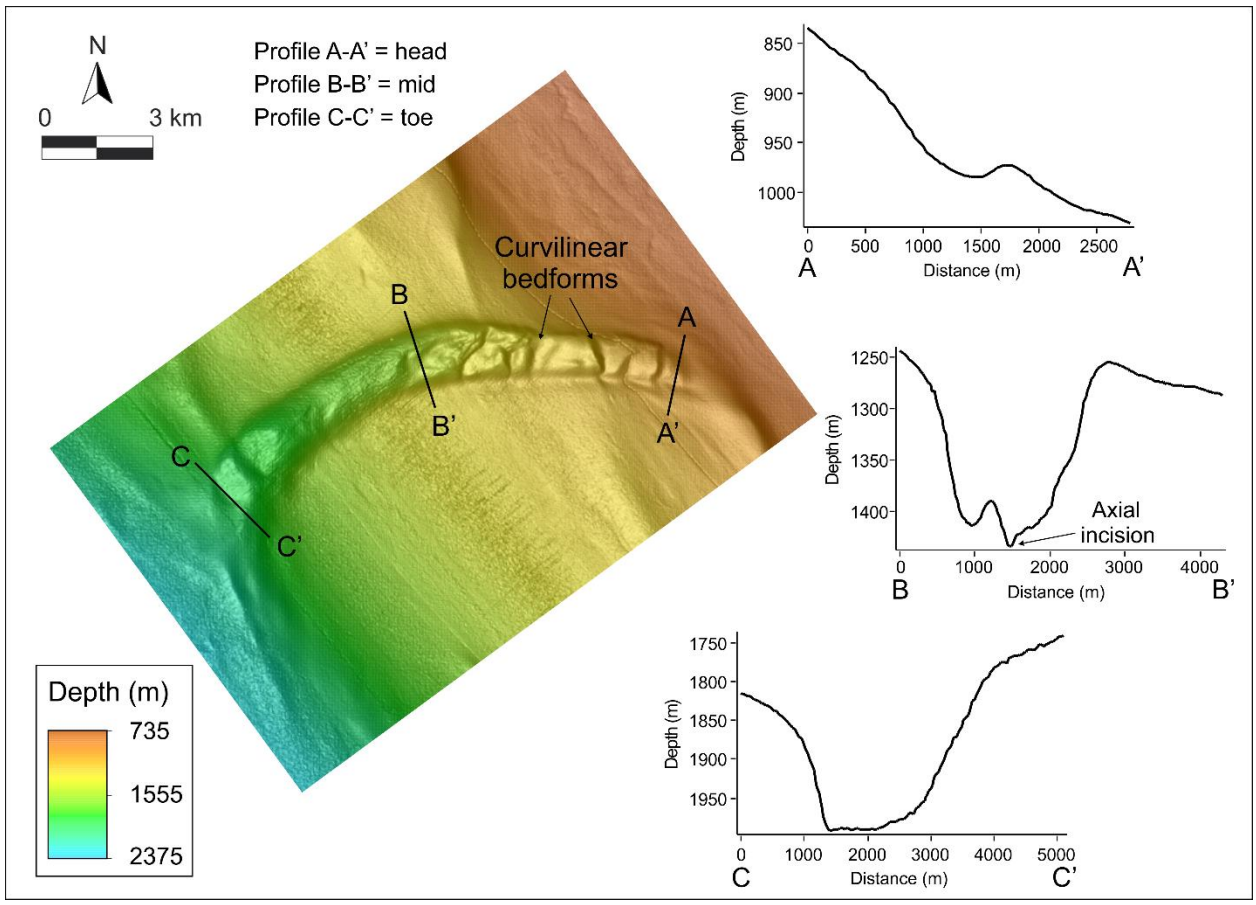

Figure 5.2.19: The bathymetry and corresponding bathymetric cross-sections of the head (A-A'), mid-canyon (B-B') and toe (C-C') of the Coffee Canyon. Note the arcuate hook type morphology with multiple crescentic bedforms that are concentrated in the head and mid-canyon regions.

The Reznor Canyon

The Reznor Canyon is located 2000 m south-west to a major pockmark field (Chapter 5, Section 5.3). It is moderately sinuous (1.43) and one of the longest canyons in this zone (30 km). The head forms a narrow (850 m) V-shape (Fig. 5.2.20a) and is associated with abundant pockmarks that reach up to 900 m in diameter (Fig. 5.2.20b). The canyon widens with depth (1800 m) (Fig. 5.2.20a), with the beginnings of an axial incision that extends for 6100 m downslope (Fig. 5.2.20a & b). Several curvilinear bedforms (orientated SW, with downslope dipping lee faces) converge into this incision (Fig. 5.2.20b). The canyon terminates in a U-shaped profile (Fig. 5.2.20a), adjacent to a cluster of pockmarks up to 1250 m in diameter (Fig. 5.2.20c). There is a minor, linear canyon to the NW of the main Reznor Canyon, with a substantial number of downslope-orientated, curvilinear bedforms (Fig. 5.2.20a). A prominent zone of disturbed seafloor topography, ~84 km^2 in size, marks the terminus of the canyon system (Fig. 5.2.20a).

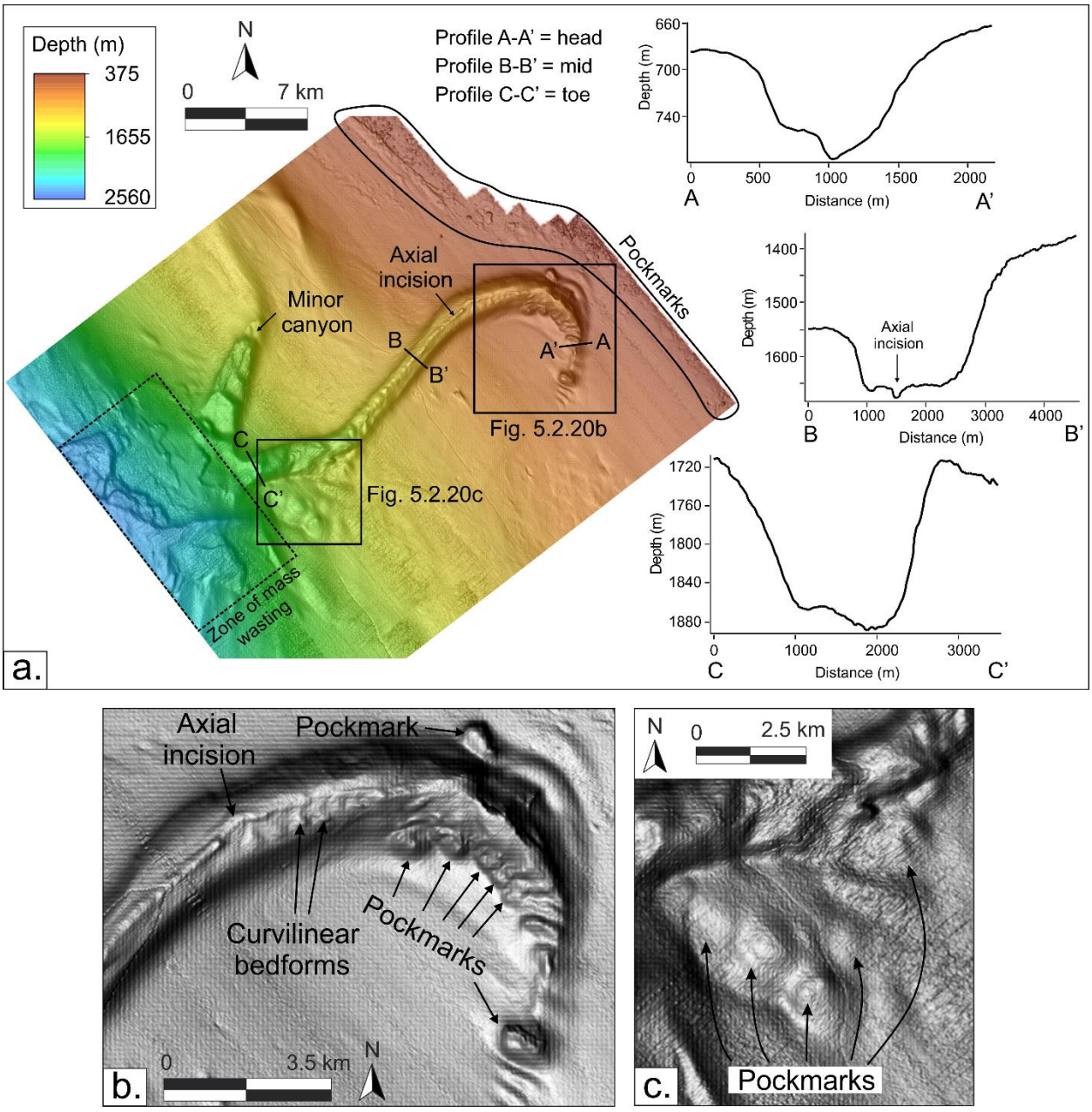

Figure 5.2.20: Features of the Reznor Canyon (A – C). **A.** Bathymetry showing the main Reznor canyon channel with an axial incision, a minor canyon and an extensive zone of mass wasting downslope from the toe. The corresponding cross sections of the head (A-A'), mid-canyon (B-B') and toe (C-C') are also shown. **B.** A hillshaded image of the bathymetric data at the canyon head, showing multiple pockmarks, curvilinear bedforms and an axial incision. **C.** Hillshaded image of pockmarks adjacent to the toe region of the Reznor Canyon.

The Lewis Canyon

This canyon is 7500 m in length, characterised by multiple sinuous bedforms that manifest on the canyon flanks. The bedform wavelengths range from 500 to 2000 m, and the crests are orientated perpendicular to the canyon axis (Fig. 5.2.21b). The canyon head begins as a 1000 m wide V-shaped valley (Fig. 5.2.21a) and widens to 1500 m with a gentler U-shaped geometry that progressively deepens (200 m) (Fig. 5.2.21a). The canyon narrows to the toe (700 m) and maintains a near uniform incision depth (~150 m). Notably, this canyon expresses steep gradients of its walls at ~24° throughout its length. A peculiarly prominent axial incision extends for 28 km downslope (Fig. 5.2.21a). This incision has a relief of 40 m and width of 200 m along a strict V-shape profile (Fig. 5.2.21c).

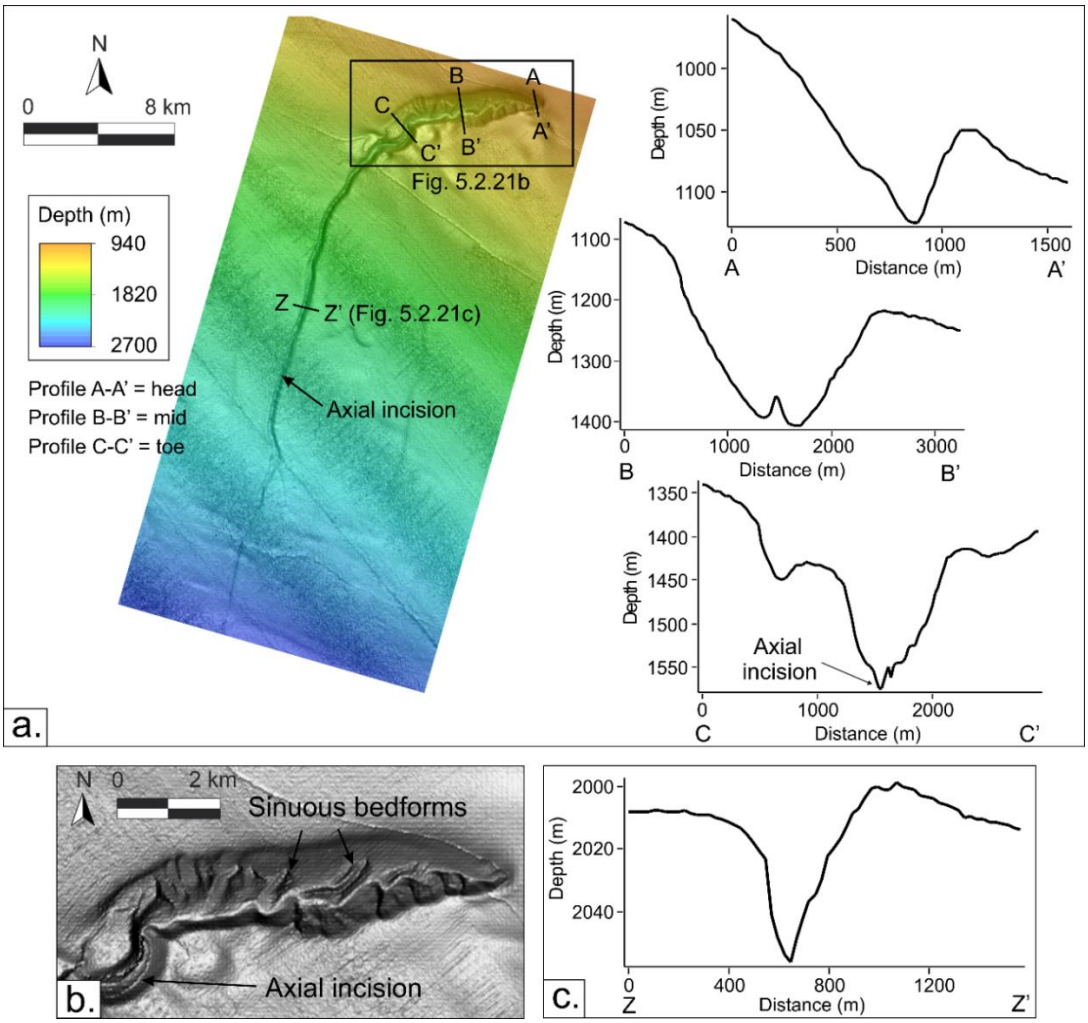

Figure 5.2.21: The features of the Lewis Canyon (A – C). **A.** Bathymetry and associated bathymetric cross sectional profiles of the head (A-A'), mid-canyon (B-B') and toe (C-C'). The bathymetry shows a 28 km axial incision which

extends beyond the toe of the canyon. **B.** A hillshaded bathymetric data associated with the actual Lewis Canyon channel which express numerous sinuous bedforms and the axial incision in the toe region. **C.** The cross section of the axial incision shows maximum dimensions that are 200 m wide and 40 m deep.

The Layne Canyon

The Layne Canyon is the southern-most hook canyon in the study area. It is a low sinuosity system (1.04). It is associated with numerous occurrences of downslope-orientated, subdued, curvilinear bedforms that coalesce into an axial incision that defines the canyon thalweg (Fig. 5.2.22a). The head component of this canyon is not included in this bathymetric dataset, it is therefore assumed that the edge of this dataset represents the canyon head. There is a widening of this canyon from 1200 m at the head to 2100 m at the mid-canyon, narrowing toward the toe (1200 m) (Fig. 5.2.22a). The head is defined by a narrow V-shaped cross section 1200 m wide and with a relief of 70 m. The mid-canyon transforms to a gentler U-shaped geometry (2100 m wide and 150 m deep) with a lengthy axial incision (Fig. 5.2.22a) that becomes more pronounced down-canyon. The axial incision extends beyond the toe for a further 12.5 km (Fig. 5.2.22a). This incision has a relief of 15 m and a width of 110 m and has a distinctive channel-levee geometry (Fig. 5.2.22b). There are prominent gas pipes and brightened parabolic reflectors associated with this canyon (Fig. 5.2.23). The pipes consist of either brightened reflectors or acoustic blanking (Fig. 5.2.23). Notably, SF4a and surface D is missing in the seismic data.

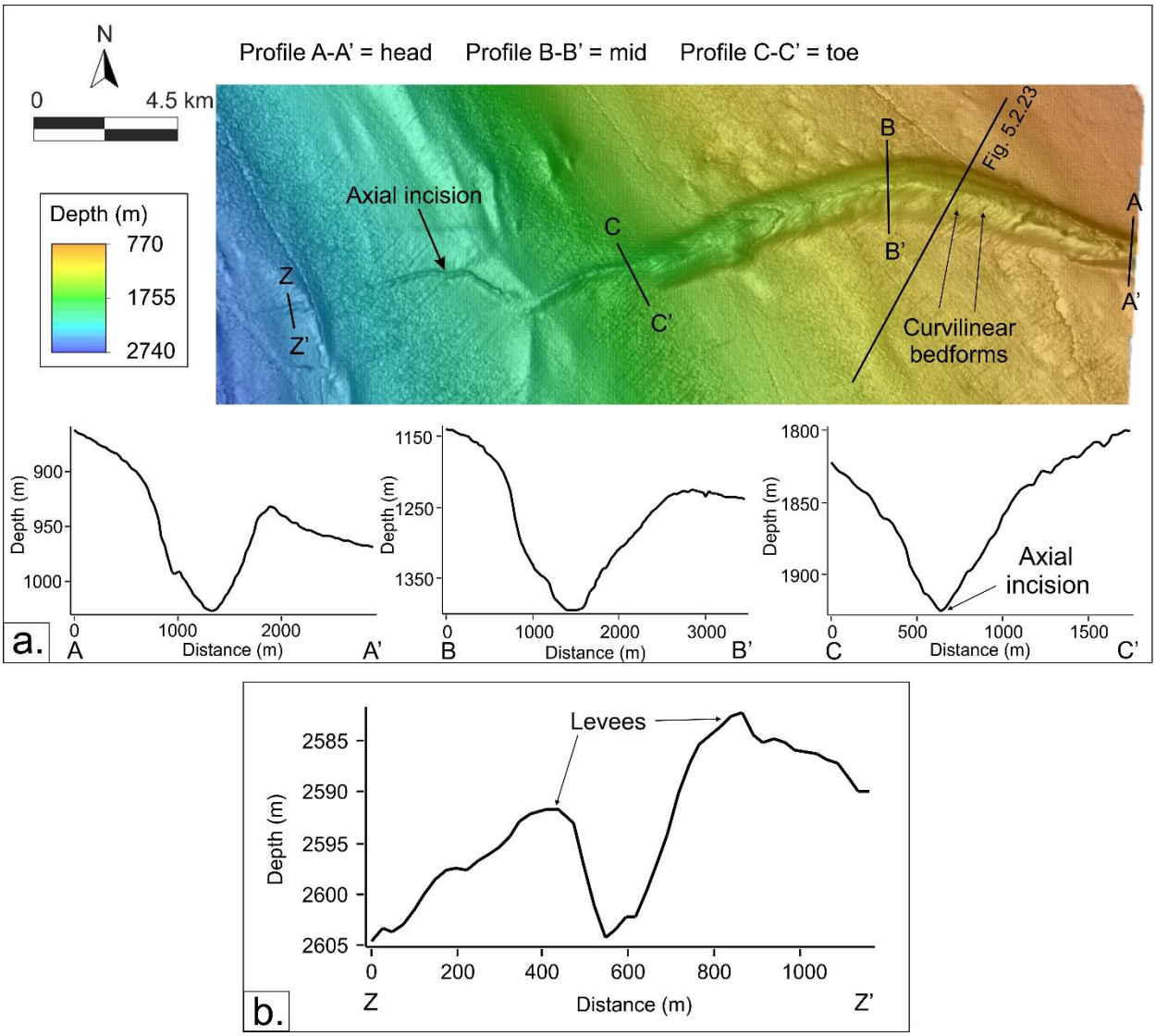

Figure 5.2.22: The morphological features of the Layne Canyon (A – B). **A.** Bathymetry and associated bathymetric cross-sectional profiles of the head (A-A'), mid-canyon (B-B') and toe (C-C'). The bathymetry shows a 12.5 km axial incision which extends beyond the toe of the canyon. **B.** The cross section of the axial incision (110 m wide and 15 m deep).

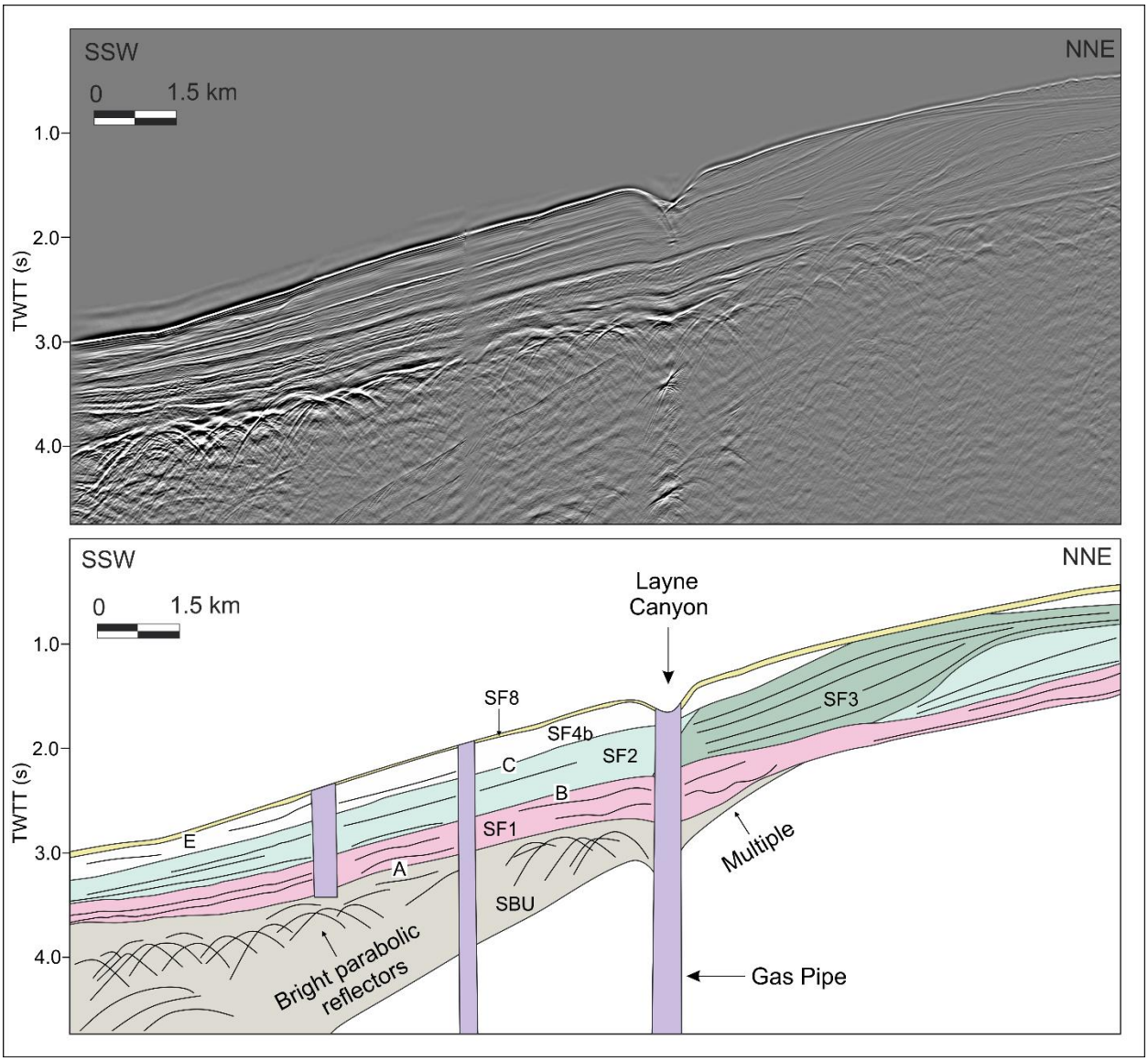

Figure 5.2.23: Seismic profile through the Layne Canyon (above) showing its association with gas pipes and brightened parabolic reflectors (below).

5.3. FLUID FLOW AND POCKMARK FEATURES

The pockmark occurrences within the study area amount to 2219 features with varying morphologies. The pockmarks are all confined to the uppermost continental slope between depths of 325 m and 1196 m. The most prominent pockmark occurrences are in Zone A (950) and C (1251), whereas only 18 pockmarks are found in Zone B.

Zone A Pockmark Field

Zone A contains 950 pockmarks over an area of 2048 km^2. This pockmark field ranges in depth between 325 and 1251 m (Fig. 5.3.1a). There are three distinct clusters of pockmarks (Fig. 5.3.1b): a major accumulation in the 325 – 680 m range (Cluster 1), and two lesser accumulations in the 680 – 1070 m (Cluster 2) and 1070 – 1251 m (Cluster 3), ranges respectively. There is a cluster of high-relief pockmarks (between 43 and 77 m pockmark depth) located at deeper seafloor depths (1000 and 1200 m) (Fig. 5.3.1b). Spatially, these deeper pockmarks tend to cluster around the distinct change in canyon orientation of the Cape Canyon, and the arcuate heads of the Oli Canyon Systems (Fig. 5.3.1a). The morphologies associated with Zone A include: circular, elongate, crescentic or stringed (Fig. 5.3.2a). Of particular interest is the peculiar crescentic, string-like morphology (Fig. 5.3.2b) of pockmarks located in the northern regions of Zone A.

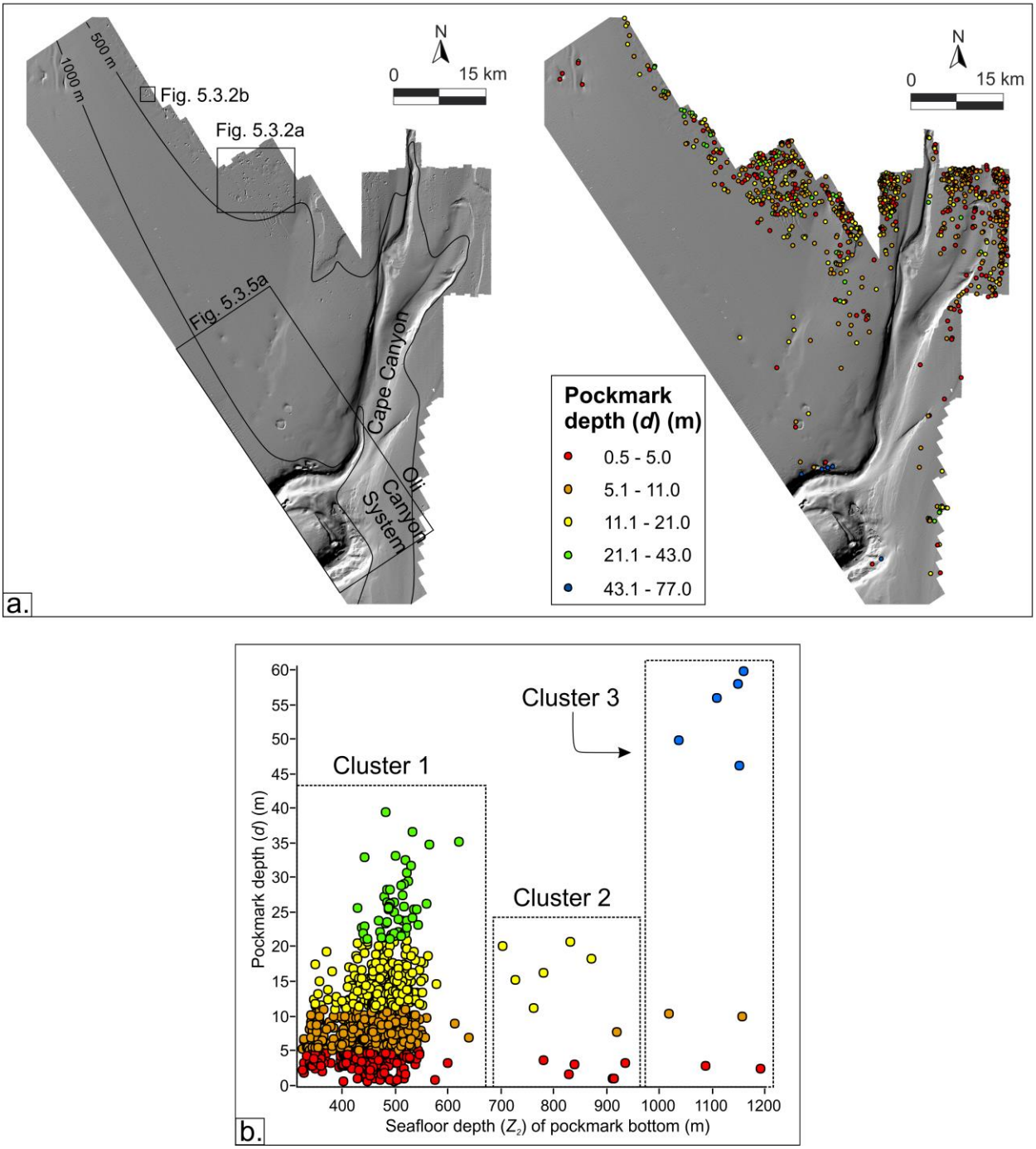

Figure 5.3.1: The pockmarks of Zone A. **A.** Hillshaded bathymetry showing the overall extent of pockmark field, as well as the quantification of their bottom depths. **B.** A scatter plot of the pockmark depth (d) versus the seafloor depth (Z_2) showing three clustering pockets.

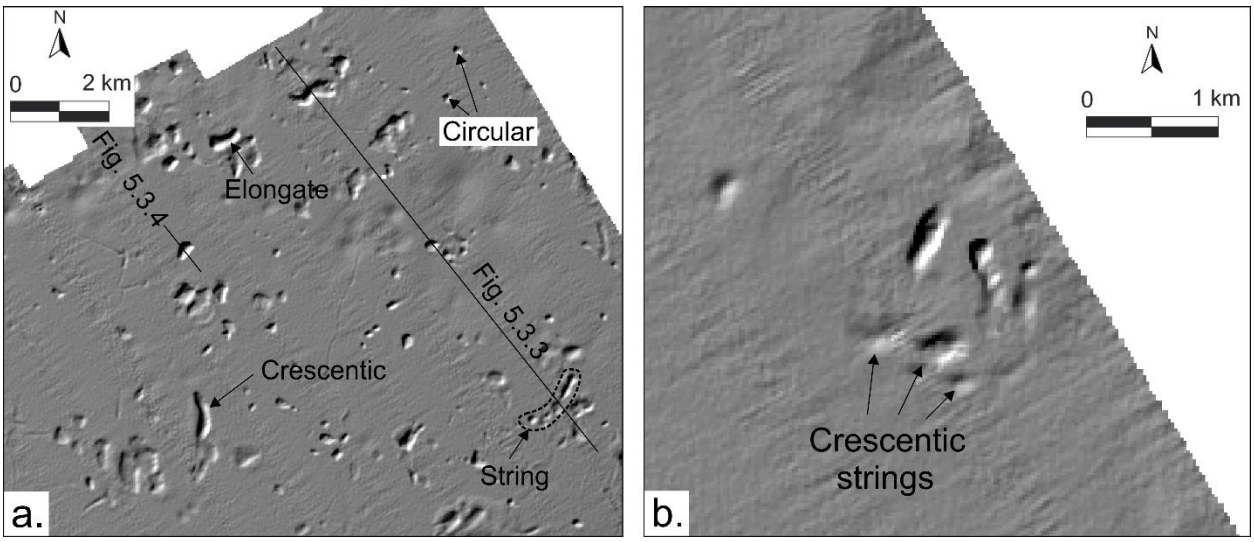

Figure 5.3.2: The various morphological expressions of pockmarks in Zone A. **A.** Circular, elongate, crescentic and stringed pockmark morphologies with seismic line. **B.** The crescentic string morphology.

The pockmarks are associated with subsurface gas pipes which are narrow (<400 m) and deep-seated (>800 m) features that have a sub-vertical to vertical long axis (Fig. 5.3.3 & 5.3.4). The contents of these pipes show stacked high amplitude reflectors with a convex upward relief (Fig. 5.3.3 & 5.3.4). They are generally the same width as the surface pockmarks (100 – 600 m). Stratigraphically, they appear to originate from the brightened parallel reflectors of SF1 or SF4a.

There are three cases in which the gas pipes interact with the host stratigraphy:

1. They cut across the entire seismic stratigraphic sequence along a sub-vertical axis to emerge as seafloor pockmarks, evident on the bathymetry (Fig. 5.3.3).
2. Pipes truncate along the SF2 – SF4a boundary, adjacent to which a neighbouring pipe emerges from the SF4a – SF4b boundary towards the seafloor, terminating as a surficial pockmark giving an overall "stepping" pattern (Fig. 5.3.4).
3. Some pipes emerge from the SF4a unit and terminate on the seafloor as a surficial pockmark (Fig. 5.3.3).

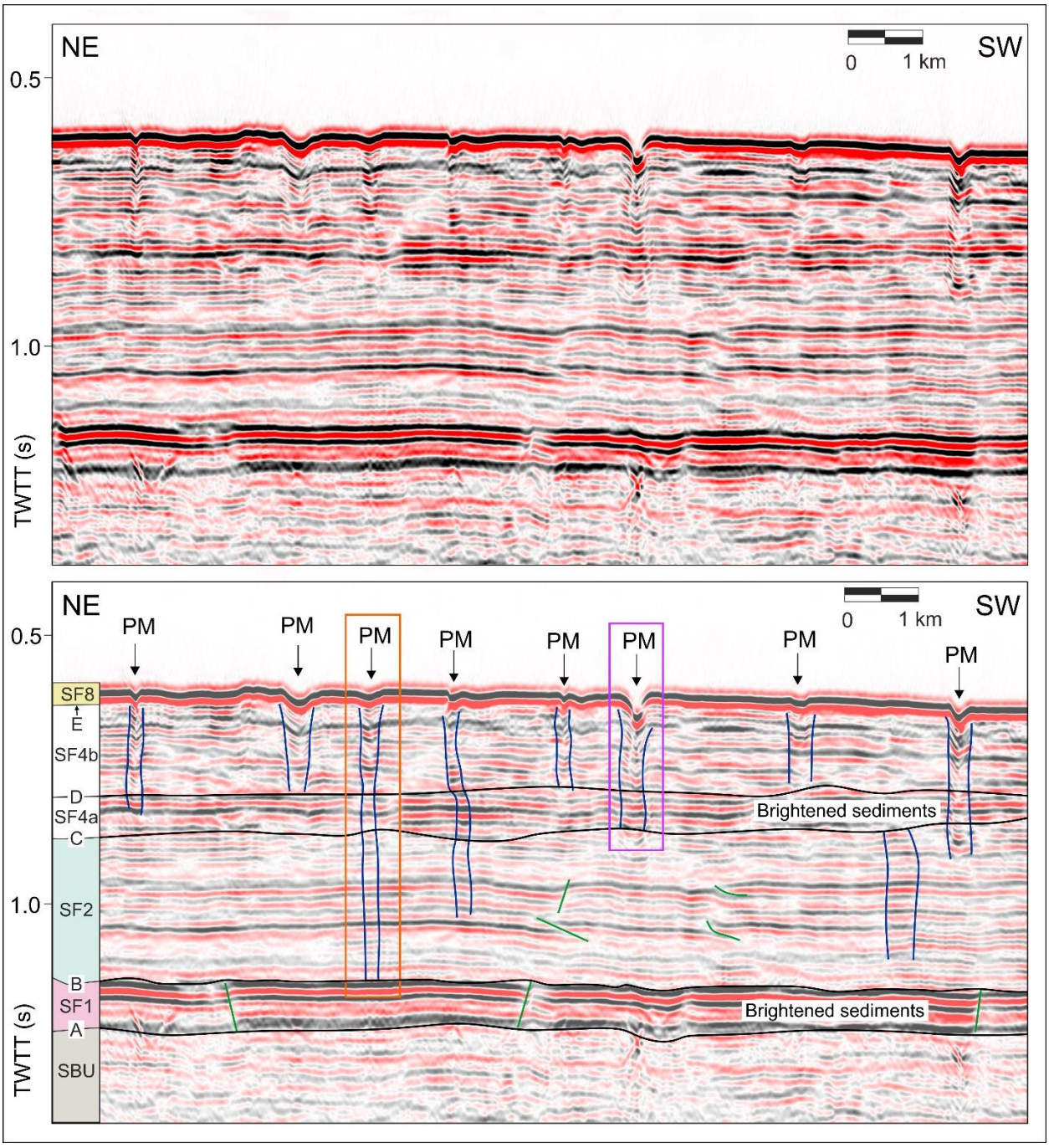

Figure 5.3.3: Seismic reflection profile (above) across the various pockmark morphologies in Zone A and interpretations (below). Pockmarks are marked on the seafloor as "PM", gas pipes are indicated by solid blue lines and faults marked by solid green lines. The orange box indicates a continuous pipe which emerges from SF1 and terminates as a pockmark on the seafloor and the purple box indicates a pipe that emerges from SF4a and terminates on the seafloor.

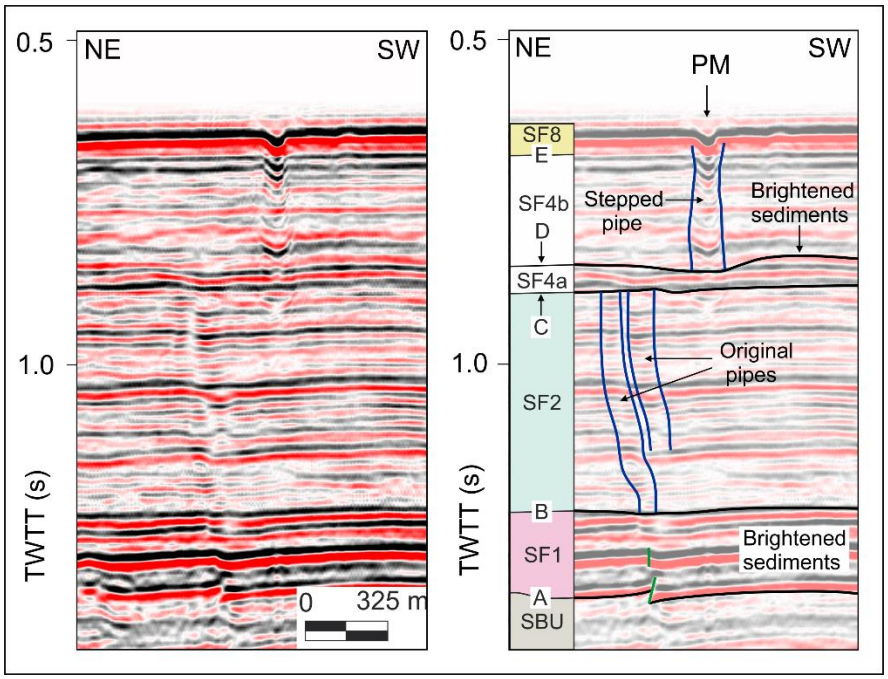

Figure 5.3.4: Seismic reflection profile (left) intersecting a circular pockmark in Zone A (from Fig. 5.3.2a) and interpretation (right). The pockmark is indicated by the "PM" on the seafloor, pipes are marked by the blue outline and faults are marked by the green solid line. Note the "stepping" pattern of the original pipes originating from SF1 and the stepped pipes originating from SF4a.

There are 18 mega-pockmarks all of which are circular in morphology (<1700 m diameter), located in the western-most portion of Zone A between 900 and 1200 m depth (Fig. 5.3.5a). These features are located adjacent to the walls of the Cape Canyon where it changes orientation, and the heads of the Oli Canyon System (Fig. 5.3.5a). Seismic data towards the edge of the largest pockmark (1700 m diameter) reveals a gas pipe ~750 m wide (Fig. 5.3.5b). The body of this pipe contains stacked columnar reflectors in a strict convex upward manner (Fig. 5.3.5b). Notably, the continuity of the reflectors is maintained relative to the adjacent strata without any terminations at the boundaries of the pipe (Fig. 5.3.5b).

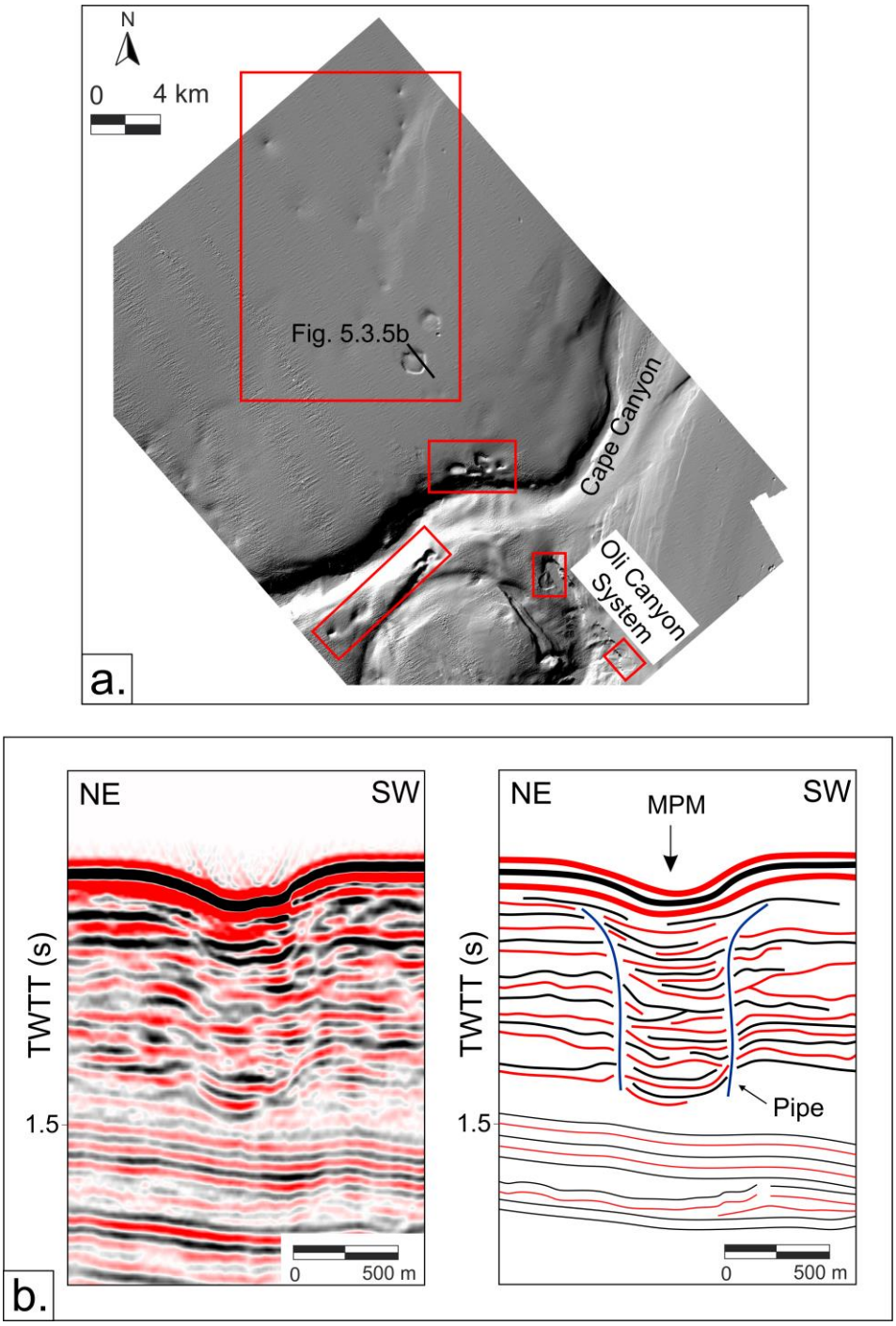

Figure 5.3.5: Mega-pockmarks of Zone A. **A.** Hillshaded bathymetric data of the mega-pockmarks in Zone A, many of which are located along the walls of the Cape Canyon and the heads of the Oli Canyon System (indicated by the red boxes). **B.** Seismic reflection profile (left) intersecting the largest mega-pockmark in the study area. The adjacent interpretation of seismic data (right) emphasizes the extent of the mega-pockmark (MPM) and associated pipe (indicated by blue solid line) that consists of convex up stacked reflectors. These reflectors merely bend and do not terminate along the boundaries of the pipe.

Zone B Pockmarks

There are a total of 21 widely spread pockmarks over an area of 251 km^2 (Fig. 5.3.6a). These span depths of 422 to 1191 m. The pockmarks mostly tend to cluster in the shallower regions in this portion of the dataset (Fig. 5.3.6b) and take the form of circular and elongate seafloor features (Fig. 5.3.7). In some instances, single circular pockmarks have merged with neighbouring pockmarks to form composite morphologies (Fig. 5.3.7).

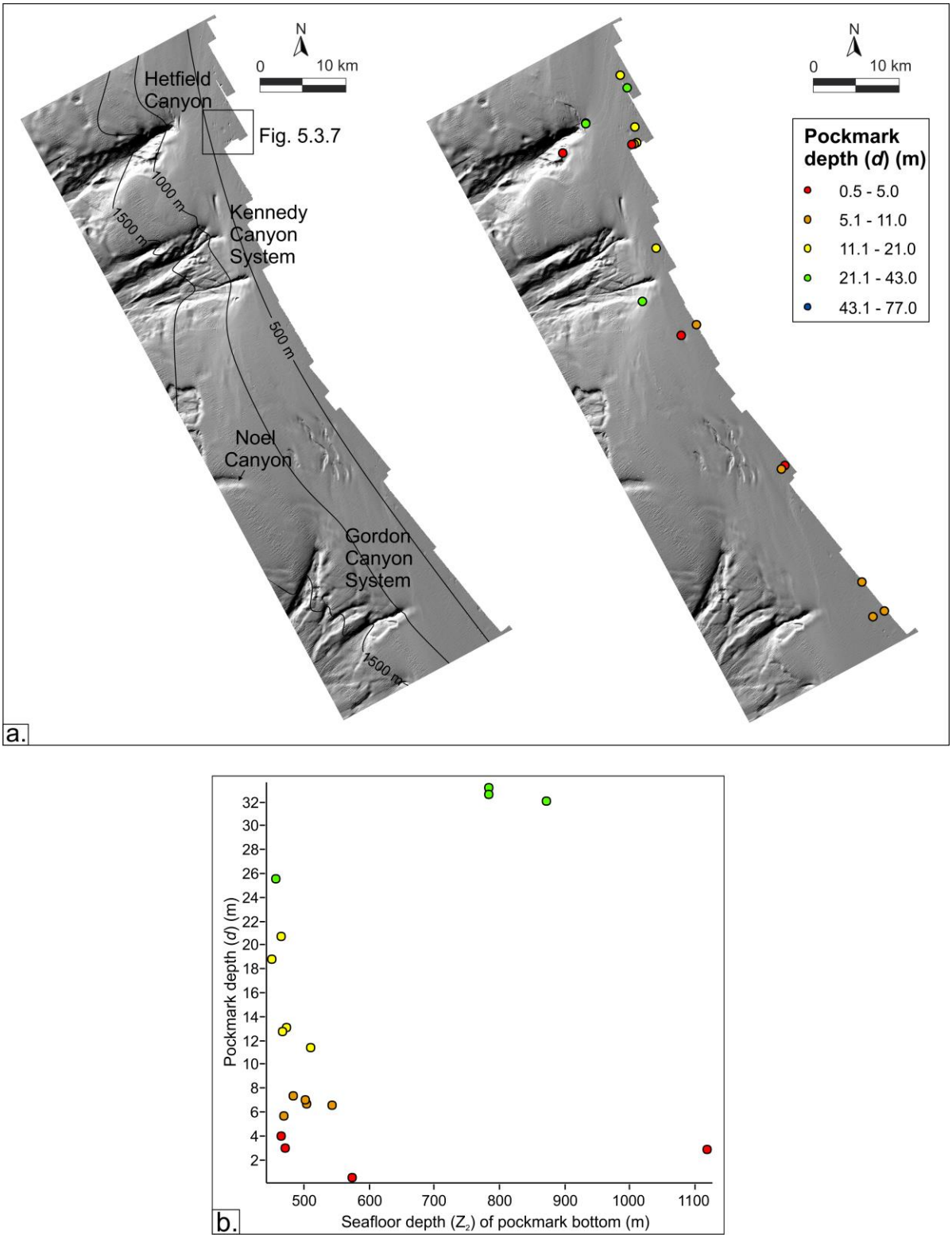

Figure 5.3.6: The pockmarks of Zone B (A - B). **A.** Hillshaded bathymetric image showing overall extent of the pockmark field as well as their respective floor-depths. **B.** A scatter plot of the pockmark floor-depth (d) versus the seafloor depth (Z_2) showing a single cluster at shallower depths.

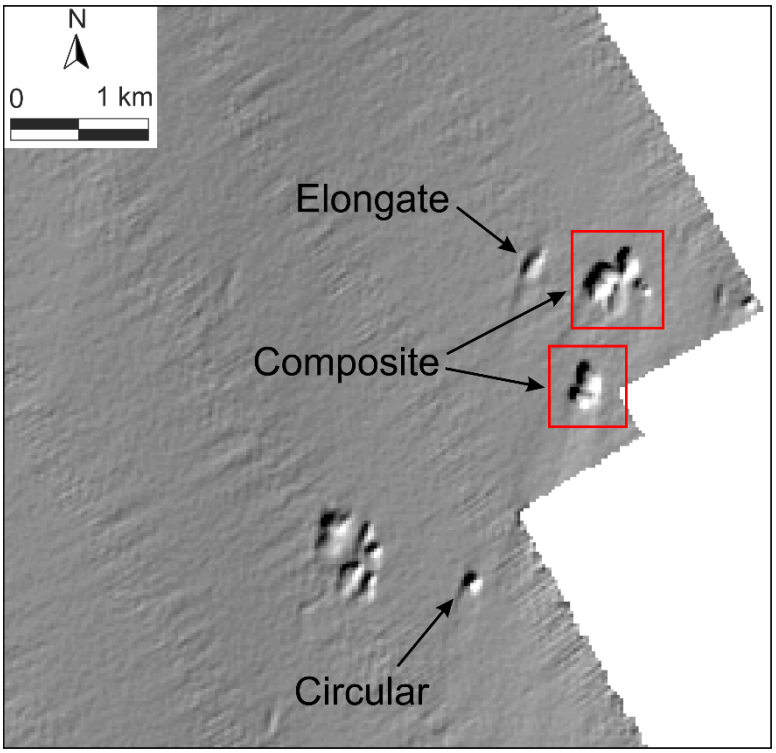

Figure 5.3.7: The elongate and circular pockmark morphologies in Zone B. The composite pockmarks are marked by the red boxes.

Zone C Pockmarks

Zone C has a total of 1251 pockmarks that span an area of 1712 km^2. These are located at seafloor depths between 391 to 1196 m (Fig. 5.3.8a). The pockmarks are unusually dense and as such, lack appreciable inter-pockmark space (usually several tens of meters). Adjacent to these pockmarks are large, NW-SE orientated elongated lobes of seafloor measuring up to 60 km^2 (Fig. 5.3.8a) and 29 km^2 (Fig. 5.3.9b). There is a subdued linear canyon, orientated NE-SW, that coalesces into the lobe shown in Figure 5.3.8a. Statistically, there are three accumulations of pockmarks in relation to seafloor depths (Fig. 5.3.8b): a 390 – 630 m range (Cluster 1); a 670 – 840 m range (Cluster 2); and a 980 – 1196 m (Cluster 3) range. Many of these features are linked with one another at their rim, and are defined by circular, elongate, stringed, or composite morphologies (Fig. 5.3.9a).

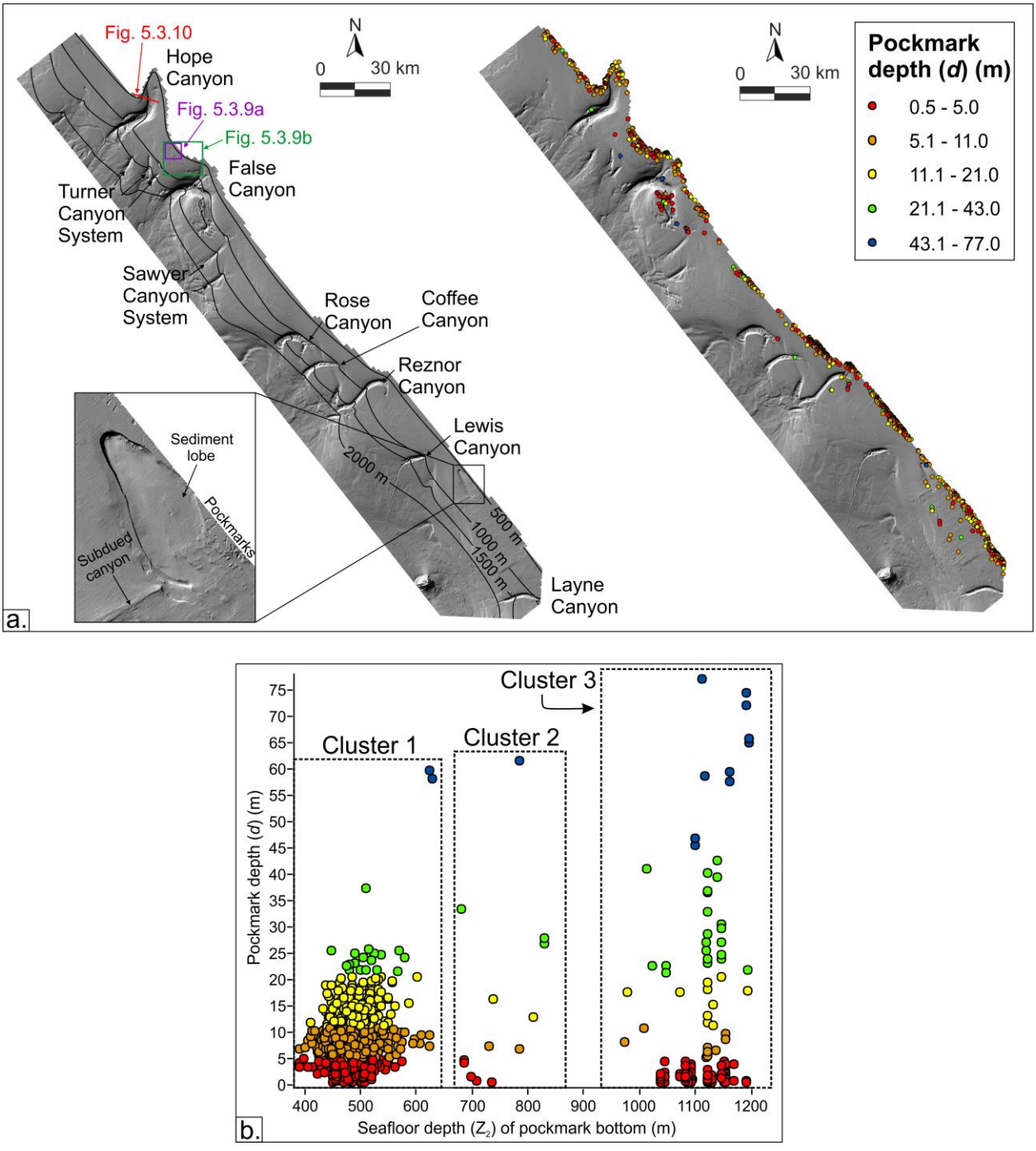

Figure 5.3.8: The pockmarks of Zone C. **A.** Hillshaded bathymetric image showing the overall extent of the pockmark field as and their respective floor-depths. Notable features associated with the pockmarks is a large sediment lobe and a subdued canyon. **B.** A scatter plot of the pockmark floor-depth (d) versus the seafloor depth (Z_2) showing three clusters of pockmarks.

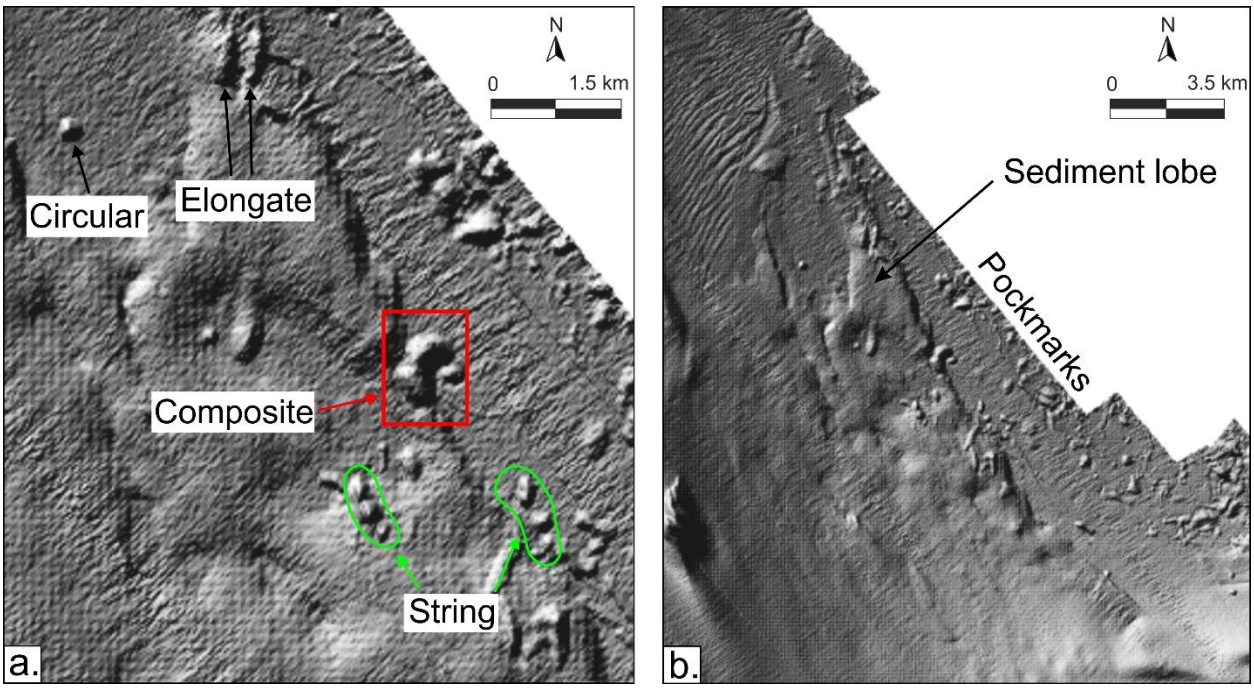

Figure 5.3.9: The pockmarks of Zone C (A – B). **A.** The morphologies of Zone C pockmarks showing circular, elongate, stringed (indicated by the green outline) and composite (indicated by the red box) forms. **B.** A large sediment lobe associated with the pockmarks of Zone C.

Notably, these pockmarks generally lack defined gas pipes and linkages between pockmarks and pipes cannot be established in most cases. However, there are minor occurrences of gas pipes (up to 400 m in width) connecting to a present-day pockmark or terminating along surface C (Fig. 5.3.10). Their seismic cross sections consist of either stacked convex up reflectors, brightened reflectors or acoustic blanking (Fig. 5.3.10). The pockmark rims tend to amalgamate with one another creating a complex undulating surface along the present-day seafloor (Fig. 5.3.10). There is a prominent seismic signal attenuation under the Hope Canyon, which precludes a seismic stratigraphic appraisal (Fig. 5.3.10).

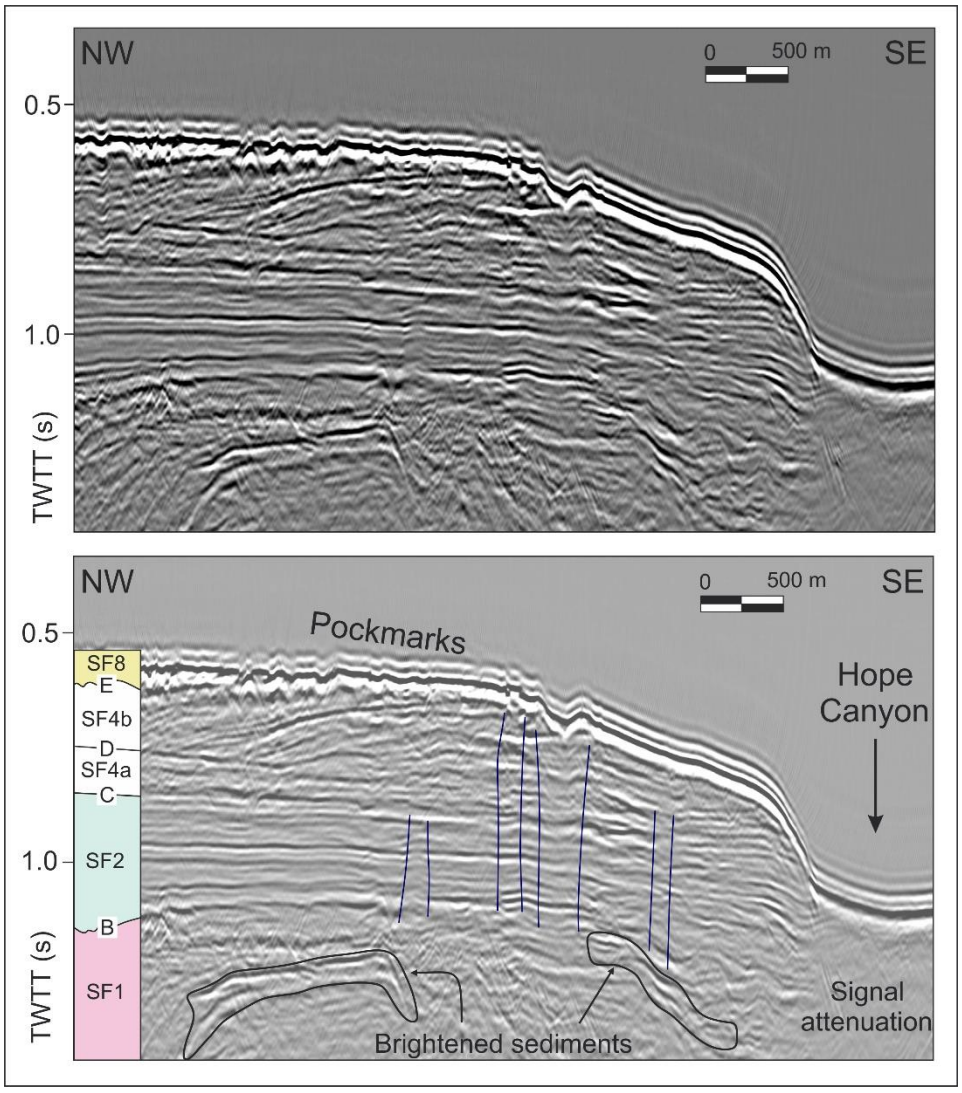

Figure 5.3.10: Seismic profile intersecting several pockmarks of Zone C (top). The interpretation (below) shows the seismic stratigraphy, surficial pockmarks and gas pipes (blue outline) and brightened sediments within the body of the SF1 unit. Note the lack of pipe continuation to the seafloor in some cases and termination along surface C (SF2 – SF4a boundary). There is a key signal attenuation under the Hope Canyon of which no stratigraphy is recorded.

CHAPTER 6

DISCUSSION

This chapter summarises the results with respect to the genesis of the linear, sinuous and hooked canyons of the southwestern Cape continental margin. Conceptual models are presented to relate the role fluid venting plays in the geographic positioning of particular canyon morphologies, and their evolution to their contemporary geomorphologies.

6.1. GENERAL SEISMIC STRATIGRAPHY

The ages of the shallow seismic stratigraphic units and their bounding surfaces provide meaningful insights into fluid (gas) liberation and the development of the canyon systems in the area. These bounding surfaces and their timing in relation to sea-level changes are displayed in Figure 6.1.1. The establishment of the fully opened Atlantic Ocean during the Late Cretaceous breakup of Gondwana (Watkeys & Sokoutis, 1998) led to the continuation of the drift phase of deposition on the passive margin within the Orange Basin (Dingle, 1992). This stage reconciles with surface A – E and seismic units SF1 – SF8 of this study. Notably, the transitional phase which hosts the first marine incursions (Aptian age) are absent on this southern part of the basin, confirmed by Van der Spuy (2003).

Surface A marks the contact between crystalline basement rocks and the onset of Albian sedimentation within the basin (e.g. Broad et al., 2006). SF1, which overlies this surface, correlates to the first occurrences of marine sediments along the western margin of South Africa after the establishment of the fully opened Atlantic Ocean in the drift phase at ~93 Ma (cf. Broad et al., 2006; Kuhlmann et al., 2010). The seismic characteristics of SF1 indicate its potential as a source rock (Turonian age - Kuhlmann et al., 2010). The strong parallel reflectors of the SF1 unit in the gas-rich domains of Zone A and C are interpreted to have acquired their high amplitudes through gas brightening (Løseth et al., 2009; Weschenfelder et al., 2016). The lateral continuity of this was considered to be the product of margin-parallel currents that transported sediment along the newly forming continental slope during this time (Dingle et al., 1983).

Surface B, marks the Turonian – Coniacian boundary and hosts the first occurrence of major palaeo-canyons on the margin (e.g. Fig. 5.2.3 & 5.2.10) and reflector corrugations (e.g. Fig. 5.3.10). These corrugations have the exact scale and shape as the contemporary inter-canyon rill features (e.g. Fig. 5.2.10) and are therefore interpreted as palaeo-rill features, which are suggested to be the precursor to canyon formation (Pratson & Coakley, 1996; Green, 2011a). Importantly, there was a global sea-level fall at the Turonian – Coniacian boundary (Fig. 6.1.1), imprinting the first rills and canyons in the stratigraphy.

The multiple canyon incisions that characterise the Maastrichtian – Danian boundary, surface C, have been attributed to increased erosion by slope confined canyons (Uenzelmann-Neben & Huhn, 2009). Previous studies have similarly recognised a regional signal in the dominant erosional patterns of the Maastrichtian – Danian crossover along the South African coastline (Dingle et al., 1983; Green, 2011b; Kuhlmann et al., 2010).

From the observations (e.g. Fig. 5.1.4 & 5.2.10), the palaeo-canyons filled by SF7 have incised SF4, which lies above surface D that represents the Palaeocene – Eocene boundary. Therefore, the palaeo-canyon channels that define the base of SF7 are interpreted to be of Early Oligocene age (cf. Petters, 1984). This corresponds to a hinterland uplift episode in southern Africa (Partridge & Maud, 1987) and a global sea-level low (Fig. 6.1.1) which would have permitted canyoning during this time. The infills of SF7 itself are likely to be of Late Oligocene – Early Miocene age, corresponding to a rise in sea-level (Fig. 6.1.1) which will permit the development of canyon fill sequences (cf. Petters, 1984).

Surface E is interpreted to be the Mid-Miocene unconformity (Hicks & Green, 2017) and can be traced all over southern Africa, which formed in response to epeirogenic uplift of the hinterland by 150 – 300 m (Partridge & Maud, 1987). Overlying this surface is the Holocene-age unit SF8. Its transparent acoustic properties and general draped nature point to recent (at the least Holocene) low-energy conditions with an overall quiescence of the canyons. A similar situation is documented on the east coast of South Africa (Green, 2011b).

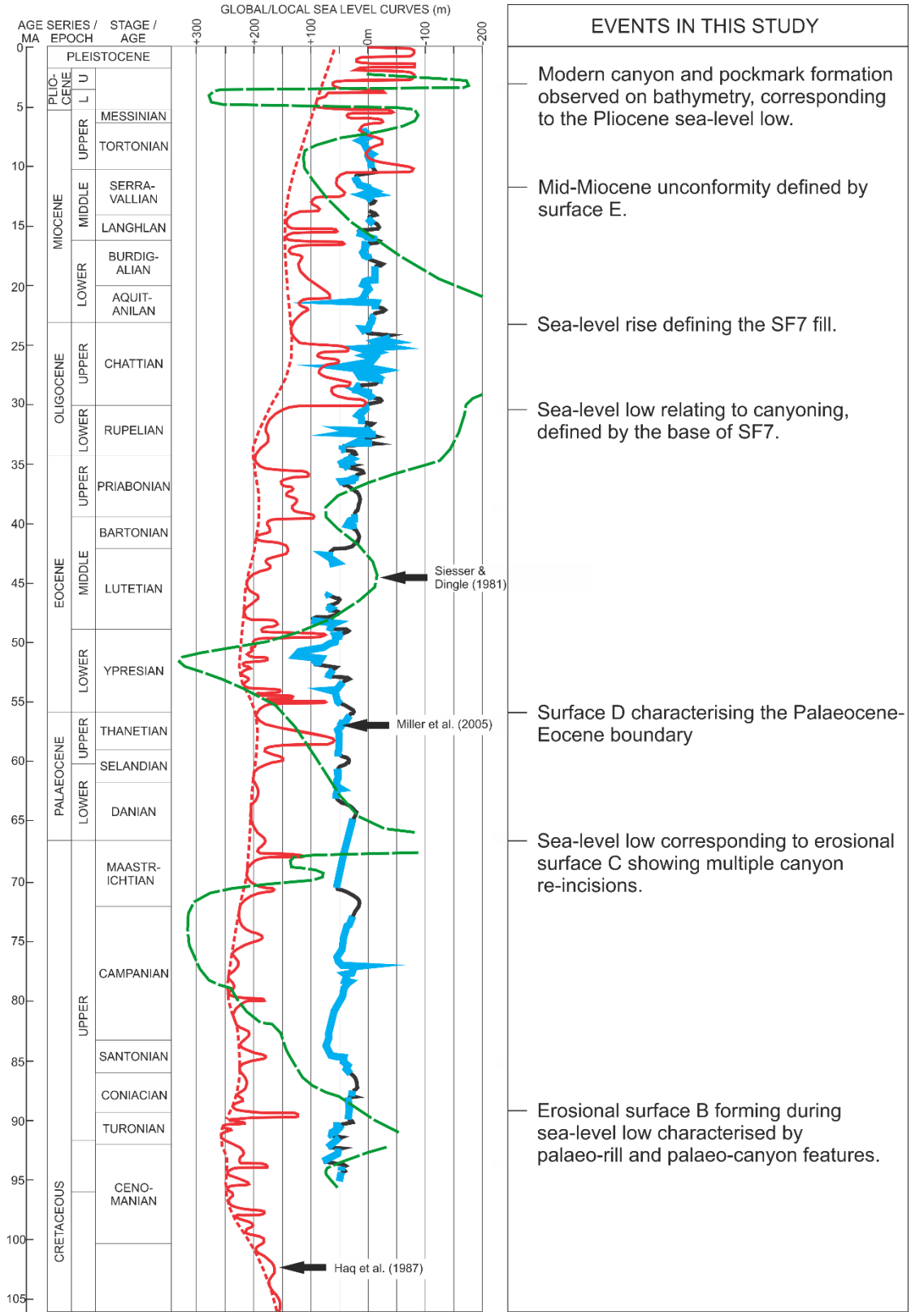

Figure 6.1.1: Global (Haq et al., 1987; Miller et al., 2005) and local (Siesser & Dingle, 1981) sea-level curves relating the events of canyoning and filling in the study area.

6.2. SUBMARINE CANYONS

All the submarine canyons in the study area are suspected to have formed in the Pliocene, in response to uplift of the hinterland (Wigley & Compton, 2006). They reside on the continental slope (~60 km offshore) with the exception of the Cape Canyon which incises the shelf (Dingle et al., 1983; Wigley & Compton, 2006; Compton & Wiltshire, 2009). It is therefore suggested that the formation of these canyons are not associated with the river-fed hyperpycnal plumes, especially as there is no direct present-day fluvial linkage or strong evidence for an ancient one. Hill et al. (2005) suggested that an external sediment source, such as a fluvial one, is not essential to initiate canyon incision through sediment mobilisation. Slope and/or shelf sediment is therefore sufficient to initiate oversteepening and/or turbidity currents (Piper & Normark, 2009). Furthermore, the canyons in this study do not have corresponding fan lobes attached to their trunks, thereby reinforcing the idea that the sediment being reworked is of strict marine origin (cf. Piper et al., 2005). It is proposed by Wiles et al. (2013) that the absence of fan lobes is due to bottom current winnowing which would have either removed existing fans or prohibited their development. It is well known that the North Atlantic Deep Water (NADW) bottom current exists between the depths of 1500 to 4000 m (Weigelt & Uenzelmann-Neben, 2004) where fan lobes are suspected to form. It is therefore accepted that fan lobes are winnowed away by the NADW system (Wiles et al., 2013). This peculiar phenomenon exists in the Durban Basin on the east coast of South Africa (Wiles et al., 2013; Hicks & Green, 2017).

Many current canyons inherit older canyon channels, particularly that of the Early Oligocene canyon systems filled by SF7 (e.g. Fig. 5.2.3, 5.2.10 & 5.2.18). This is likely to have occurred due to the remaining topographic low of the palaeo-canyon caused by the incomplete fill of SF7, allowing for modern turbidity currents to get caught within this palaeo-channel forcing re-incision (cf. Bertoni & Cartwright, 2005; Green, 2011a; Hicks & Green, 2016). Furthermore, the sediments that comprise SF7 could be softer and therefore more vulnerable to erosion by turbidity flows (cf. Pratson et al., 1994).

6.2.1. Linear Canyons

The linear canyons of the study area are considered as the youngest canyons of the study area and are suspected to be the product of submarine rill amalgamation (Pratson & Coakley, 1996), evidenced by a series of rills at the O2 Canyon toe (Fig. 5.2.5), G1 Canyon toe (Fig. 5.2.8) and in the Noel Canyon System (Fig. 5.2.10). This thesis proposes that slope failure of an initial oversteepened slope occurs and cuts narrow and shallow rills which increase in relief over time (Pratson et al., 1994) due to turbidity flows. This is apparent from the deepening and general increase in relief of many of the smaller rill systems in the canyons (e.g. Fig. 5.2.7 & 5.2.8).

The linear evolution of these rills into larger systems causes subsequent retrogressive failure and the beginnings of both lateral and headward erosion (Pratson & Coakley, 1996) to set up incipient canyons (Lastras et al., 2011). This can be seen in the U-shaped portions of many of the canyon features, which form by widening and headward-extension. This mechanism displays a simultaneous bimodal erosive phenomenon involving the initial slope failure in a downslope direction together with retrogressive erosion creating a strong turbidity current (Piper & Normark, 2009). The slopes of this area are steep enough (2 – 3.5°) to sustain fully erosive turbidity currents (Piper & Normark, 2009).

Axial incision of the canyon floor is believed to be an important pre-conditioning factor for mass wasting events along linear canyon channels (Baztan et al., 2005; Arzola et al., 2008). This is evidenced by the abundance of these features within the linear systems pointing to a more youthful phase in the canyon development continuum, when compared to the sinuous and hooked canyons that lack the prominence of these intra-canyon features (Chapter 6.2.2 & 6.2.3). Rather, they are associated with older subdued intra-canyon axial incisions or axial incisions that are attached downslope from the toe regions, suggesting the onset of extending the length of the canyon channel (Baztan et al., 2005).

The absence of pockmarks associated with the linear canyons implies that there is no interaction between venting and canyon form. As described above, these morphologies can be simply formed through sediment failures and the resulting high energy turbidity currents (Mitchell, 2004; Pratson et al., 2007; Piper & Normark, 2009). Their relatively short lengths affirm their youth when compared to the more elaborate erosion styles of the neighbouring sinuous and hooked canyons.

6.2.2. Sinuous Canyons

The sinuous canyons are believed to have evolved from further retrogressive erosion of the linear canyons. These systems all have associated gas pockmark features along the walls of the head and mid-canyon regions, and as such, these may act as a preconditioning mechanism for sediment failure (Valle & Gamberi, 2011). Evidenced by multiple depositional bodies sediment lobes and mass transport deposits (MTDs), flow interaction is therefore suggested to be disrupted (Babonneau et al., 2002). Each of the sinuous canyons are discussed individually below due to their unique characteristics.

The Cape Canyon

The protracted change in channel orientation of the Cape Canyon (1000 – 1200 m depth) is marked by the presence of mega-pockmarks adjacent to the canyon walls. Slope failure due to gas liberation is a well-documented phenomenon (Nakajima et al., 2014; Sun et al., 2017), and the venting features may have played a role in influencing the canyon behavior in these regions. Similarly, the neighbouring Oli Canyon System has a clear change in orientation at the same depth, likewise associated with numerous mega-pockmarks in the adjacent canyon interfluves and walls. It appears that the Cape Canyon was in the process of establishing a hooked morphology, before the head subsequently straightened. The straight head and its position as a shelf-indenting canyon suggests that at some point, the canyon intercepted a new source of sediment gravity flow which allowed it to then extend linearly towards the shelf break (cf. Pratson et al., 1994).

The Noel Canyon System

The chaotic strata beneath the subdued headscarps located upslope from the Noel Canyon System are interpreted as buried mass transport deposits (MTDs) (Dawei et al., 2013; Mosher et al., in press). These are products of a progressive slump failure that evolved to a downslope slide along a glide plane (cf. Mosher et al., 2010) (Fig. 6.2.1). The large-scale Cenozoic slumping along concave glide planes is documented from other parts of the basin (e.g. Dingle et al., 1983; Broad et al., 2006; Kuhlmann et al., 2010), who suggest that this occurred due to the collapse of

increasingly unstable sediments along the shelf edge. Considering the proximal shelf break at ~500 m depth, this would most likely be the case involving the re-suspension of shelf material similar to the southeastern Canadian margin (Piper & Normark, 2009) and the western US margin (Mosher et al., 2004). This appears to distort the entire stratigraphy and as such is interpreted to be a response to a falling sea-level during the Mid-Miocene that allowed sediments to prograde downslope (Kuhlmann et al., 2010).

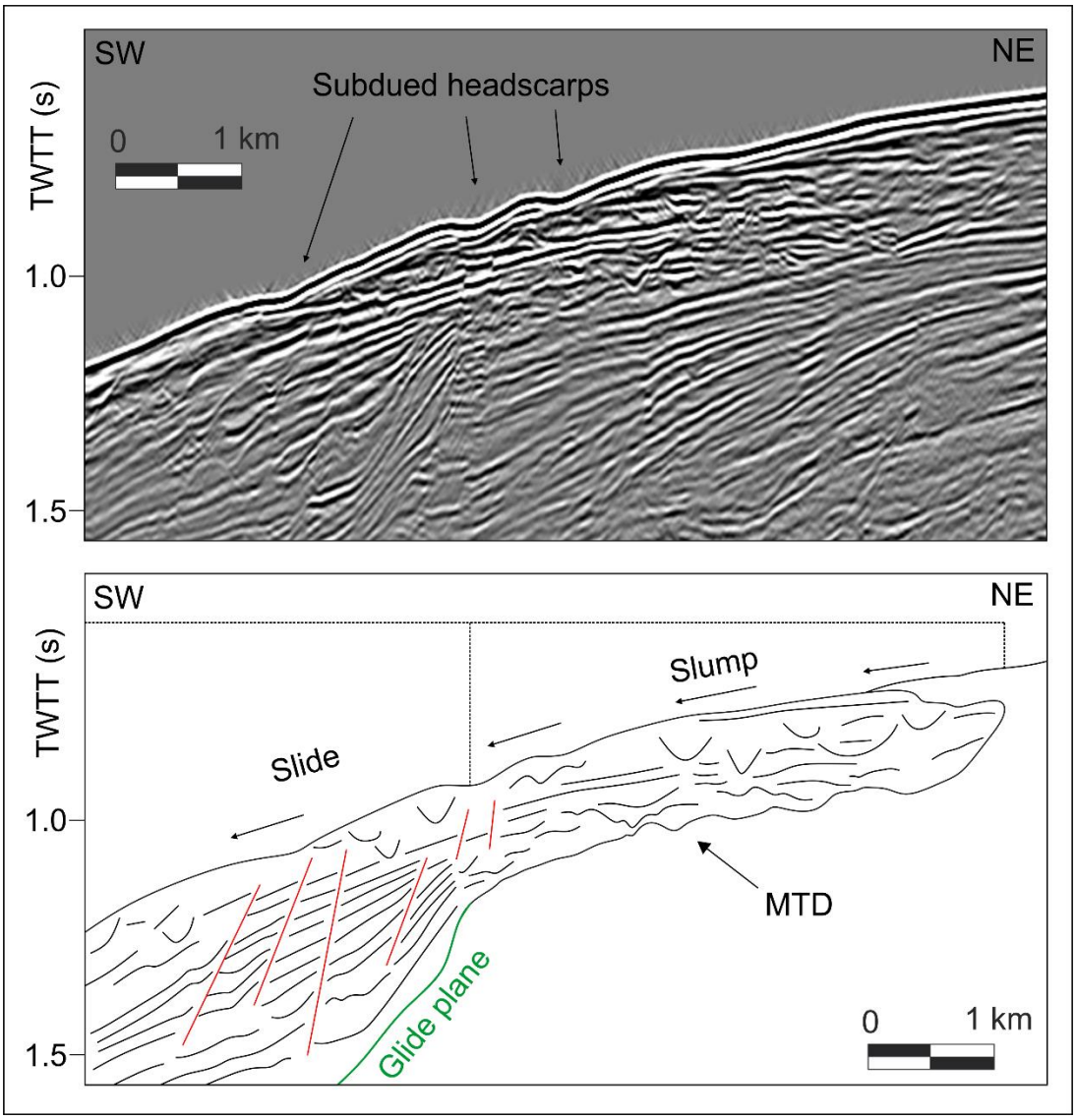

Figure 6.2.1: Seismic reflection profile of a set of subdued headscarps and underlying mass transport deposits (MTDs) (above) and interpretation of the mass movement processes (below). Note the disturbance of the entire sediment package up to the seafloor, indicating recent activity.

The seismic line in Figure 5.2.10b, collected in 1991, shows the presence of multiple rills along the N1 Canyon interfluve which are now not evident in the multibeam dataset. These rill features appear to have coalesced and slumped (observable on the bathymetric data collected in 2013). These rills are considered as canyon precursors, whereby they will eventually merge to create the main canyon channel (Pratson & Coakley, 1996; Green, 2011a; Puig et al., 2017), or incise to the point where the surrounding walls are unstable and cause retrogressive failures, provided there is a persistent sediment flow (Pratson et al., 1994). The N1 Canyon rills and the interfluve rills are interpreted to have collectively failed either by a slump and progressive slide mechanism (Mosher et al., 2010) or a debris flow (Masson et al., 1998) to produce the resultant hummocky topography. The channel of the N2 Canyon is underlain by a series of canyons which had previously occupied this area and this points to palaeo-topographic control and inheritance of the canyons and their incipient rill systems (Fig. 5.2.10b).

The Hope Canyon

The head of the Hope Canyon shows a pronounced gas curtain, observable on the seismic data, which is interpreted to be a gas-charged, mud-rich fill (cf. Andresen et al., 2009; Weschenfelder et al., 2016). The crescentic bedforms (Fig. 5.2.11b) are interpreted to be cyclic steps (Parker, 1996) caused by strong bottom current activity (Lastras et al., 2011). The merging of this cyclic step train into the central axial incision indicates the activity of high-density turbidity currents (Babonneau et al., 2013). The axial incision, which serves as a terminus for these bedforms, is interpreted to have formed from an erosive dilute turbidity current which followed a downslope mass wasting event (Baztan et al., 2005) of which the remnant sediment lobes provide evidence for (Fig. 5.2.11b). The sinuous nature of the incision within the canyon channel suggests that this flow was maintained rather than episodic (Baztan et al., 2005). The distributary is interpreted to have formed at a later post-canyon inception stage through the process of flow stripping (Peakall et al., 2000). This would involve a post-canyon turbidity flow which spilled sediment over the bend of the existing Hope Canyon channel (Piper & Normark, 1983) and formed the adjacent zone.

6.2.3. Hooked Canyons of Zone A and C

The extreme arcuate nature of the heads of the hooked canyons in the study area are undescribed in the literature and thus showcase a unique and complex formative process that is undescribed to date. Notably, the heads of these canyons are associated with numerous pockmark assemblages found in Zone A and C respectively. It is crucial to note that the pockmark fields of Zone A and C are orientated in a coast-parallel (NW-SE) fashion (Chapter 5, Section 5.3). Furthermore, the seismic data through the Layne Canyon (Fig. 5.2.23), for example, shows clear gas interaction with the host stratigraphy in the form of gas pipes, defined as columnar zones of acoustic blanking, chaotic reflections or reflector brightening (Løseth et al., 2009; Andresen et al., 2011; Horozal et al., 2017). These surface and sub-surface observations provide evidence for considerable gas migration that is in clear association with the hooked canyon morphologies. Previous authors have considered that the eustatic sea-level falls of the Pleistocene allowed for the liberation of residual gas to permit, which led to the destabilisation of slope sediment (Kayen & Lee, 1991; Hurst et al., 2011; Andresen, 2012). This, in conjunction with simultaneous canyon incision through a lowered sea-level (Baztan et al., 2005) is believed to produce the arcuate head morphology, evidenced by the hook systems that still preserve pockmark features around their existing heads (e.g. Oli Canyon System and Reznor Canyon). In other cases, it appears that these pockmark and/or gas features have completely destabilised the sediment (cf. Nakajima et al., 2014) to form an arcuate zone of slumping, as apparent from the head of the False Canyon. Importantly, these arcuate heads are also orientated in a coast-parallel fashion, corresponding to the orientation of the pockmark fields, suggesting strong venting interaction with canyon formation.

The curvilinear, crescentic and sinuous bedforms found throughout the bodies of the southeastern-most hooked canyons of Zone C are interpreted to be asymmetrical cyclic steps (Parker, 1996; Tubau et al., 2015; Covault et al., 2017). The bedforms are suggested to have matured from a curvilinear to a crescentic to a continuous sinuous depression due to bottom current activity (cf. Lastras et al., 2011). The lack of high resolution seismic data leaves this interpretation open to other possibilities such as upslope migrating sandwaves (Zhong et al., 2015) or dunes (Cartigny et al., 2011) as the nature of the bedding is unknown. However, based on bathymetric and cross-sectional comparisons from Fildani et al. (2013) and Covault et al. (2017), as well as the logical assumption of the close turbidity current influence on canyon formation (Babonneau et al., 2013),

the cyclic step hypothesis is favoured. These bedforms indicate hydraulic jumps of the flow within the canyon channel itself (Fildani et al., 2006; Kostic, 2014) and are assumed to be precursors to canyon formation (Covault et al., 2017). They are believed to have formed in response to strong bottom current activity (Lastras et al., 2011) and progressive turbidity flows (Kostic, 2011) whereby flow direction is perpendicular to the wave crests (Babonneau et al., 2013). It is noteworthy that these appear to be mostly associated with smaller, strongly hooked or sinuous systems.

6.3. FLUID FLOW AND POCKMARK FEATURES

The numerous sub-surface fluid flow features described in this study (Chapter 5, Section 5.3) are considered to have originated from a deeper-seated gas reservoir (e.g. Cartwright et al., 2007; Andresen et al., 2011). In the Orange Basin, authors have suggested deep Aptian and shallower Turonian source rocks (Van der Spuy, 2003; Kuhlmann et al., 2010). In this part of the basin, however, the Aptian intersection is missing (Van der Spuy, 2003) and only the Turonian source rock is observed, correlating to SF1. The migration of these fluids results in either storage in shallow sedimentary successions or expulsion onto the seafloor to form pockmarks (Hovland & Judd, 1988; Løseth et al., 2009). Fluid migration is evidenced in this study by numerous gas pipes, brightening of reflectors or outright acoustic blanking. Most pipes show stacked reflector bending which are classified as "blowout pipes" (Andresen et al., 2012) which indicates strong cross-stratal fluid migration (Cartwright et al., 2007). Less frequently observed are gas chimneys that are columnar zones of chaotic reflectors (Andresen et al., 2012). Assuming these vertical migratory structures have acquired their gaseous contents from a deeper reservoir, it can then be suggested that faulting mechanisms acted as a conduit to feed these pipes (Cartwright et al., 2003; Ostanin et al., 2017) which can clearly be observed in seismic section (Fig. 5.3.3 & 5.3.4). Fluid storage in both SF1 and SF4a is evidenced by the lateral gas brightened zones which charge the stratigraphy and indicate the presence of free gas (Judd & Hovland, 1992; Mazumdar et al., 2009). Essentially, this is a porous layer which acts as a "shallow gas reservoir" that traps gases originating from the deeper reservoir (Cukur et al., 2013). It is understood that gas must first accumulate in the sediments to create a pressure gradient and is subsequently forced abruptly upward to the seafloor (Cukur et al., 2013). Given the above evidences for gas storage and vertical migration (majorly in

the form of blowout pipes), it is suggested that the pockmarks in this study were created in a violent and episodic manner (Traynor & Sladen, 1997; Løseth et al., 2001).

Statistically, the high concentration of Zone A and C pockmarks in Cluster 1 (Fig. 5.3.1 & 5.3.8) indicates that vertical fluid flow was more active in the shallower regions between 350 to 700 m depth, pointing towards a larger pockmark field inshore from the bathymetry portrayed in this thesis. The Cluster 3 pockmarks of Zone A and C are found adjacent to the walls of the hooked canyon systems, suggesting that gas migration had caused major orientation and morphological changes within these canyon channels due to sediment mobility (Hovland et al., 2002; Valle & Gamberi, 2011; Andresen, 2012). The elongate, crescentic and stringed pockmark morphologies are interpreted to have been shaped to their present forms through bottom current controls modifying simplistic circular-type morphologies (cf. Hovland et al., 2002, Andresen et al., 2008). Similarly, composite morphologies are interpreted to have formed from single circular pockmark amalgamation through bottom current activity (cf. Hovland et al., 2002).

The mega-pockmark occurrences along the walls of the Cape Canyon, Oli Canyon System and Reznor Canyon are interpreted as "canyon margin" pockmarks (Benjamin et al., 2015). The fluid flows required to establish a canyon margin pockmark are considered to have migrated along a discontinuity or unconformity (Gay et al., 2006; Deptuck et al., 2007; Benjamin et al., 2015; Chen et al., 2015). In this case, one such discontinuity would be the postulated Early Oligocene canyon channels (filled by Late Oligocene – Early Miocene SF7) which could permit fluid migration along its walls (Fig. 6.3.1). These Early Oligocene canyons are marked by strong bright reflectors at their thalwegs which are interpreted to be gas brightened zones (Judd & Hovland, 1992), where free gas is believed to accumulate before migrating along the palaeo-canyon walls (Fig. 6.3.1) (cf. Orange et al., 2002; Benjamin et al., 2015).

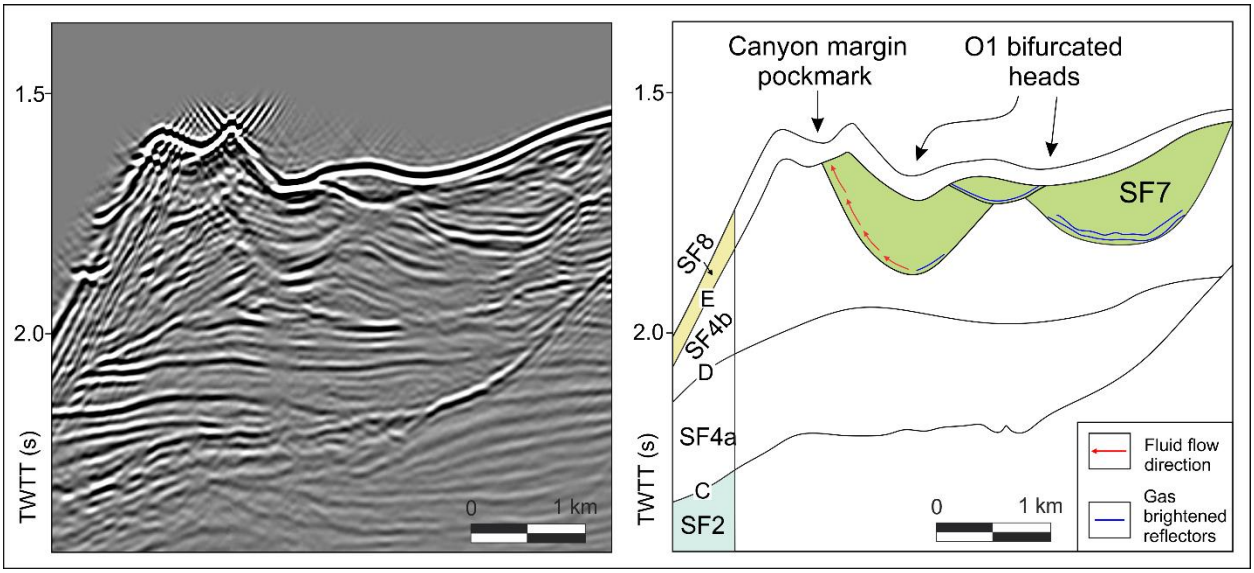

Figure 6.3.1: Seismic data across the canyon margin pockmark of the O1 Canyon (left). The interpretation (right) showing the suggested fluid flow pathway along the Early Oligocene canyon walls (which are filled by SF7).

The absence of pockmarks in Zone B is not clearly understood. The most plausible explanation would be the geological heterogeneity that exists within a gas reservoir (Zhou et al., 2016). Changes in the depositional facies can affect the permeability and porosity of a reservoir which are related to changes in energy settings (Haile et al., in press). In the case of a lack of gas features, it is believable that there is a greater mud to sand ratio thereby creating a weaker reservoir potential (cf. Sahoo et al., 2016). Alternatively, the lateral continuity of the assumed dominant sandy reservoir in Zone A and C may be poor in Zone B. Unfortunately, this cannot be confirmed due to the lack and limitations of seismic and well data.

6.4. MODELS FOR FLUID MIGRATION AND CANYON DEVELOPMENT

It is suggested that fluid flow interaction is directly related to the formation of certain canyon morphologies (sinuous, hooked and shelf-indenting). Therefore, a fluid flow model is proposed showing pathways for fluid migration within the stratigraphy. Relating to this is a canyon evolution model is to explain canyon maturation in relation to fluid flow and retrogressive erosion.

Conceptual model for fluid flow for the southwestern Cape continental margin

It is proposed that there are three main mechanisms for fluid flow in the area (1, 2 and 3 – Fig. 6.4.1):

1. Pipes cutting across the established seismic stratigraphy from SF1 in a vertical manner, without terminations, to the seafloor.
2. Pipes creating a stepping pattern along the SF2 – SF4a boundary.
3. Pipes emerging from SF4a to the seafloor.

It is assumed that the Aptian source rock within the basin (Kuhlmann et al., 2010) plays a role in fluid migration and thus pockmark formation, however not directly observed in this study. The Turonian source rock (SF1), however, sees gas pipes emerge and cut through the established seismic units and terminate on the seafloor as pockmarks (case 1).

Case 2 sees a stepping pattern, which considers that the original fluid flow was vertical from the SF1 unit, which then went through a phase of lateral flow within the SF4a unit and re-emerged as vertical flow from this unit, thereby creating a new pipe to reach the seafloor as a pockmark.

Case 3 characterises pipes that merely emerge from the gas rich unit of SF4a. The idea being that this could be a free gas zone (e.g. Chen et al., 2015) dominated by lateral flow (also characteristic of case 2).

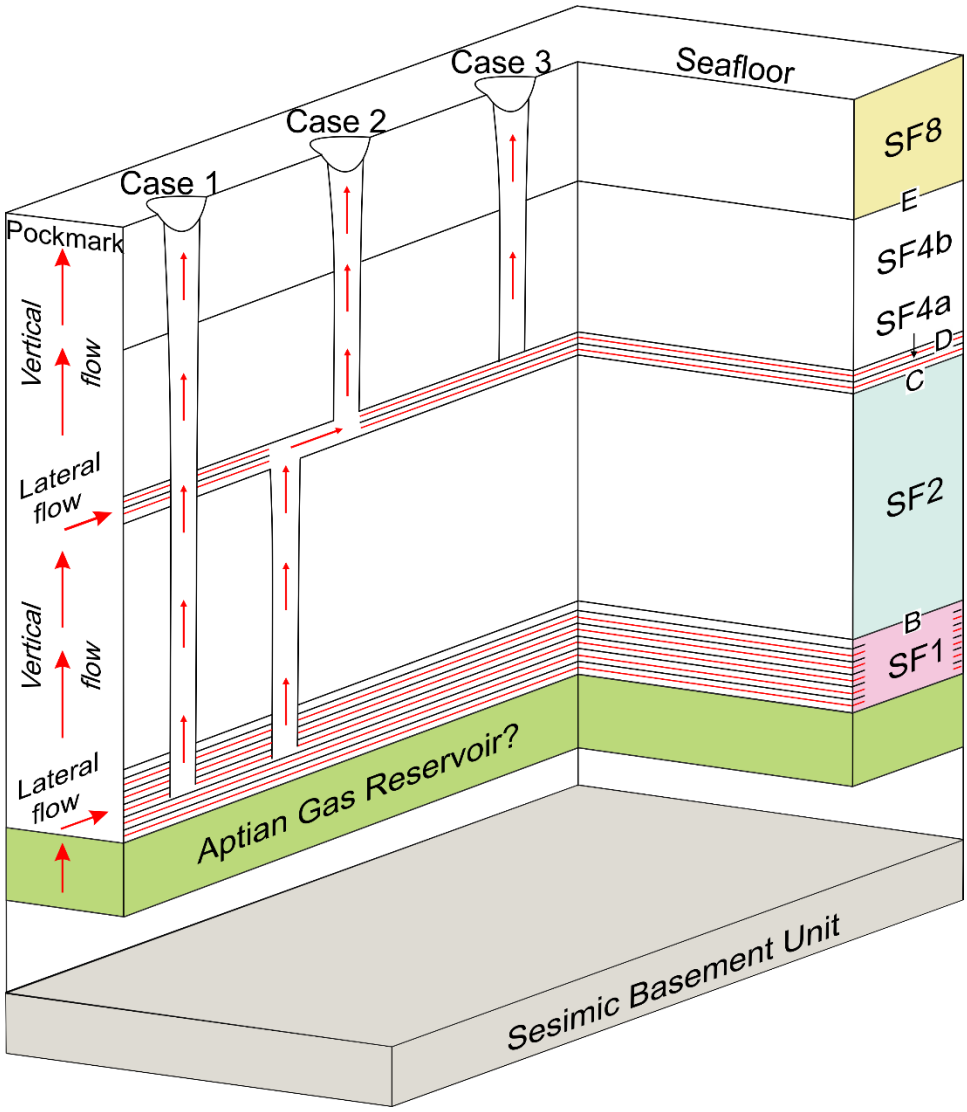

Figure 6.4.1: Conceptual model for fluid flow for the southwestern Cape continental margin showcasing three idealised fluid pathways (case 1, 2 and 3). The main source for gas is believed to be from Aptian and Turonian source rocks (Kuhlmann et al., 2010).

Conceptual canyon evolution model for the southwestern Cape continetnal margin

It is proposed that the various canyon morphologies along the southwestern Cape continental margin express different levels of maturity which occurred in five stages (Fig. 6.4.2):

1. Pre-canyon phase accounting for the development of intra-slope rills
2. The development of the linear canyon morphologies
3. The progression to the sinuous channel morphology
4. The development of the arcuate head to produce a hooked canyon morphology
5. Continued retrogressive erosion to indent the shelf

Initially, there needs to be the formation of a series of relatively small intra-slope rills, considered here as the "pre-canyon phase" (stage 1). These rill features (no wider than 200 m) are suggested to amalgamate through turbidity current processes to form incipient canyons (Lastras et al., 2011), or provide a localised preconditioning for slope oversteepening and later canyon excavation both upslope and downslope (cf. Green & Uken, 2008).

Based on the comparably short lengths and lack of mass wasting features, it is proposed that the linear canyons are the youngest canyons in the study area. Formation of these canyons would be attributed to the widening of the incipient canyons by the collapsing of its walls to set up subsequent retrogressive erosion (stage 2) (Pratson & Coakley, 1996; Green & Uken, 2008).

Upon retrogressing into the active pockmark fields, the linear canyons acquire a sinuous nature due to sediment mobilisation from gas expulsion (Løseth et al., 2009), where they transform to sinuous canyons (stage 3). Also, depending on the amount and character of the sediment flows supplied to the system in the downslope eroding phases, the canyons may also transform to more sinuous features that may not be associated with pockmarks (cf. Hicks & Green, 2017). These canyons remain merely as sinuous systems.

The hooked canyons acquired their arcuate heads from frequent sediment failure due to continued gas expulsion (Løseth et al., 2009) in a coast-parallel fashion to establish a NW-SE arcuate head and NE-SW mid-canyon and toe (stage 4). In some cases, such as the Oli Canyon System, the entire head would fail to form a circle-like appearance.

The final stage in canyon evolution involves the reworking of the arcuate head of a hooked canyon and subsequent large scale retrogressive erosion, evidenced by the shelf-indenting Cape Canyon (defined in this study as a sinuous system according to its overall morphological appearance and sinuosity). The mid-canyon is defined as being in the process of "hooking" due to sediment failure from gas expulsion (Løseth et al., 2009), upon which a proposed slump reignited further retrogressive erosion which breached the shelf to form its head (Pratson et al., 1994).

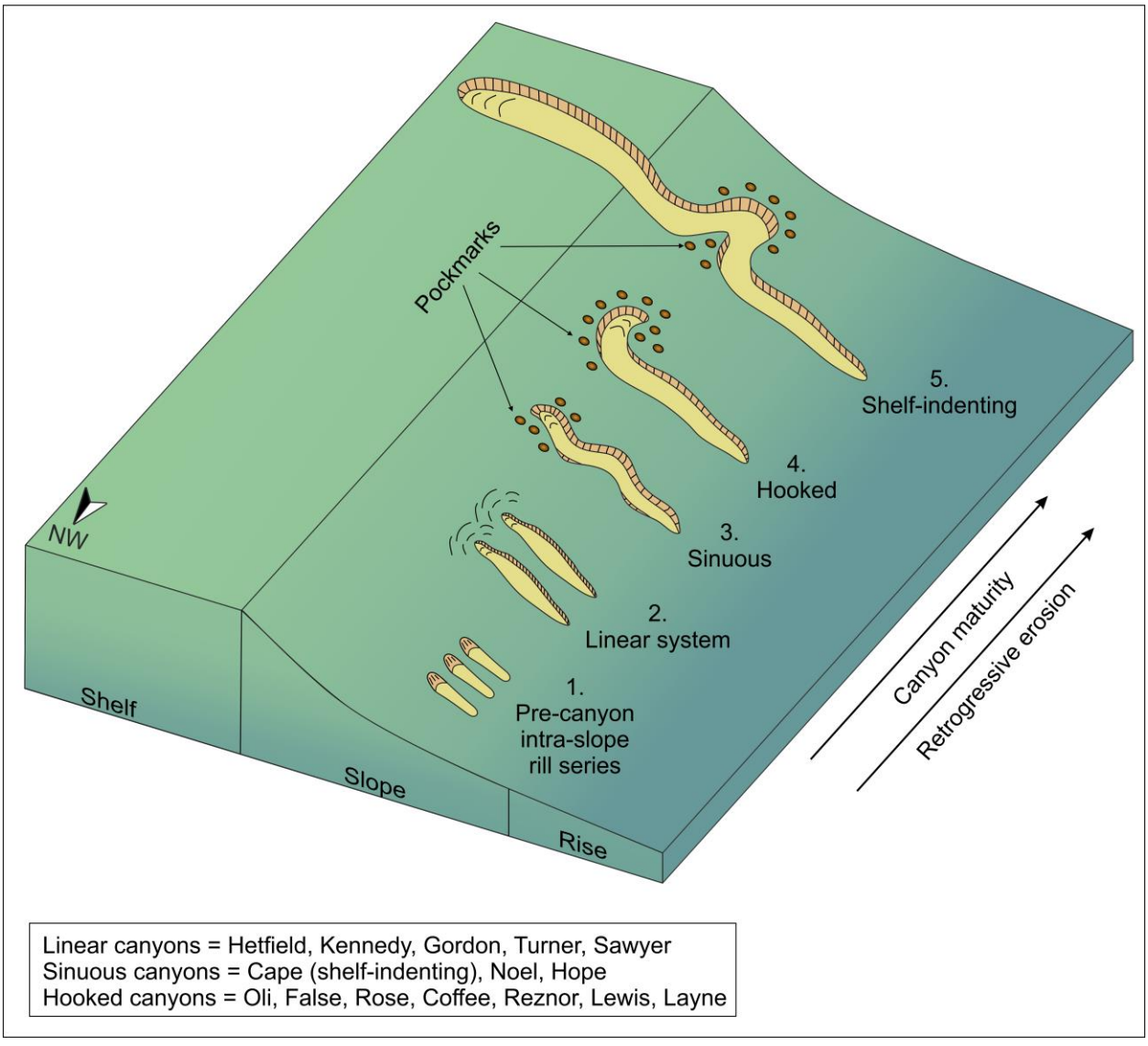

Figure 6.4.2: Conceptual evolution model for the southwestern Cape continental margin canyons relating erosive mechanisms and gas expulsion to canyon maturity.

CHAPTER 7

CONCLUSIONS

Canyon evolution on the southwest Cape continental margin is complex, controlled by simultaneous downslope-eroding turbidity flows and upslope-eroding retrogressive erosion. Complicating the evolution of these canyons are sediment failures related to prominent gas venting of the mid-slope. Of less importance are bottom current circulations (the North Atlantic Deep Water in this case), which are unlikely to cause slope incision and canyon formation but would have rather played a role in denuding any associated fan lobes. Strong bottom currents are evidenced further by the elongate, crescentic, composite and string-type pockmarks that occur on the mid-slope.

The proposed fluid flow model demonstrates the distinctive pathways for sub-surface fluid migration that have the potential to mobilise sediments, revealed by the occurrences of blowout pipes, pockmarks and mass wasting deposits. Canyon evolution along the Cape margin appears to be directly linked to fluid flow interaction with both the down- and upslope erosion processes interacting with the pockmark fields and venting processes. This is evidenced by dense pockmark associations with the sinuous, hooked and shelf-indenting canyon types, and the absence of pockmarks around linear-type canyons. It is therefore suggested that the linear canyons in this study are the most youthful canyon types, following a pre-canyon rilling phase. Succeeding this are the sinuous canyons which increase in sinuosity due to fluid migration, transforming linear-types to sinuous-types. The hooked-type canyons are especially unusual and this thesis proposes that their morphologies are indubitably linked with active vertical fluid flows which destabilise the slope and lead to the arcuate canyon heads failing retrogressively. The most mature canyon system is the Cape Canyon which has sustained significant retrogressive erosion. It is suggested that this system was in the process of "hooking" around its mid-canyon region, whereby it stepped out of the zone controlled by venting and fully retrogressed beyond the shelf break.

Based on the spatial distribution of the pockmarks, it appears that there is a continuation of these features located inshore from the bathymetric coverage of this thesis. Future research would therefore include a collection and analysis of bathymetric data located inshore from the bathymetry documented here. In addition to this, a detailed sequence stratigraphic framework of the study area needs to be established to determine the controls affecting reservoir quality and gas migration.

This would also include further detailed seafloor mapping seaward of the bathymetry described. These analyses would allow an expansion of the knowledgebase of how fluid flow affects canyon evolution along the margins of the world.

REFERENCES

Aldrich, J., Zilinski, R., Edman, J., Leu, W., Berge, T. & Corbett, K. (2003). Documentation of a New Petroleum System in the South Atlantic. AAPG Annual Convention, May 11–14, 2003, Salt Lake City, Utah.

Andresen, K.J. (2012). Fluid flow features in hydrocarbon plumbing systems: What do they tell us about the basin evolution? Marine Geology 332–334, 89–108.

Andresen, K.J., Clausen, O.R. & Huuse, M. (2009). A giant (5.3×107 m^3) middle Miocene (c. 15 Ma) sediment mound (M1) above the Siri Canyon, Norwegian–Danish Basin: origin and significance. Marine and Petroleum Geology 26, 1640–1655.

Andresen, K.J., Huuse, M. & Clausen, O.R. (2008). Morphology and distribution of Oligocene and Miocene pockmarks in the Danish North Sea — implications for bottom current activity and fluid migration. Basin Research 20, 445–466.

Andresen, K.J., Huuse, M., Schødt, N.H., Clausen, L.F. & Seidler, L. (2011). Hydrocarbon plumbing systems of salt minibasins offshore Angola revealed by three-dimensional seismic analysis. AAPG Bulletin 95 (6), 1039–1065.

Andrews, B.D., Brothers, L.L. & Barnhardt, W.A. (2010). Automated feature extraction and spatial organization of seafloor pockmarks, Belfast Bay, Maine, USA. Geomorphology 124, 55–64.

Arzola, R., Wynn, R.B., Lastras, G., Masson, D.G. & Weaver, P.P.E. (2008). Sedimentary features and processes in submarine canyons: a case study from the Nazaré and Setúbal Canyons, west Iberian margin. Marine Geology 250, 64–88.

Babonneau, N., Delacourt, C., Cancouët, R., Sisavath, E., Bachèlery, P., Mazuel, A., Jorry, S.J., Deschamps, A., Ammanna, J. & Villeneuve, N. (2013). Direct sediment transfer from land to deep-sea: Insights into shallow multibeam bathymetry at La Réunion Island. Marine Geology 346, 47–57.

Babonneau, N., Savoye, B., Cremer, M. & Klein, B. (2002). Morphology and architecture of the present day canyon and channel system of the Zaire deep-sea fan. Marine and Petroleum Geology 19, 445–467.

Baztan, J., Berné, S., Olivet, J.-L., Rabineau, M., Aslanian, D., Gaudin, M., Réhault, J.P. & Canals, M. (2005). Axial incision: the key to understand submarine canyon evolution (in the western Gulf of Lion). Marine and Petroleum Geology 22, 805–826.

Benjamin, U., Huuse, M. & Hodgetts, D. (2015). Canyon-confined pockmarks on the western Niger Delta slope. Journal of African Earth Sciences 107, 15–27.

Berger, W. H. & Wefer, G. (2002). On the reconstruction of upwelling history: Namibia upwelling in context. Marine Geology 180, 3–28.

Berndt, C., Bunz, S. & Mienert, J. (2003). Polygonal fault systems on the mid-Norwegian margin: a long-term source for fluid flow. In: Van Rensbergen, P., Hillis, R.R. & Morley, C.K. (Eds.), Subsurface Sediment Mobilization, Geological Society of London, Special Publication 216, pp. 283–290.

Bertoni, C. & Cartwright, J. (2005). 3D seismic analysis of slope-confined canyons from the Plio–Pleistocene of the Ebro Continental Margin (Western Mediterranean). Basin Research 17 (1), 43–62.

Birch, G.F. (1977). Surficial sediments on the continental margin off the west coast of South Africa. Marine Geology 23, 305–337.

Boyd, R., Ruming, K., Goodwin, I., Sandstrom, M. & Schroder-Adams, C. (2008). Highstand transport of coastal sand to the deep ocean: A case study from Fraser Island, southeast Australia. Geology 36 (1), 15–18.

Broad, D.S., Jungslager, E.H.A., McLachlan, I.R. & Roux, J. (2006). Offshore Mesozoic Basins. In: Johnson, M.R., Anhaeusser, C.R. & Thomas, R.J. (Eds.), The Geology of South Africa. Geological Society of South Africa, Johannesburg/Council for Geosciences, Pretoria, pp. 553–571.

Brothers, D.S., Ruppel, C., Kluesner, J.W., ten Brink, U.S., Chaytor, J.D., Hill, J.C., Andrews, B.D. & Flores, C. (2014). Seabed fluid expulsion along the upper slope and outer shelf of the U.S. Atlantic continental margin. Geophysical Research Letters 41, 96–101.

Brothers, D.S., ten Brink, U.S., Andrews, B.D., Chaytor, J.D. & Twitchell, D.C. (2013). Geomorphic process fingerprints in submarine canyons. Marine Geology 337, 53–66.

Brown Jr., L.F., Benson, J.M., Brink, G.J., Doherty, S., Jollands, A., Jungslager, E.H.A., Keenan, J.H.G., Muntingh, A. & Van Wyk, N.J.S. (1995). Sequence stratigraphy in offshore South African divergent basins: an atlas on exploration for Cretaceous lowstand traps by SOEKOR (Pty) Ltd. AAPG Studies in Geology 41, 184.

Canals, M., Puig, P., de Madron, X.D., Heussner, S., Palanques, A. & Fabres, J. (2006). Flushing submarine canyons. Nature 444, 354–357.

Carlson, P.R. & Karl, H.A. (1988). Development of large submarine canyons in the Bering Sea indicated by morphologic, seismic, and sedimentologic characteristics. Geological Society of America Bulletin 100, 1594–1615.

Cartigny, M.J., Postma, G., van den Berg, J.H. & Mastbergen, D.R. (2011). A comparative study of sediment waves and cyclic steps based on geometries, internal structures and numerical modeling. Marine Geology 280 (1), 40–56.

Cartwright, J. (1996). Volumetric contraction during the compaction of mudrocks: A mechanism for the development of regional-scale polygonal fault systems. Basin Research 8 (2), 183–193.

Cartwright, J. & Santamarina, C. (2015). Seismic characteristics of fluid escape pipes in sedimentary basins: Implications for pipe genesis. Marine and Petroleum Geology 65, 126–140.

Cartwright, J., Huuse, M. & Aplin, A. (2007). Seal bypass systems. AAPG bulletin 91 (8), 1141–1166.

Cartwright, J.A., James, D.M.D. & Bolton, A.J. (2003). The genesis of polygonal fault systems: A review. In: Van Rensbergen, P., Hillis, R., Maltman, A., Morley, C. (Eds.), Subsurface sediment mobilization. Special Publication, vol. 216. Geological Society, London, pp. 223–242.

Cathles, L.M., Su, Z. & Chen, D. (2010). The physics of gas chimney and pockmark formation, with implications for assessment of seafloor hazards and gas sequestration. Marine and Petroleum Geology 27, 82–91.

Catuneanu, O. (2006). Principles of Sequence Stratigraphy. Elsevier, Amsterdam, pp. 37.

Chen, J., Song, H., Guan, Y., Yang, S., Pinheiro, L.M., Bai, Y., Liu, B. & Geng, M. (2015). Morphologies, classification and genesis of pockmarks, mud volcanoes and associated fluid escape features in the northern Zhongjiannan Basin, South China Sea. Deep-Sea Research II 122, 106–117.

Compton, J.S. & Wiltshire, J.G. (2009). Terrigenous sediment export from the western margin of South Africa on glacial to interglacial cycles. Marine Geology 226, 212–222.

Covault, J.A. & Graham, S.A. (2010). Submarine fans at all sea-level stands: Tectono-morphologic and climatic controls on terrigenous sediment delivery to the deep sea. Geology 38 (10), 939–942.

Covault, J.A., Kostic, S., Paull, C.K., Sylvester, Z. & Fildani, A. (2017). Cyclic steps and related supercritical bedforms: Building blocks of deep-water depositional systems, western North America. Marine Geology 393, 4–20.

Covault, J.A., Normark, W.R., Romans, B.W. & Graham, S.A. (2007). Highstand fans in the California borderland: The overlooked deep-water depositional systems. Geology 35 (9), 783–786.

Covault, J.A., Romans B.W., Graham, S.A., Fildani, A. & Hilley, G.E. (2011). Terrestrial source to deep-sea sink sediment budgets at high and low sea levels: Insights from tectonically active Southern California. Geology 39 (7), 619–622.

Cukur, D., Krastel, S., Tomonaga, Y., Cagatay, N., Meydan, A.F. & PaleoVan Science Team. (2013). Seismic evidence of shallow gas from Lake Van, eastern Turkey. Marine and Petroleum Geology 48, 341–353.

Cunningham, M.J., Hodgson, S., Masson, D.G. & Parson, L.M. (2005). An evaluation of along- and down-slope sediment transport processes between Goban Spur and Brenot Spur on the Celtic Margin of the Bay of Biscay. Sedimentary Geology 179, 99–116.

Currie, R. (1953). Upwelling in the Benguela Current. Nature 171, 497–500.

Dandapath, S., Chakraborty, B., Karisiddaiah, S.M., Menezes, A., Ranade, G., Fernandes, W., Naik, D.K. & Prudhvi Raju, K.N. (2010). Morphology of pockmarks along the western

continental margin of India: Employing multibeam bathymetry and backscatter data. Marine and Petroleum Geology 27, 2107–2117.

Davies, R., Bell, B.R., Cartwright, J.A. & Shoulders, S. (2002). Three-dimensional seismic imaging of Paleogene dike-fed submarine volcanoes from the northeast Atlantic margin. Geology 30, 223–226.

Dawei, W., Shiguo, W., Zhiliang, Q., Spence, G. & Fuliang, L. (2013). Seismic characteristics of the Huaguang mass transport deposits in the Qiongdongnan Basin, South China Sea: Implications for regional tectonic activity. Marine Geology 346, 165–182.

Deptuck, M.E., Sylvester, Z., Pirmez, C. & O'Byrne, C. (2007). Migration aggradation history and 3-D seismic geomorphology of submarine channels in the Pleistocene Benin-major Canyon, western Niger Delta slope. Marine and Petroleum Geology 24 (6–9), 406–433.

Diester-Haass, L., Meyers, P.A. & Vidal, L. (2001). The late Miocene onset of high productivity in the Benguela Current upwelling system as part of a global pattern: Marine Geology 180, 87–104.

Dingle, R.V. (1992). Structural and sedimentary development of the continental margin off southwestern Africa. Communications of the Geology Survey of Namibia 8, 35–43.

Dingle, R.V. & Robson, S.H. (1992). Southwestern Africa continental rise: Structural and Sedimentary evolution. In: Poag, C.W. & de Graciansky, P.C. (Eds.), Geologic Evolution of Atlantic Continental Rises, New York, Von Nostrand Reinhold, pp. 62–76.

Dingle, R.V., Siesser, W.G. & Newton, A.R. (1983). Mesozoic and Tertiary Geology of Southern Africa. Balkema, Rotterdam, pp. 262–316.

Duarte, J.C., Terrinha, P., Rosas, F.M., Valadares, V., Pinheiro, L.M., Matias, L., Magalhães, V. & Roque, C. (2010). Crescent-shaped morphotectonic features in the Gulf of Cadiz (offshore SW Iberia). Marine Geology 271, 236–249.

Emery, D. & Myers, K. (1996). Sequence Stratigraphy. Blackwell Publishing, Oxford, U.K., pp. 178–191.

Falvey, D.A. (1974). The development of continental margins in plate tectonic theory. Australian Petroleum Exploration Association Journal 14, 95–106.

Farre, J.A., McGreggor B.A., Ryan, W.B.F. & Robb, J.M. (1983). Breaching the shelf break: Passage from youthful to mature phase in submarine canyon evolution. In: Stanley, D.J. & Moore, G.T. (Eds.), The shelf-break: Critical interface on continental margins. Society of Economic Paleontologists and Mineralogists Special Publication 33, pp. 25–39.

Fildani, A., Hubbard, S.M., Covault, J.A., Maier, K.L., Romans, B.W., Traer, M. & Rowland, J.C. (2013). Erosion at inception of deep-sea channels. Marine and Petroleum Geology 41, 48–61.

Fildani, A., Normark, W.R., Kostic, S. & Parker, G. (2006). Channel formation by flow stripping: large-scale scour features along the Monterey East Channel and their relation to sediment waves. Sedimentology 53 (6), 1265–1287.

Fouché, J., Bate, K.J. & Van der Merwe, R. (1992). Plate tectonic setting of the Mesozoic basins, southern offshore, South Africa: a review. In: De Wit, M.J. & Ransome, I.G.D. (Eds.), Inversion Tectonics of the Cape Fold Belt, Karoo and Cretaceous Basins of Southern Africa. A.A. Balkema, Rotterdam, pp. 33– 45.

Gay, A., Lopez, M., Berndt, C. & Séranne, M. (2007). Geological controls on focused fluid flow associated with seafloor seeps in the Lower Congo Basin. Marine Geology 244, 68–92.

Gay, A., Lopez, M., Cochonat, P., Séranne, M., Levaché, D. & Sermondadaz, G. (2006). Isolated seafloor pockmarks linked to BSRs, fluid chimneys, polygonal faults and stacked Oligocene–Miocene turbiditic palaeochannels in the Lower Congo Basin. Marine Geology 226, 25–40.

Gerrard, I. & Smith, G.C. (1982). Post-Paleozoic succession and structure of the southwestern African continental margin. In: Watkins, J.S. & Drake, C.L. (Eds.), Studies in Continental Margin Geology. AAPG Memoir 34, 49–74.

Gladczenko, T.P., Skogseid, J. & Eldholm, O. (1998). Namibia volcanic margin. Marine Geophysical Researches 20 (4), 313–341.

Gradstein, F.M., Ogg, J.G., Smith, A.G., Agterberg, F.P., Bleeker, W., Cooper, R.A., Davydov, V., Gibbard, P., Hinnov, L., House, M.R., Lourens, L., Luterbacher, H.-P., McArthur, J., Melchin, M.J., Robb, L.J., Shergold, J., Villeneuve, M., Wardlaw, B.R., Ali, J., Brinkhuis, H., Hilgen, F.J., Hooker, J., Howarth, R.J., Knoll, A.H., Laskar, J., Monechi, S., Powell, J., Plumb, K.A., Raffi, I., Rohl, U., Sanfilippo, A., Schmitz, B., Shackleton, N.J., Shields, G.A., Strauss, H., Van Dam, J., Veizer, J., van Kolfschoten, T. & Wilson, D. (2004). A new Geologic Time Scale, with special reference to Precambrian and Neogene. Cambridge University Press, pp. 500.

Green, A.N. (2011a). Submarine canyons associated with alternating sediment starvation and shelf-edge wedge development: northern KwaZulu-Natal continental margin, South Africa. Marine Geology 289, 114–126.

Green, A.N. (2011b). The late Cretaceous to Holocene sequence stratigraphy of a sheared passive upper continental margin, northern KwaZulu-Natal, South Africa. Marine Geology 289, 17–28.

Green, A.N. & Uken, R. (2008). Submarine landsliding and canyon evolution on the northern KwaZulu-Natal continental shelf, South Africa, SW Indian Ocean. Marine Geology 254 (3 – 4), 152–170.

Green, A.N., Goff, J.A. & Uken, R. (2007). Geomorphological evidence for upslope canyon forming processes on the northern KwaZulu-Natal shelf, South Africa. Geo-Marine Letters 27, 399–409.

Haile, B.G., Klausen, T.G., Czarniecka, U., Xi, K., Jahren, J. & Hellevang, H. (in press). How are diagenesis and reservoir quality linked to depositional facies? A deltaic succession, Edgeøya, Svalbard. Marine and Petroleum Geology (in press).

Hammer, Ø., Webb, K.E. & Depreiter, D. (2009). Numerical simulation of upwelling currents in pockmarks, and data from the Inner Oslofjord, Norway. Geo-Marine Letters 29, 269–275.

Hampton, M. (1972). The role of subaqueous debris flow in generating turbidity currents. Journal of Sedimentary Petrology 42, 775–993.

Haq, B.U., Hardenbol, J. & Vail, P.R. (1987). Chronology of fluctuating sea levels since the Triassic. Science 235, 1156–1167.

Harris, P.T. & Whiteway, T. (2011). Global distribution of large submarine canyons: geomorphic differences between active and passive continental margins. Marine Geology 285, 69–86.

Harris, P.T., Heap, A., Post, T., Whiteway, A., Potter, A. & Bradshaw, M. (2007). Marine zone management and the EPBC Act – How environmental marine geological information provides certainty for petroleum exploration. APPEA Journal 47 (1), 329–345.

Hasiotis, T., Papatheodorou, G. & Ferentinos, G. (2002). A string of large and deep gas-induced depressions (pockmarks) offshore Killini peninsula, western Greece. Geo-Marine Letters 22, 142–149.

Henrich, R., Cherubini, Y. & Meggers, H. (2010). Climate and sea level induced turbidite activity in a canyon system offshore the hyperarid Western Sahara (Mauritania): The Timiris Canyon. Marine Geology 275, 178–198.

Hicks, N. & Green, A. (2016). Sedimentology and depositional architecture of a submarine delta-fan complex in the Durban Basin, South Africa. Marine and Petroleum Geology 78, 390–404.

Hicks, N. & Green, A. (2017). A Mid-Miocene erosional unconformity from the Durban Basin, SE African margin: A combination of global eustatic sea level change, epeirogenic uplift, and ocean current initiation. Marine and Petroleum Geology 86, 798–811.

Hill, P.J., De Deckker, P. & Exon, N.F. (2005). Geomorphology and evolution of the gigantic Murray canyons on the Australian southern margin. Australian Journal of Earth Science 52, 117–136.

Hirsch, K.K., Scheck-Wenderoth, M., van Wees, J.D. & Kuhlmann, G. (2010). Tectonic subsidence history and thermal evolution of the Orange Basin. Marine and Petroleum Geology 27, 565–584.

Horozal, S., Bahk, J.J., Urgeles, R., Kim, G.Y., Cukur, D., Kim, S.P., Lee, G.H., Lee, S.H., Ryu, B.J. & Kim, J.H. (2017). Mapping gas hydrate and fluid flow indicators and modeling gas hydrate stability zone (GHSZ) in the Ulleung Basin, East (Japan) Sea: Potential linkage between the occurrence of mass failures and gas hydrate dissociation. Marine and Petroleum Geology 80, 171–191.

Hovland, M. & Judd, A.G. (1988). Seabed Pockmarks and Seepages: Impact on Geology, Biology and the Marine Environment. Graham and Trotman Ltd, London, pp. 14–32.

Hovland, M., Gardner, J.V. & Judd, A.G. (2002). The significance of pockmarks to understanding fluid flow processes and geohazards. Geofluids 2, 127–136.

Huang, Z., Nichol, S.L., Harris, P.T. & Caley, M.J. (2014). Classification of submarine canyons of the Australian continental margin. Marine Geology 357, 362–383.

Hurst, A., Scott, A. & Vigorito, M. (2011). Physical characteristics of sand injectites. Earth Science Reviews 106, 215–246.

Hustoft, S., Bünz, S. & Mienert, J. (2010). Three-dimensional seismic analysis of the morphology and spatial distribution of chimneys beneath the Nyegga pockmark field, offshore mid-Norway. Basin Research 22, 465–480.

Huvenne, V.A.I. & Davies, J.S. (2013). Towards a new integrated approach to submarine canyon research. Deep-Sea Research Part II: Topical Studies in Oceanography 104, 1–5.

Jobe, Z.R., Lowe, D.R. & Uchytil, S.J. (2011). Two fundamentally different types of submarine canyons along the continental margin of Equatorial Guinea. Marine and Petroleum Geology 28 (3), 843–860.

Josenhans, H.W., King, L.H. & Fader, G.B. (1978). A side-scan sonar mosam of pockmarks on the Scotian Shelf. Canadian Journal of Earth Sciences 15, 831–840.

Judd, A.G. & Hovland, M. (1992). The evidence of shallow gas in marine sediments. Continental Shelf Research 12 (10), 1081–1095.

Judd, A.G. & Hovland, M. (2007). Seabed Fluid Flow: The Impact on Geology, Biology, and the Marine Environment. Cambridge University Press, Cambridge, UK, pp. 9–15, 189–194.

Kayen, R. & Lee, H. (1991). Pleistocene slope instability of gas hydrate-laden sediment on the Beaufort sea margin. Marine Geotechnology 10, 125–141.

Kennett, J.P. (1982). Marine Geology. Prentice-Hall, Englewood Cliffs, NJ, pp. 813.

King, L.H. & MacLean, B. (1970). Pockmarks on the Scotian Shelf. Geological Society of America Bulletin 81 (10), 3141–3148.

Kostic, S. (2011). Modeling of submarine cyclic steps: controls on their formation, migration, and architecture. Geosphere 7 (2), 294–304.

Kostic, S. (2014). Upper flow regime bedforms on levees and continental slopes: turbidity current flow dynamics in response to fine-grained sediment waves. Geosphere 10 (6), 1094–1103.

Kuhlmann, G., Adams, S., Campher, C., Van der Spuy, D., di Primio, R. & Horsfield, B. (2010). Passive margin evolution and its controls on natural gas leakage in the southern Orange Basin, blocks 3/4, offshore South Africa. Marine and Petroleum Geology 27, 973–992.

Lastras, G., Acosta, J., Munoz, A. & Canals, M. (2011). Submarine canyon Formation and evolution in the argentine continental margin between 44°30'S and 48°S. Geomorphology 128, 116–136.

Lastras, G., Arzola, R.G., Masson, D.G., Wynn, R.B., Huvenne, V.A.I., Huhnerbach, V. & Canals, M. (2009). Geomorphology and sedimentary features in the Central Portuguese submarine canyons, Western Iberian margin. Geomorphology 103, 310–329.

Li, X.S., Zhou, Q.J., Su, T.Y., Liu, L.J., Gao, S. & Zhou, S.W. (2016). Slope-confined submarine canyons in the Baiyun deep-water area, northern South China Sea: variation in their modern morphology. Marine and Geophysical Research 37 (2), 95–112.

Light, M.P.R., Maslanyj, M.P., Greenwood, R.J. & Banks, N.L. (1993). Seismic sequence stratigraphy and tectonics offshore Namibia. In: Willams, G. & Dobb, A. (Eds.), Tectonic and Seismic Sequence Stratigraphy, Geological Society, London, Special Publications 71, pp. 163–191.

Long, D. (1992). Devensian late-glacial gas escape in the central North Sea. Continental Shelf Research 12, 1097–1110.

Løseth, H., Gading, M. & Wensaas, L. (2009). Hydrocarbon leakage interpreted on seismic data. Marine and Petroleum Geology 26, 1304–1319.

Løseth, H., Wensaas, L., Arntsen, B., Hanken, N., Basire, C. & Graue, K. (2001). 1000 m long gas blow out pipes. 63rd EAGE Conference and Exhibition, Extended abstract, 524–527.

Løseth, H., Wensaas, L., Arntsen, B., Hanken, N., Basire, C. & Graue, K. (2011). 1000 m long gas blow-out pipes. Marine and Petroleum Geology 28, 1047–1060.

Lutjeharms, J.R.E. & Stockton, P.L. (1987). Kinematics of the upwelling front off southern Africa. South African Journal of Marine Science 5, 35–49.

Macdonald, D., Gomez-Perez, I., Franzese, J., Spalletti, L., Lawver, L., Gahagan, L., Dalziel, I., Thomas, C., Trewin, N., Hole, M. & Paton, D. (2003). Mesozoic break-up of SW Gondwana: implications for regional hydrocarbon potential of the southern South Atlantic. Marine and Petroleum Geology 20, 287–308.

Maia, A.R., Cartwright, J. & Andersen, E. (2016). Shallow plumbing systems inferred from spatial analysis of pockmark arrays. Marine and Petroleum Geology 77, 865–881.

Marcon, Y., Ondréas, H., Sahling, H., Bohrmann, G. & Olu, K. (2014). Fluid flow regimes and growth of a giant pockmark. Geology 42 (1), 63–66.

Masson, D.G., Canals, M., Alonso, B., Urgeles, R. & Huhnerbach, V. (1998). The canary debris flow; source area morphology and failure mechanisms. Sedimentology 45, 411–432.

Mazumdar, A., Peketi, A., Dewangan, P., Badesab, F., Ramprasad, T., Ramana, M.V., Patil, D.J. & Dayal, A. (2009). Shallow gas charged sediments off the Indian west coast: genesis and distribution. Marine Geology 267, 71–85

Mazzini, A., Svensen, H.H., Planke, S., Forsberg, C.F. & Tjelta, T.I. (2016). Pockmarks and methanogenic carbonates above the giant Troll gas field in the Norwegian North Sea. Marine Geology 373, 26–38.

McMillan, I.K. (2003). Foraminiferally defined biostratigraphic episodes and sedimentation pattern of the Cretaceous drift succession (Early Barremian to Late Maastrichtian) in seven basins on the South African and southern Namibian continental margin. South African Journal of Science 99, 537–576.

Miller, K.G., Kominz, M.A., Browning, J.V., Wright, J.D., Mountain, G.S., Katz, M.E., Sugarman, P.J., Cramer, B.S., Christie-Blick, N. & Pekar, S.F. (2005). The Phanerozoic record of global sea-level change. Science 310, 1293–1298.

Mitchell, N.C. (2004). Form of submarine erosion from confluences in Atlantic USA continental slope canyons. American Journal of Science 304, 590–611.

Mohrig, D. & Marr, J.G. (2003) Constraining the efficiency of turbidity current generation from submarine debris flows and slides using laboratory experiments. Marine and Petroleum Geology 20, 883–899.

Mosher, D.C., Campbell, D.C., Gardner, J.V., Piper, D.W.J., Chaytor, J.D. & Rebesco, M. (in press). The role of deep-water sedimentary processes in shaping a continental margin: The Northwest Atlantic. Marine Geology (in press).

Mosher, D.C., Monahan, P.A., Barrie, J.V. & Courtney, R.C. (2004). Coastal submarine failures in the Strait of Georgia, British Columbia: Landslides of the 1946 Vancouver Island earthquake, Journal of Coastal Research 20 (1), 277–291.

Mosher, D.C., Xu, Z. & Shimeld, J. (2010). The Pliocene Shelburne mass-movement and consequent tsunami, western Scotian Slope, In: Mosher, D.C., Shipp, R.C., Moscardelli, L., Chaytor, J.D., Baxter, C.D.P., Lee, H.J. & Urgeles, R. (Eds.), Submarine Mass Movements and their Consequences, Advances in Natural and Technological Hazards Research, v. 28, Springer, the Netherlands, pp. 765-775.

Moss, J.L. & Cartwright, J. (2010). The spatial and temporal distribution of pipe formation, offshore Namibia. Marine & Petroleum Geology 27, 1216–1234.

Nakajima, T., Kakuwa, Y., Yasudomi, Y., Itaki, T., Motoyama, I., Tomiyama, T., Machiyama, H., Katayama, H., Okitsu, O., Morita, S., Tanahashi, M. & Matsumoto, R. (2014). Formation of pockmarks and submarine canyons associated with dissociation of gas hydrates on the Joetsu Knoll, eastern margin of the sea of Japan. Journal of Asian Earth Sciences 90, 228–242.

Netzeband, G.L., Krabbenhoeft, A., Zillmer, M., Petersen, C.J., Papenberg, C. & Bialas, J. (2010). The structures beneath submarine methane seeps: seismic evidence from Opouawe Bank, Hikurangi Margin, New Zealand. Marine Geology 272, 57–70.

National Oceanic and Atmospheric Administration (2017). http://www.noaa.gov/ [Dec. 01, 2017]

Orange, D.L., Yun, J., Maher, N., Barry, J. & Greene, G. (2002). Tracking California seafloor seeps with bathymetry, backscatter and ROVs. Continental Shelf Research 22, 2273–2290.

Ortega-Sánchez, M., Lobo, F.J., López-Ruiz, A., Losada, M.A. & Fernández-Salas, L.M. (2014). The influence of shelf-indenting canyons and infralittoral prograding wedges on coastal morphology: The Carchuna system in Southern Spain. Marine Geology 347, 107–122.

Ostanin, I., Anka, Z. & di Primio, R. (2017). Role of Faults in Hydrocarbon Leakage in the Hammerfest Basin, SW Barents Sea: Insights from Seismic Data and Numerical Modelling. Geosciences 7, 28.

Ostanin, I., Anka, Z., di Primio, R. & Bernal, A. (2013). Hydrocarbon plumbing systems above the Snøhvit gas field: Structural control and implications for thermogenic methane leakage in the Hammerfest Basin, SW Barents Sea. Marine and Petroleum Geology 43, 127–146.

Palanques, A., Durrieu de Madron, X., Puig, P., Fabres, J., Guillén, Calafat, A., Canals, M., Heussner, S. & Bonnin, J. (2006). Suspended sediment fluxes and transport processes in the Gulf of Lions submarine canyons. The role of storms and dense water cascading. Marine Geology 234 (1–4), 43–61.

Panieri, G., Bünz, S., Fornari, D.J., Escartin, J., Serov, P., Jansson, P., Torres, M.E., Johnson, J.E., Hong, W., Sauer, S., Garcia, R. & Gracias, N. (2017). An integrated view of the methane system in the pockmarks at Vestnesa Ridge, 79°N. Marine Geology 390, 282–300.

Parker, G. (1996). Some speculations on the relation between channel morphology and channel-scale flow structures. In: Ashworth, P.J. & Bennet, J.L. (Eds.), Coherent Flow Structures in Open Channels. Wiley, New York, pp. 429–432.

Parsons, J.D., Bush, J.W.M. & Syvitski, J.P.M. (2001). Hyperpycnal plumes with small sediment concentrations. Sedimentology 48, 465–478.

Partridge, T.C. & Maud, R.R. (1987). Geomorphic evolution of southern Africa since the mesozoic. South African Journal of Geology 90, 179–208.

Paull, C., Ussler III, W., Maher, N., Greene, H.G., Rehder, G., Lorenson, T. & Lee, H. (2002). Pockmarks off Big Sur, California. Marine Geology 181, 323–335.

Peakall, J., McCaffrey, B. & Kneller, B. (2000). A process model for the evolution, morphology, and architecture of sinuous submarine channels. Journal of Sedimentary Research 70, 434–448.

Petroleum Agency SA (PASA). (2003). South African Exploration Opportunities. South African Agency for Promotion of Petroleum Exploration and Exploitation, Parow, Cape Town, pp. 28.

Petters, S.W. (1984). An ancient submarine canyon in the Oligocene-Miocene of the western Niger Delta. Sedimentology 31 (6), 805–810.

Pilcher, R. & Argent, J. (2007). Mega-pockmarks and linear pockmark trains on the West African continental margin. Marine Geology 244, 15–23.

Piper, D.J.W., MacDonald, A.W.A., Ingram, S.I., Williams, G.L. & McCall, C. (2005). Late Cenozoic architecture of the St. Pierre Slope. Canadian Journal of Earth Science 42 (11), 1967–1985.

Piper, D.J.W. & Normark, W.R. (1983). Turbidite depositional patterns and flow characteristics, Navy Submarine Fan, California Borderland, Sedimentology 30, 681–694.

Piper, D.J.W. & Normark, W.R. (2009). Processes that initiate turbidity currents and their influence on turbidites: a marine geology perspective. Journal of Sedimentary Research 79 (6), 347–362.

Plaza-Faverola, A., Westbrook, G.K., Ker, S., Exley, R.J.K., Gailler, A., Minshull, T.A. & Broto, K. (2010). Evidence from three-dimensional seismic tomography for a substantial accumulation of gas hydrate in a fluid-escape chimney in the Nyegga pockmark field, offshore Norway. Journal of Geophysical Research 115, B08104.

Posamentier, H.W., Erskine, R.D. & Mitchum, R.M. (1991). Models for Submarine-Fan Deposition within a Sequence-Stratigraphic Framework. In: Weimer, P. & Link, M.H. (Eds.), Seismic Facies and Sedimentary Processes of Submarine Fans and Turbidite Systems. Springer-Verlag, New York, pp. 127–136.

Pratson, L.F. & Coakley, B.J. (1996). A model for the headward erosion of submarine canyons induced by downslope eroding sediment flows. Geological Society of America Bulletin 108, 225–234.

Pratson, L., Nittrouer, C., Wiberg, P., Steckler, M., Swenson, J., Cacchione, D., Karson, J., Murray, A.B., Wolinsky, M., Gerber, T., Mullenbach, B., Spinelli, G., Fulthorpe, C., O'Grady, D., Parker, G., Driscoll, N., Burger, C., Paola, C., Orange, D., Field, M., Friedrichs, C. & Fedele, J. (2007). Seascape evolution on clastic continental shelves and slopes. In: Nittrouer, C.A., Austin Jr., J.A., Field, M.E., Kravitz, J.H., Syvitski, J.P.M. & Wiberg, P.L. (Eds.), Continental-Margin Sedimentation: from Sediment Transport to Sequence Stratigraphy. Blackwell Publishing Ltd, Oxford, pp. 339–380.

Pratson, L.F., Ryan, W.B.F., Mountain, G.S. & Twitchell, D.C. (1994). Submarine canyon initiation by downslope-eroding sediment flows: evidence in late Cenozoic strata on the New Jersey continental slope. Geological Society of America Bulletin 106, 395–412.

Puga-Bernabéu, Á., Webster, J.M., Beaman, R.J & Guilbaud, V. (2013). Variation in canyon morphology on the Great Barrier Reef margin, north-eastern Australia: the influence of slope and barrier reefs. Geomorphology 191, 35–50.

Puig, P., Durán, R., Muñoz, A., Elvira, E. & Guillén, J. (2017). Submarine canyon-head morphologies and inferred sediment transport processes in the Alías-Almanzora canyon system (SW Mediterranean): On the role of the sediment supply. Marine Geology 393, 21–34.

Puig, P., Palanques, A. & Martín, J. (2014). Contemporary sediment-transport processes in submarine canyons. Annual Reviews of Marine Science 6, 53–77.

Sahoo, H., Royhan Gani, M., Hampson, G.J., Gani, N.D. & Ranson, A. (2016). Facies- to sandbody-scale heterogeneity in a tight-gas fluvial reservoir analog: Blackhawk Formation, Wasatch Plateau, Utah, USA. Marine and Petroleum Geology 78, 48–69.

Sánchez, F., González-Pola, C., Druet, M., García-Alegre, A., Acosta, J., Cristobo, J., Parra, S., Ríos, P., Altuna, A., Gómez-Ballesteros, M., Muñoz-Recio, A., Rivera, J. & Díaz del Río, G. (2014). Habitat characterization of deep-water coral reefs in LaGaviera canyon (Avilés Canyon System, Cantabrian Sea). Deep-Sea Research II 106, 118–140.

Scarselli, N., McClay, K. & Elders, C. (2016). Seismic geomorphology of cretaceous megaslides offshore Namibia (Orange Basin): Insights into segmentation and degradation of gravity-driven linked systems. Marine and Petroleum Geology 75, 151–180.

Shanmugam, G. (2006). Deep-water Processes and Facies Models: Implications for Sandstone Petroleum Reservoirs. Handbook of Petroleum Exploration and Production, 5. Elsevier Science, pp. 207.

Shanmugam, G. (2016). Submarine fans: a critical retrospective (1950 – 2015). Journal of Palaeogeography 5 (2), 110–184.

Shannon, L.V. (1985). The Benguela ecosystem: Part I. Evolution of the Benguela, physical features and processes: Oceanography and Marine Biology 23, pp. 105–182.

Shepard, F.P. & Dill, R.F. (1966). Submarine Canyons and Other Sea-valleys. Rand McNally, Chicago, IL, pp. 381.

Siesser, W.G. & Dingle, R.V. (1981). Tertiary sea-level movements around southern Africa. The Journal of Geology 89, 83–96.

Sun, Q., Alves, T., Xie, X., He, J., Li, W. & Ni, X. (2017). Free gas accumulations in basal shear zones of mass-transport deposits (Pearl River Mouth Basin, South China Sea): An important geohazard on continental slope basins. Marine and Petroleum Geology 81, 17–32.

Sun, Q., Wu, S., Hovland, M., Luo, P., Lu, P. & Qu, T. (2011). The morphologies and genesis of mega-pockmarks near the Xisha Uplift, South China Sea. Marine and Petroleum Geology 28, 1146–1156.

Talling, P.J (2014). On the triggers, resulting flow types and frequencies of subaqueous sediment density flows in different settings. Marine Geology 352, 155–182.

Traynor, J.J. & Sladen, C. (1997). Seepage in Vietnam – onshore and offshore examples. Marine and Petroleum Geology 14 (4), 345–362.

Tubau, X., Paull, C.K., Lastras, G., Caress, D.W., Canals, M., Lundsten, E., Anderson, K., Gwiazda, R. & Amblas, D. (2015). Submarine canyons of Santa Monica Bay, Southern California: variability in morphology and sedimentary processes. Marine Geology 365, 61–79.

Uenzelmann-Neben, G. & Huhn, K. (2009). Sedimentary deposits on the southern South African continental margin: Slumping versus non-deposition or erosion by oceanic currents? Marine Geology 266, 65–79.

Valle, G.D. & Gamberi, F. (2011). Pockmarks and seafloor instability in the Olbia continental slope (northeastern Sardinian margin, Tyrrhenian Sea). Marine Geophysical Research 32, 193–205.

Van Der Spuy, D. (2003). Aptian source rocks in some South African Cretaceous basins. In: Arthur, T.J., MacGregor, D.S. & Cameron, N.R. (Eds.), Petroleum Geology of Africa: New Themes and Developing Technologies. Geological Society of London, Special Publication 207, pp. 185–202.

Van Rensbergen, P., Hillis, R.R., Maltman, A.J. & Morley, C.K. (2003). Subsurface sediment mobilization, introduction. In: Van Rensbergen, P., Hillis, R.R., Maltman, A.J. & Morley, C.K. (Eds.), Subsurface Sediment Mobilization: Geological Society Special Publication, 216, pp. 1–8.

Verdicchio, G. & Trincardi, F. (2006). Short-distance variability in slope bed-forms along the Southwestern Adriatic Margin (Central Mediterranean). Marine Geology 234, 271–292.

Watkeys, M.K. (2006). Gondwana break-up: A South African perspective. In: Johnson, M.R., Annhauser, C.R. & Thomas, R.J. (Eds.), The Geology of South Africa. Geological Society of South Africa, Johannesburg/Council for Geoscience, Pretoria, pp. 531–539.

Watkeys, M.K. & Sokoutis, D. (1998). Transtension in south-east Africa during Gondwana break-up. In: Holdsworth, R.E., Strachan, R., Dewey, J.F. (Eds.), Continental Transpressional and Transtensional Tectonics, vol. 135. Geological Society of London, pp. 203–214.

Wefer, G., Berger, W.H. & Richter, C. (1998). Proceedings of Ocean Drilling Program, Initial Reports 175, College Station, Texas.

Weigelt, E. & Uenzelmann-Neben, G. (2004). Sediment deposits in the Cape Basin: Indications for shifting ocean currents? AAPG Bulletin 88 (6), 765–780.

Weschenfelder, J., Klein, A.H.F., Green, A.N., Aliotta, S., de Mahiques, M.M., Neto, A.A., Terra, L.C., Corrêa, I.C.S., Calliari, L.J., Montoya, I., Ginsberg, S.S. & Griep, G.H. (2016). The control of palaeo-topography in the preservation of shallow gas accumulation: examples from Brazil, Argentina and South Africa. Estuarine Coastal and Shelf Science 172, 93–107.

Wigley, R.A. & Compton, J.S. (2006). Late Cenozoic evolution of the outer continental shelf at the head of the Cape Canyon, South Africa. Marine Geology 226, 1–23.

Wiles, E., Green, A.N., Watkeys, M., Jokat, W. & Krocker, R. (2013). The evolution of the Tugela canyon and submarine fan: a complex interaction between margin erosion and bottom current sweeping, southwest Indian Ocean, South Africa. Marine and Petroleum Geology 44, 60–70.

Zachos, J., Pagani, M., Sloan, L., Thomas, E. & Billups, K. (2001). Trends, rhythms, and aberrations in global climate 65 Ma to Present. Science 292, 686–693.

Zhong, G., Cartigny, M.J., Kuang, Z. & Wang, L. (2015). Cyclic steps along the South Taiwan Shoal and West Penghu submarine canyons on the northeastern continental slope of the South China Sea. GSA Bulletin 127 (5–6), 804–824.

Zhou, Y., Ji, Y., Xu, L., Che, S., Niu, X., Wan, L., Zhou, Y., Li, Z. & You, Y. (2016). Controls on reservoir heterogeneity of tight sand oil reservoirs in Upper Triassic Yanchang Formation in Longdong area, southwest Ordos Basin, China: implications for reservoir quality prediction and oil accumulation. Marine and Petroleum Geology 78, 110–135.

Zhu, M., Graham, S.A., Pang, X. & McHargue, T. (2009). Characteristics of migrating submarine canyons from the middle Miocene to present: implications for paleoceanographic circulation, northern South China Sea. Marine and Petroleum Geology 27 (1), 307–319.

Zühlsdorff, L. & Spiess, V. (2004). Three-dimensional seismic characterization of a venting site reveals compelling indications of natural hydraulic fracturing. Geology 32 (2), 101–104.

APPENDIX A

Table A1: Morphometric information of all canyon systems along the Cape continental margin.

	Cape	**O1**	**O2**	**O3**	**Hetfield**	**K1**	**K2**	**K3**
Morphology	Sinuous	Hooked	Hooked	Hooked	Linear	Linear	Linear	Linear
Sub-division (Zone)	A	A	A	A	B	B	B	B
Thalweg Length (km)	100	51	27	42	17.50	12.40	17.00	17.31
Sinuosity	1.33	1.10	1.22	1.00	1.00	1.00	1.00	1.00
Gradient of walls at head (°)	Unavailable	14	27	13.50	15.50	7.30	14	12.90
Gradient of walls at mid-canyon (°)	16	15	16	15.50	24.50	7.60	20	14.40
Gradient of walls at toe (°)	17	4	12.50	6	18	7	9	10.10
Width of head (m)	Unavailable	1000	1500	1000	2000	500	1000	750
Width of mid-canyon (m)	4000	4000	3000	1000	4000	2200	3800	3500
Width of toe (m)	300	1750	1000	1500	1500	2800	1000	1300
Relief of head (m)	Unavailable	50	200	200	300	30	250	130
Relief of mid-canyon (m)	300	200	400	250	200	150	150	100
Relief of toe (m)	40	100	100	150	100	70	60	100

Table A1 (continued): Morphometric information of all canyon systems along the Cape continental margin.

	N1	**N2**	**G1**	**G2**	**Hope**	**T1**	**T2**	**T3**
Morphology	Sinuous	Sinuous	Linear	Linear	Sinuous	Linear	Linear	Linear
Sub-division (Zone)	B	B	B	B	C	C	C	C
Thalweg Length (km)	10	20	30.50	12.90	34	14.50	7.50	5.50
Sinuosity	1.10	1.10	1.00	1.02	1.12	1.00	1.00	1.00
Gradient of walls at head (°)	Unavailable	14.20	14.10	20.80	11.70	14.30	14.00	5.00
Gradient of walls at mid-canyon (°)	Unavailable	14	13.60	11.10	23.80	16.70	20.00	11.20
Gradient of walls at toe (°)	Unavailable	9.5	13.20	10.30	13.60	11.20	14.30	11.90
Width of head (m)	Unavailable	2000	1200	1000	5000	1700	650	1400
Width of mid-canyon (m)	Unavailable	1500	600	1500	5500	2300	1900	1700
Width of toe (m)	Unavailable	500	2500	1500	2500	2100	1800	1500
Relief of head (m)	Unavailable	80	200	110	150	130	120	40
Relief of mid-canyon (m)	Unavailable	220	80	60	500	150	125	70
Relief of toe (m)	Unavailable	20	70	100	100	150	110	50

Table A1 (continued): Morphometric information of all canyon systems along the Cape continental margin.

	False	**S1**	**S2**	**Rose**	**Coffee**	**Reznor**	**Lewis**	**Layne**
Morphology	Hooked	Linear	Linear	Hooked	Hooked	Hooked	Hooked	Hooked
Sub-division (Zone)	C	C	C	C	C	C	C	C
Thalweg Length (km)	34	11	9	18.5	17	30	7	18
Sinuosity	1.70	1.00	1.00	1.78	1.20	1.43	1.30	1.04
Gradient of walls at head (°)	6.70	5.60	4.46	28.50	9.00	10.12	24.07	11.45
Gradient of walls at mid-canyon (°)	12.21	6.50	12.40	14.00	22.00	15.65	25.65	26.40
Gradient of walls at toe (°)	15.24	3.00	19.01	10.52	25.64	14.96	23.32	9.20
Width of head (m)	1000	2500	1500	3000	1000	750	1000	1200
Width of mid-canyon (m)	3500	1500	850	4250	2500	2000	1500	2100
Width of toe (m)	4000	2800	1200	4500	2500	1700	1000	1200
Relief of head (m)	300	60	90	250	25	80	70	150
Relief of mid-canyon (m)	400	170	150	400	200	200	200	150
Relief of toe (m)	250	70	150	200	250	160	150	120